ROYAL SOCIETY
OF CHEMISTRY

Check for updates

Design, synthesis, and structure–activity relationship studies of 4-substituted phenylpyrazolidinone derivatives as potent Ku70/80 targeted DNA-PK inhibitors

Narva Deshwar Kushwaha,[a] Pamela VanderVere-Carozza,[b] Tyler L. Vernon,[b] Pamela L. Mendoza-Munoz, [iD][b] Jitender D. Gaddameedi,[a] Karim Ben Ali Gacem,[cd] Joseph Engel,[a] Jean-Baptiste Charbonnier,[c] Navnath S. Gavande [iD] *[ae] and John J. Turchi [iD] *[bfg]

The Ku70–Ku80 (Ku) heterodimer complex plays a central role in the non-homologous end joining (NHEJ) double-strand break (DSB) repair pathway and the DNA damage response (DDR). Like DNA–PK, Ku is a promising drug target for cancer treatment when combined with radiotherapy or DSB-inducing agents. We have previously reported the first-in-class, early-generation, highly potent, and specific Ku–DNA binding inhibitors (Ku-DBi's) that block the Ku interaction with DNA and inhibit DNA-PK kinase activity. These early-generation Ku-DBi's also inhibit cellular DNA-PK, NHEJ-catalyzed DSB repair, sensitize non-small cell lung cancer (NSCLC) cells to DSB-inducing agents, and potentiate the cellular effects of these agents *via* p53 phosphorylation through the activation of the ATM pathway. In this study, we report a comprehensive structure–activity relationship (SAR) analysis around the initial **X80** hit molecule to develop highly potent Ku-DBi's. Early generation Ku-DBi's display a potent Ku–DNA binding inhibitory activity with a range of 2 to 6 μM, and DNA-PK inhibitory activity in the nanomolar range of approximately 110 nM. Microscale thermophoresis assay shows that these compounds inhibit Ku70–Ku80 binding to DNA with a Kd value of 0.4–6.4 μM. The thermal stability analysis also supports the notion that these Ku-DBi's bind to the Ku as measured by nanoDSF (Differential Scanning Fluorimetry), which is consistent with the observed SAR trends. These Ku-DBi's may serve as candidate compounds for further modification and development as anticancer therapeutics in combination with radiotherapy or DSB-inducing agents to treat certain DNA repair-deficient cancers.

1. Introduction

DNA double-strand breaks (DSBs) are considered the most lethal form of all DNA lesions that threaten genomic integrity and if not correctly repaired, lead to genomic instability, cell-cycle arrest, and oncogenic transformation.[1,2] To safeguard inherent genomic integrity and stability, cancer cells have developed a complex DNA damage response (DDR) mechanism, in which the majority of DSBs are detected and repaired *via* homologous recombination (HR) and non-homologous end joining (NHEJ) pathways.[3–5] Alternative NHEJ (alt-NHEJ) or microhomology-mediated end joining (MMEJ), also called polymerase theta-mediated end joining (TMEJ), and single-strand annealing (SSA), are considered backup pathways.[6–8] Canonical or classical NHEJ is the predominant pathway in human cells and is active throughout the cell cycle, rapidly repairing up to ~80% of all DSBs.[9,10]

The members of the PI-3 kinase-related-kinase (PIKK) superfamily (ATM, ATR, and DNA-PK) are the central regulators of the DDR initiated at the DSBs and DNA discontinuities that orchestrate many phosphorylation events in response to DNA damage and replication stress. Among

[a] Department of Pharmaceutical Sciences, Eugene Applebaum College of Pharmacy and Health Sciences (EACPHS), Wayne State University, Detroit, MI 48201, USA. E-mail: ngavande@wayne.edu; Fax: +1 (313) 577 2033; Tel: +1 (313) 577 1523

[b] Department of Medicine, Indiana University School of Medicine (IUSM), Indianapolis, IN 46202, USA. E-mail: jturchi@iu.edu; Fax: +1 317 274 0396; Tel: +1 317 278 1996

[c] Institute for Integrative Biology of the Cell (I2BC), Institute Joliot, CEA, CNRS, Université Paris-Sud, 91198 Gif-sur-Yvette Cedex, France

[d] Structure-Design-Informatics, Sanofi R&D, 94400 Vitry sur Seine, France

[e] Molecular Therapeutics Program, Barbara Ann Karmanos Cancer Institute, Wayne State University, Detroit, MI 48201, USA

[f] Department of Biochemistry and Molecular Biology, Indiana University School of Medicine, Indianapolis, Indiana 46202, USA

[g] NERx Biosciences, Indianapolis, IN 46202, USA

them, the DNA-PK holoenzyme plays a crucial role in cellular DDR, consisting of the 469 kDa catalytic subunit, DNA-PKcs, and the Ku70/Ku80 heterodimeric (Ku) DNA-binding complex. DNA-PKcs kinase activity requires Ku70/80 DNA binding to enable NHEJ recognition and repair of DSBs.[2,11] In addition, DNA-PK also phosphorylates ATM and other downstream targets, and it is also a phosphorylation substrate for both ATM and ATR. In this context, Ku is involved in modulating ATM activity by signaling the ATM-dependent DDR cascade in response to DSBs to regulate cell fate after DNA damage. This collective response ensures that cancer cells respond to all types of DNA damage, thereby promoting their survival. In addition to its role in NHEJ, Ku70/80 is also playing a critical role in other biological processes, including telomere maintenance and protection, post-translational modifications, and other important cellular mechanisms such as regulation of RNA polymerase II-mediated transcription and chromatin dynamics, mitochondrial function, apoptosis regulation, and involvement in cellular senescence and aging.[12,13]

DNA-PKcs and Ku70/80 are dysregulated in various cancers, including lung, breast, cervix, pancreatic, leukemia, and multiple myeloma, as tumors become reliant on increased DNA-PK activity to respond to genomic instability.[2,14–17] Overall, upregulated expression of DNA-PKcs and Ku70/80 has been shown to instigate aggressive tumor behavior, tumor cell proliferation, metastasis, inferior clinical outcome, and poor overall survival.[16,18] The enhanced ability of tumor cells to repair DSBs is also a major contributor to chemo- and radiotherapy resistance.

DNA-PK has been regarded as an excellent drug target, and many DNA-PK inhibitors have been developed, which are currently in preclinical and clinical trials for cancer treatment. Although DNA-PK is considered a feasible genetic target for cancer therapy, no DNA-PK inhibitors are currently FDA-approved. The selective DNA-PK inhibitors such as M3814/nedisertib (Merck, phase 1/2, multiple clinical trials undergoing), AZD7648, (AstraZeneca, phase 1/2, NCT03907969), and VX-984/M9831/peposertib (Vertex/Merck, phase 1, NCT02644278) and non-selective inhibitors such as CC-115 (Celgene, phase 1, NCT01353625 and NCT02833883,), LY3023414/samotolisib (Eli Lilly, phase 1/2, multiple clinical trials undergoing) and XRD-0394 (XRad, phase 1, NCT05002140) are undergoing for their therapeutic utility in combination with radiotherapy, DNA-damaging chemotherapeutics, and monoclonal antibodies for treating various cancers.[19–22] Since these inhibitors compete with ATP for binding, their effectiveness can be significantly reduced when ATP levels are elevated, as is often the case in aggressive cancers. This ATP abundance leads to drug resistance and metastasis, requiring higher drug concentrations to achieve therapeutic effects, which in turn exacerbates pharmacokinetic and pharmacodynamic challenges.[23] Recent clinical analyses of M3814 (peposertib), AZD7648, and CC-115 revealed that the maximum tolerable dose of these drugs failed to achieve prolonged DNA-PK

inhibition and provided insufficient targeting of tumor tissue in combination therapy.[24–26] An alternative approach for DNA-PK inhibition is targeting Ku, and the unique capacity of Ku–DNA binding inhibitors (Ku-DBi's) to block the formation of end-joining complexes and DNA-PK activity. This mechanism, working independently of ATP concentration, can achieve more specific inhibition under physiological conditions of high ATP concentrations. The significance of targeting Ku also lies in the fact that DSBs are first recognized by the Ku70/Ku80 heterodimeric complex, which recruits and activates the DNA-PKcs, subsequently activating a series of DNA repair enzymes in the NHEJ pathway. Thus, blocking this interaction leaves the DNA ends free for processing by other DNA repair and genome stability pathways, unlike DNA-PKcs targeted agents, which block the Ku–DNA-PKcs complex on the DNA end and occlude other processing activities.

We are the first to report a new class of inhibitors that block the interaction between Ku70/80 heterodimer and DNA, which displayed nanomolar activity *in vitro*, inhibit cellular DNA-PK, NHEJ-catalyzed DSB repair, and sensitize non-small cell lung cancer (NSCLC) cells to DSB-inducing agents.[27,28] Herein, we report our efforts to identify these more potent Ku-DBi's of the Ku–DNA interaction through extensive structure–activity relationships (SARs) efforts. Other molecules exhibiting Ku inhibitory activity include STL127705 (compound L) and the promiscuous inhibitor UMI-77, which are identified through computational and high-throughput screening of small-molecule inhibitors targeting the Ku complex using a fluorescence polarization-based DNA binding assay, respectively.[29,30] More recently, we showed that Ku-DBi's abolish DNA-PKcs autophosphorylation to impact DSB repair and DDR signaling through activating the ATM pathway.[31] In addition, *in vivo* studies in an NSCLC xenograft model demonstrated that the Ku-DBi treatment blocked IR-dependent DNA-PKcs autophosphorylation, modulated DDR, and reduced tumor cell proliferation.[32]

2. Results and discussion

2.1 SAR design

As described in our earlier report,[27] we identified an **X80** (phenylpyrazolidinone) scaffold with modest *in vitro* inhibitory activity of Ku in electrophoretic mobility shift assay (EMSA) and DNA-PK phosphorylation assay. We utilized the existing crystal structures of the Ku70/80 heterodimer (PDB: 1JEQ) and the Ku70/80 dimer bound to a 55-nucleotide DNA substrate (PDB: 1JEY) to explore the interactions of the **X80** molecule with Ku70/80 heterodimer.[33] Based on our previous findings through molecular docking,[27] we embarked on a multidisciplinary structure-guided synthetic chemistry effort to obtain high-affinity Ku-DBi's with favorable DNA-PK inhibitory activity. The initial substitutions on ring A of the **X80** molecule furnished compounds **5102** and **5135**, which displayed around a 25-fold increase in potency.[28] However, both compounds exhibited poor solubility, making them of

limited utility for further *in vitro* or cellular studies. Based on the promising initial data, a library of more than 38 novel analogs was designed and synthesized, relying on iterative logic-based SAR exploration of the chemical space around the **X80** molecule. The overall SAR approach for identifying potent Ku-DBi's is outlined in Fig. 1.

The SAR approach involves 1) substitutions on ring A with aryl and alkyl moieties to occupy a hydrophobic pocket, which spans the interface between the two Ku subunits; 2) replacement of furan ring with thiophene/1*H*-pyrrole to obtain a single *Z* isomer; 3) assess the effect of the *meta*-substituted carboxylic acid group on ring C over *para* on inhibitory activity; 4) replacement of CH_3 group of pyrazolone ring with bioisosteric CF_3 to improve Ku inhibitory and DNA-PK activity; 5) Reduction of carbon–carbon double bond (alkene) between the furan/thiophene and pyrazolone rings to single bond to enhance molecular flexibility and improve binding affinity; 6) the last modification is to replace phenyl carboxylic acid with a bioisosteric moiety to improve the metabolic stability and cellular permeability of lead molecules.

This approach to structural optimization was organized around iterative cycles of structure-based drug design, synthesis, and evaluation of Ku and DNA-PK activity. At each stage, experimentally obtained Ku and DNA-PK inhibitory activities were used to refine the decision model for the next synthetic planning.

2.2 Chemistry

The general synthetic route of the target compounds **35–63** is depicted in Scheme 1. We synthesized these target molecules by slightly modifying existing synthetic approaches reported earlier by our and other groups to improve overall chemical yields.[34–36] The 3′- or 4′-benzoic acid substituted dihydro-1*H*-pyrazol-1-yl **4a–c** were prepared in good yields by refluxing corresponding 3′- or 4′-benzoic acid substituted phenylhydrazines **1a** and **1b** with either ethyl acetoacetate or ethyl trifluoroacetoacetate in acetic acid. The esterification of

carboxylic acids of compound **4a–c** using H_2SO_4 in ethanol furnished **5a–c** in good yields. Aldehydes **8a–c** were prepared in moderate to high yield by optimizing Pd-catalyzed Suzuki coupling of 5-borono-2-chlorobenzoic acid **7**, with either 5-bromofuran-2-carbaldehyde **6a** or 5-bromothiophene-2-carbaldehyde **6b** or 5-bromo-1*H*-pyrrole-2-carbaldehyde **6c**. Compounds **9–14** were prepared in moderate to excellent yields as a mixture of *E/Z* isomers by condensing corresponding 3′- or 4′-carboxylic acid substituted pyrazolones **5a–c** with aldehydes **8a–c** in acetic acid under Knoevenagel reaction conditions. The ratio of *E/Z* isomers was determined by 1D and 2D NOESY NMR analysis (see Fig. S1 for NOESY analysis). The *Z* isomer was the major product of a mixture of isomers (*Z*:*E* ratio ~75:25). Preparative HPLC made the separation of the *E* and *Z* isomers possible. However, each isolated isomer was rapidly equilibrated to return to the original mixture of *E* and *Z* isomers. We synthesized compounds **15–16** by the hydrolysis of the corresponding esters (**10** and **13**, respectively) using 2 N NaOH at room temperature. The substituted aryl-and alkyl-amides **17–34** were prepared from compounds **9–14** in moderate yields by utilizing the EDCI/HOBt amide synthetic protocol. The target compounds **35–52** were obtained from compounds **17–34** in moderate to good yields by hydrolysis of the corresponding esters using 10 N LiOH at room temperature. The carbon–carbon double bond (alkene) reduction between the furan/thiophene and pyrazolone rings was carried out using either $NaBH_4$ or Pd/C in MeOH to furnish the target compounds **53–63** in moderate to good yields.

The synthetic route for the replacement of the carboxylic acid group with bioisosteric sulfonamides **67–70** is described in Scheme 2. The 4′-benzenesulfonamide substituted dihydro-1*H*-pyrazol-1-yl **65** was prepared in good yield by refluxing 4-hydrazinylbenzenesulfonamide **64** with ethyl acetoacetate in acetic acid. Compound **66** was prepared in good yield as a mixture of *E/Z* isomers by condensing compound **65** with aldehyde **8a** in acetic acid under the Knoevenagel reaction condition. The target compounds **67–69** were prepared by
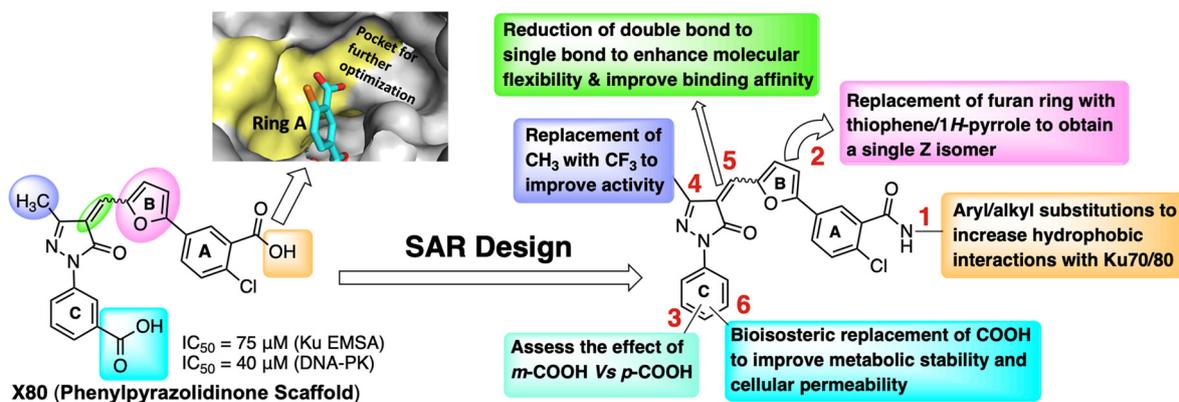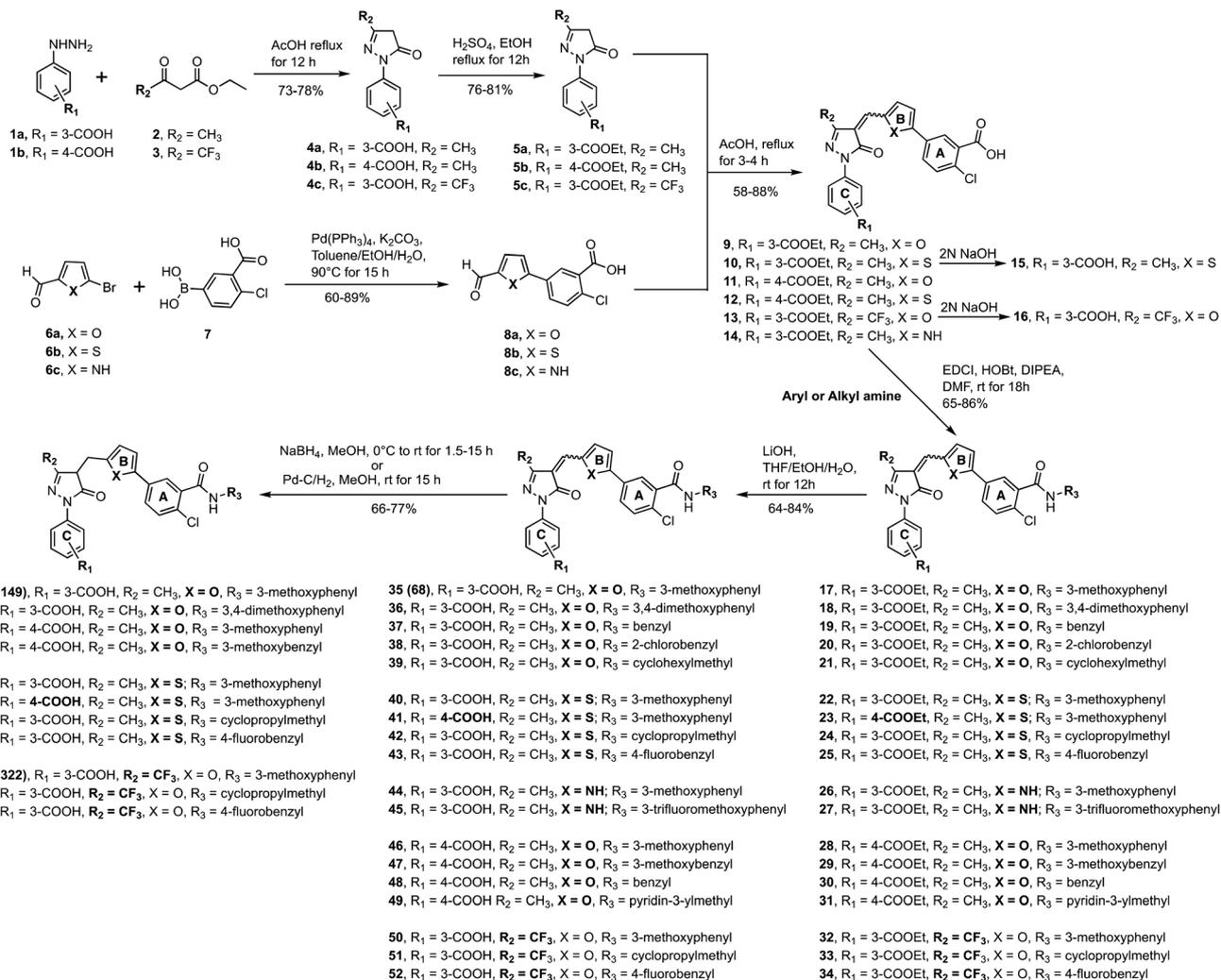

Fig. 1 Structure of **X80** with Ku EMSA and DNA-PK IC_{50} values and further SAR design strategy is highlighted for further optimization of 4-substituted phenylpyrazolidinone scaffold.

Scheme 1 The general synthetic route of the Ku/DNA-PK inhibitors, **35–63**.

coupling either an aryl- or alkyl-amine with carboxylic acid **66** in good to excellent yields using the EDCI/HOBt amide synthetic protocol. The reduced version of 3-methoxyphenyl linked phenylpyrazolidinone benzenesulfonamide **70** was synthesized from compound **67** using $NaBH_4$ in MeOH in good yield.

The synthetic route for the replacement of the carboxylic acid group with bioisosteric tetrazoles **75** and **76** (**245**) is depicted in Scheme 3. Initially, 3′-benzonitrile substituted dihydro-1*H*-pyrazol-1-yl **72** was prepared in excellent yield by refluxing 3-hydrazinylbenzonitrile **71** with ethyl acetoacetate in acetic acid.

Compound **73** was prepared in excellent yield as a mixture of *E/Z* isomers by condensing compound **72** with aldehyde **8a** in acetic acid under the Knoevenagel reaction condition. The substituted 3-methoxyphenyl derivative **74** was prepared through acid-amine coupling in good yield by utilizing the EDCI/HOBt amide synthetic protocol. A one-pot synthesis of tetrazole was achieved directly from nitriles through the [3 + 2] cycloaddition of sodium azide to the

nitrile to give 3-substituted 1*H*-tetrazole **75** in the presence of NH_4Cl and DMF at 130 °C. Finally, we utilized either $NaBH_4$ or $NiCl_2/NaBH_4$ as reducing agents in MeOH or MeOH/THF, respectively, to achieve the reduced version of tetrazole **76** (**245**).

## 2.3 Structure–activity relationship (SAR) studies of 4-substituted phenylpyrazolidinone

2.3.1 Optimization of ring A to occupy a hydrophobic pocket.
During our initial studies, we synthesized and screened similar derivatives of the **X80** compound with furan and thiophene containing phenyl carboxylic acids, **15** and **16** (Scheme 1), to reassert the **X80** (phenylpyrazolidinone) scaffold's ability to inhibit Ku and DNA-PK activity. However, compounds with free carboxylic acid on ring A displayed modest Ku inhibitory activity (**15**, Ku IC_{50} = 15.15 ± 1.24 μM and **16**, Ku IC_{50} = 16.41 ± 3.94 μM) when assessing Ku double-stranded DNA-binding activity *in vitro*. In our earlier report,[27] we performed an in-depth *in silico* analysis of the
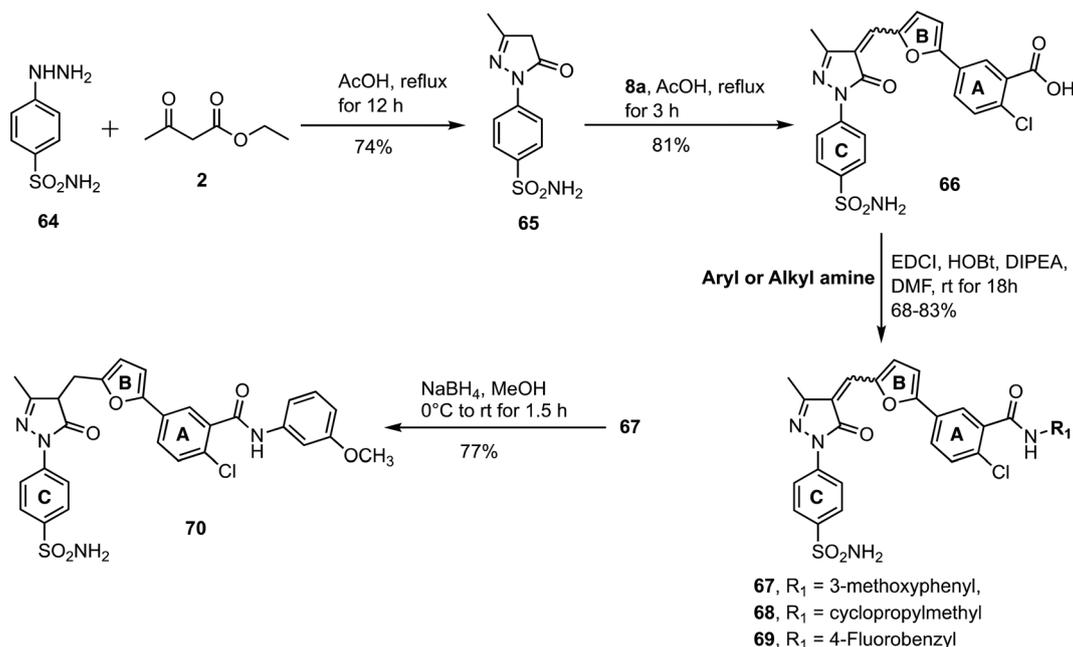
Scheme 2 The synthetic route for replacement of carboxylic acid group with bioisosteric sulfonamides, **67–70**.

67, R$_1$ = 3-methoxyphenyl,
68, R$_1$ = cyclopropylmethyl
69, R$_1$ = 4-Fluorobenzyl
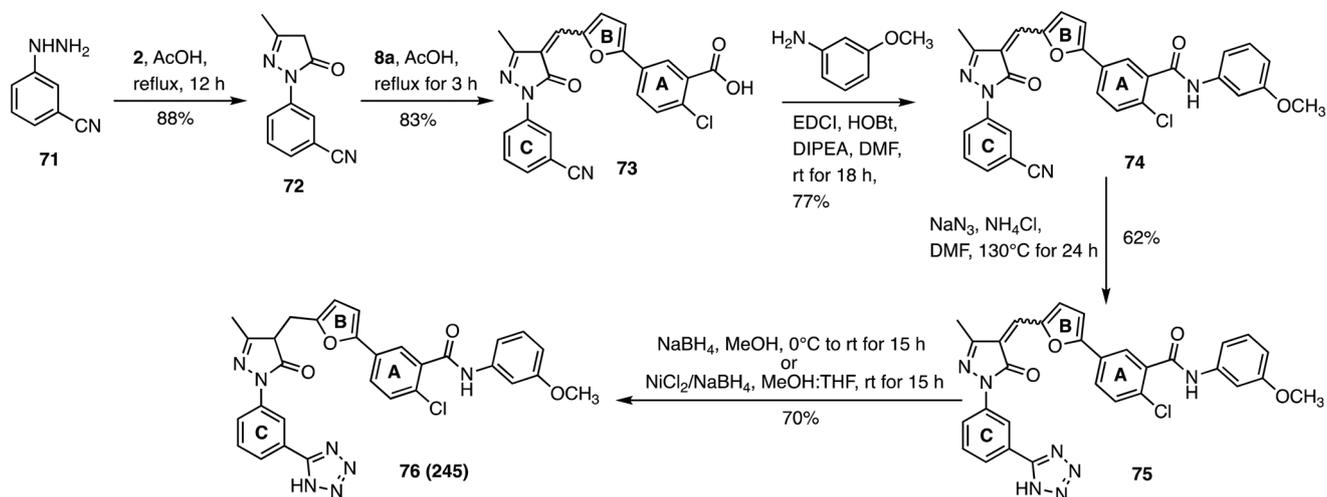
Scheme 3 The synthetic route for the replacement of the carboxylic acid group with bioisosteric tetrazoles, **75–76**.

binding interactions between the **X80** molecule and the Ku70/80 heterotrimer, utilizing the existing crystal structure of the Ku70/80 heterotrimer. We identified a space-filling hydrophobic pocket located adjacent to ring A of the **X80** molecule, which spans the interface between the two Ku subunits (Fig. 1). The initial ester-linked substitution on ring A exhibited a high clog$P$ and poor solubility; therefore, we utilized small isosteric modifications to enhance solubility and metabolic stability. This was accomplished by replacing the metabolically labile ester group with a more chemically and metabolically stable amide. We explored several arylamide- and alkylamide-containing substituents at ring A, as represented by compounds 35 (compound 68) and 37–39,

with 3-methoxyphenyl (**35/68**), benzyl (**37**), 2-chlorobenzyl (**38**), and cyclohexyl methyl (**39**) being the optimal fit in the space-filling pocket. Aryl-containing amides 35 and 37–38 (IC$_{50}$ ≈ 3–8 μM) at ring A exhibited an increase in activity compared to alkyl cyclohexyl methyl 39 (IC$_{50}$ ≈ 22 μM), aligning with our previous inhibition trend observed for extended ester derivatives, **5102** and **5135**. The benzylamide (**37**) showed better DNA-PK inhibitory activity as compared to other phenyl amides (**35 and 38**). However, there was no fine-tuning between Ku inhibitory and DNA-PK activity for benzylamide, **37** (Table 1). Importantly, amide-linked modifications on ring A displayed good physicochemical characteristics, including dramatically increased solubility

Table 1 The chemical structures of novel Ku-DBi's and their Ku–DNA binding and DNA-PK IC$_{50}$ values

Compound	Series	R$_1$	R$_2$	X	R$_3$	Ku$_{70/80}$[a] (IC$_{50}$) µM	DNA-PK[b] (IC$_{50}$) µM
Substitutions on ring A to occupy a hydrophobic pocket							
35 (**68**)	A	3-COOH	CH$_3$	—	(3-OCH$_3$ phenyl)	6.02 ± 2.19	3.12 ± 0.71
37	A	3-COOH	CH$_3$	—	(benzyl)	8.22 ± 0.45	0.83 ± 0.09
38	A	3-COOH	CH$_3$	—	(2-Cl benzyl)	3.55 ± 0.40	1.74 ± 0.61
39	A	3-COOH	CH$_3$	—	(cyclohexylmethyl)	22.58 ± 4.4	ND
Replacement of furan ring with thiophene/1H-pyrrole							
40	B	3-COOH	CH$_3$	—	(3-OCH$_3$ phenyl)	7.18 ± 2.24	1.72 ± 0.18
41	B	4-COOH	CH$_3$	—	(3-OCH$_3$ benzyl)	9.04 ± 0.36	0.53 ± 0.07
42	B	3-COOH	CH$_3$	—	(cyclopropylmethyl)	11.06 ± 0.76	3.04 ± 0.7
43	B	3-COOH	CH$_3$	—	(4-F benzyl)	10.08 ± 1.4	3.24
44	C	3-COOH	CH$_3$	—	(3-OCH$_3$ phenyl)	9.77 ± 4.16	1.57 ± 0.73
45	C	3-COOH	CH$_3$	—	(3-OCF$_3$ phenyl)	6.90 ± 1.00	0.53 ± 0.18
Replacement of meta-COOH with para-COOH on ring C							
46	A	4-COOH	CH$_3$	—	(3-OCH$_3$ phenyl)	5.06 ± 2.33	0.53 ± 0.16
47	A	4-COOH	CH$_3$	—	(3-OCH$_3$ benzyl)	>25	0.48 ± 0.048
48	A	4-COOH	CH$_3$	—	(benzyl)	22.45 ± 4.19	0.48 ± 0.016
49	A	4-COOH	CH$_3$	—	(pyridin-3-ylmethyl)	>25	2.5
Replacement of CH$_3$ group with CF$_3$ on pyrazolone ring							
50	A	3-COOH	CF$_3$	—	(3-OCH$_3$ phenyl)	3.36 ± 0.52	0.154 ± 014
51	A	3-COOH	CF$_3$	—	(cyclopropylmethyl)	11.41 ± 8.26	0.35
52	A	3-COOH	CF$_3$	—	(4-F benzyl)	9.15 ± 0.68	0.25
Reduction of carbon–carbon double bond (alkene)							
53 (**149**)	D	3-COOH	CH$_3$	O	(3-OCH$_3$ phenyl)	3.72 ± 1.49	0.5 ± 0.028
54	D	3-COOH	CH$_3$	O	(2,4-diOCH$_3$ phenyl)	9.97 ± 0.4	1.12 ± 0.17

Table 1 (continued)

Series A, Series B, Series C, Series D structures

Compound	Series	R_1	R_2	X	R_3	$Ku_{70/80}{}^a$ (IC$_{50}$) µM	DNA-PK^b (IC$_{50}$) µM
55	D	4-COOH	CH_3	O	(3-OCH$_3$ benzyl)	7.67 ± 2.95	0.808 ± 0.037
56	D	4-COOH	CH_3	O	(3-OCH$_3$ phenethyl)	12.45 ± 3.80	0.49 ± 0.08
57	D	3-COOH	CH_3	S	(3-OCH$_3$ benzyl)	6.09 ± 0.36	0.4 ± 0.04
58	D	4-COOH	CH_3	S	(3-OCH$_3$ benzyl)	9.04 ± 0.36	0.53 ± 0.07
59	D	3-COOH	CH_3	S	(cyclopropylmethyl)	11.06 ± 0.76	3.04 ± 0.07
60	D	3-COOH	CH_3	S	(4-F benzyl)	4.10 ± 0.30	2.66 ± 1.74
61 (322)	D	3-COOH	CF_3	O	(3-OCH$_3$ benzyl)	2.66 ± 0.34	0.110 ± 0.02
62	D	3-COOH	CF_3	O	(cyclopropylmethyl)	14.23 ± 0.21	ND
63	D	3-COOH	CF_3	O	(4-F benzyl)	9.15 ± 0.68	0.25
Bioisosteric replacement of phenyl carboxylic acid group with sulfonamide							
67	A	4-SO$_2$NH$_2$	CH_3	—	(3-OCH$_3$ benzyl)	11.29 ± 2.16	1.41 ± 0.27
68	A	4-SO$_2$NH$_2$	CH_3	—	(cyclopropylmethyl)	>25	ND
69	A	4-SO$_2$NH$_2$	CH_3	—	(4-F benzyl)	20.71 ± 1.84	1.53 ± 0.22
70	D	4-SO$_2$NH$_2$	CH_3	O	(3-OCH$_3$ benzyl)	7.86 ± 4.4	0.57 ± 0.12
74	A	3-CN	CH_3	—	(3-OCH$_3$ benzyl)	>25	ND
75	A	(tetrazolyl)	CH_3	—	(3-OCH$_3$ benzyl)	3.51 ± 1.81	0.98 ± 0.52
76 (245)	D	(tetrazolyl)	CH_3	O	(3-OCH$_3$ benzyl)	1.99 ± 0.88	0.24 ± 0.015

^{a} Compounds were incubated with purified Ku70/80 proteins and direct DNA binding activity was measured using EMSA. ^{b} Determined using DNA-PK phosphoryl-transferase catalytic assay, using a synthetic p53 peptide substrate and highly purified DNA-PK kinase. ND = not determined.

compared to earlier Ku inhibitors we discovered that contained ester linkages on ring A. Overall, decreased IC$_{50}$ values observed in the DNA-PK assay compared to the Ku–DNA binding assay are expected considering the difference in assay systems: DNA-PK is a catalytic assay, and Ku–DNA binding is a direct stoichiometric DNA binding assay.

2.3.2 Replacement of furan ring with thiophene/1H-pyrrole to obtain a single Z isomer. The **X80** core structure and compounds **35–39** contain a double bond between the furan
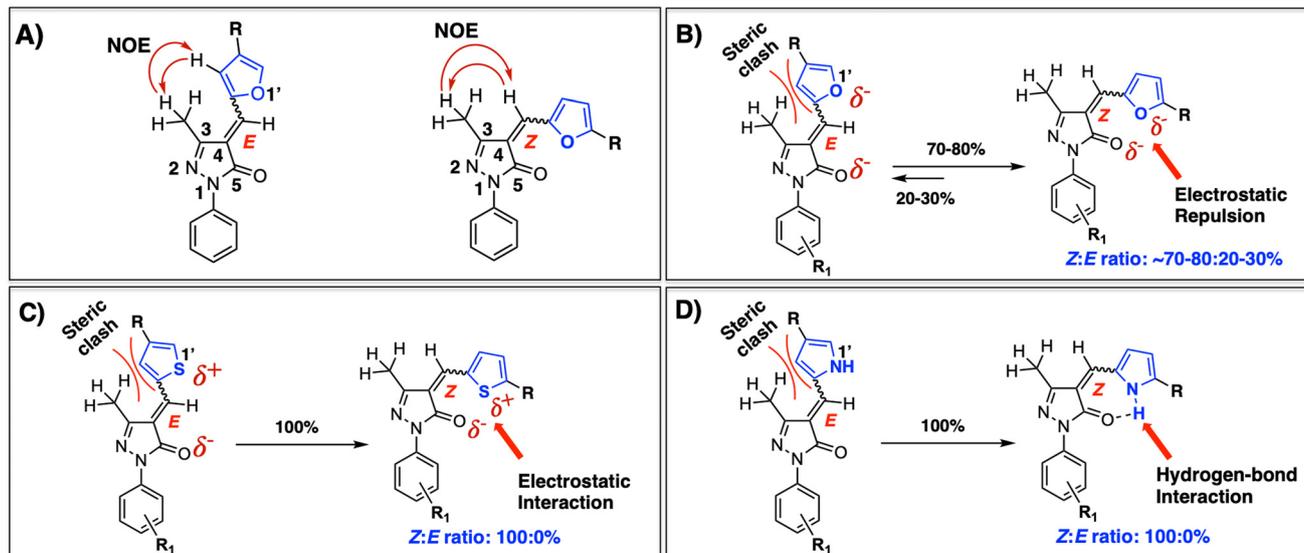
Fig. 2 A) Determination of the configurations for 4-substituted phenylpyrazolidinones using NOE experiments; B–D) rationales for the preferred *Z* or *E* configuration of 4-substituted phenylpyrazolidinones.

and pyrazolone rings. Thus, as determined by 1D and 2D NOESY NMR analysis, they exist as a mixture of *Z* and *E* isomers in roughly a 75 : 25 ratio. The *Z* isomer was the major product of a mixture of isomers. The *Z*-configured compounds should show an NOE effect between the C-3 substituted methyl proton and the proton of the C-4 substituted alkene of the pyrazolone ring. In contrast, the *E*-configured compounds should have an NOE effect between the C-3 substituted methyl proton of the pyrazolone ring and the vinylic proton of the heteroaromatic ring (Fig. 2A).

Our molecular docking studies predicted that the *Z*-isomer favors the efficient binding of our Ku-DBi's in the Ku70/80 heterodimer binding pocket. The primary goal of ring B modification is to establish an initial SAR and obtain a single *Z* isomer with high potency and selectivity as a chemical lead. To this end, we exploited chemical interactions between ring B and pyrazolone rings to obtain a single chemical entity. The mixture of *Z* and *E* isomerism of the 4-substituted phenylpyrazolidinones (35–39) may be the result of the electrostatic repulsion between the C-5 carbonyl oxygen atom of the pyrazolone ring and the O-1′ of furan (Fig. 2B).[37] This electrostatic repulsion between O-1′ of furan and C-5 carbonyl oxygen atom of the pyrazolone ring should favor more *E* isomers for our compounds, but a steric clash between the methyl proton of the pyrazolone ring and furan pushes compounds to adopt more *Z* isomers (~70–80%) than *E* isomers (~20–30%). Replacement of the furan ring with either thiophene or 1*H* pyrrole is expected to alleviate this repulsion and result in stabilization of the *Z* isomer and the existence of a single isomer (Fig. 2C and D). The electrostatic interaction between the C-5 carbonyl oxygen atom of pyrazolone ring and the partially positively charged S-1′ of the thiophene ring favors the *Z* isomer form for the compounds (Fig. 2C and S2). The predominance of the *Z*

isomerism of the 4-[(substituted pyrrolyl)methylidenyl] pyrazolone may be achieved due to the result of the intramolecular hydrogen bonding between the C-5 carbonyl oxygen atom of the pyrazolone ring and the proton on the *N*-1′ of the pyrrole ring (Fig. 2D and S3). Fig. 2C and D depicts our rationale for obtaining a single *Z* isomer by utilizing this strategy in our SAR studies.

Based on our strategy to obtain a single *Z* isomer, we initially synthesized a series of thiophene and pyrrole-containing substituted aryl and alkyl amines (40–45). We exclusively obtained the *Z* isomer, which was determined by 1D and 2D NOESY NMR analysis. Thiophene-ring-containing compounds (40–43) show similar Ku inhibitory and DNA-PK activity (Table 1) as furan-ring-containing compounds (35, 37–39); however, thiophene-ring-containing compounds showed high toxicity to normal cells. The thiophene ring is known to form reactive toxic metabolites as it undergoes CYP450-catalyzed *S*-oxidation and epoxidation.[38,39] These metabolites are highly electrophilic and react with the biochemical system, leading to a toxic effect on cells. The pyrrole-containing compounds (44–45) also exhibited similar Ku inhibitory and DNA-PK activity to the furan-ring-containing compounds (35, 37–39), but they have limited cellular uptake compared to their predecessor compounds.

2.3.3 Optimization of *meta* and *para* substitution of the acid group on ring C. Next, we focused on assessing the effects of carboxylic acid with *para* and *meta* position substitutions on ring C, using 35 (68) and 37 as our lead compounds. Interestingly, compounds 46–49 with *para* carboxylic acid (4-COOH) substitution exhibit a 2 to 6-fold increase in DNA-PK activity compared to *meta* carboxylic acid (3-COOH) substitution, demonstrating the importance of the position of the carboxylic acid moiety (Table 1). However, there was no fine-tuning between Ku inhibitory and DNA-PK

activities, so we focused our further SAR studies with *meta*-substituted derivatives on ring C.

2.3.4 Replacement of CH$_3$ with bioisosteric CF$_3$ on pyrazolidinone to improve Ku inhibitory and DNA-PK activity. The replacement of a methyl group by a bioisosteric trifluoromethyl is frequently used in medicinal chemistry.[40–42] We replaced the CH$_3$ group of pyrazolone ring B with the CF$_3$ group, and we observed a 2-fold increase in Ku inhibitory activity (compound **50**, Ku IC$_{50}$ = 3.36 ± 0.52 μM) and around a 20-fold increase in DNA-PK inhibitory activity. The other derivatives, **51–52** showed improved DNA-PK inhibitory activity but similar Ku inhibitory activity to its predecessor. The high electronegativity of the CF$_3$ group may directly alter the electron distribution of small molecules, influencing the binding interaction with surrounding protein residues.

2.3.5 Reduction of carbon–carbon double bond (alkene) between the furan/thiophene and pyrazolone rings to a single bond. Subsequently, the importance of the single bond was evaluated, as compounds containing a double bond exist as a mixture of *Z* and *E* isomers, contributing to molecular rigidity. To enhance flexibility and improve binding affinity, as predicted by molecular docking studies, we focused on reducing the double bond to a single bond. This modification, exemplified by compound **53** (**149**), resulted in a notable increase in potency across both assays (compare the Ku and DNA-PK activities of compound **35** (**68**) with those of **53** (**149**) in Table 1). The 3′,4′-dimethoxy substitution (**54**) on ring A showed a reduction in Ku and DNA-PK inhibitory activities, which may be due to structural constraints imposed by such a modification to fit in the space-filling binding pocket. Interestingly, 4-substituted carboxylic acid at ring C exhibited promising DNA-PK inhibitory activity with 3-methoxyphenyl **55** (DNA-PK IC$_{50}$ = 0.808 ± 0.037 μM) and 3-methoxybenzyl **56** (DNA-PK IC$_{50}$ = 0.49 ± 0.08 μM) but reduced in Ku inhibitory activity. To assess the importance of the double bond and its reduced version, particularly between compounds with exclusive *Z* isomer (compounds **40–43**) and the reduced version of thiophene-containing compounds, compounds **57–60** with several arylamide and alkylamide-containing substituents at ring A showed a similar Ku inhibitory activity with improved DNA-PK activity. However, these thiophene-containing compounds also exhibited toxicity to normal cells, similar to their thiophene-containing predecessor compounds.

Earlier, the replacement of the methyl group with a bioisosteric trifluoromethyl of the pyrazolone ring B showed impressive Ku and DNA-PK inhibitory activities, mainly with 3-methoxyphenyl amide (compound **50**). Thus, we reduced the double bond of compound **50** to a single bond, generating compound **61** (**322**), which resulted in a further increase in Ku (IC$_{50}$ = 2.66 ± 0.34 μM) and DNA PK inhibitory activity (IC$_{50}$ = 0.110 ± 0.02 μM) compared to compound **50**. As expected, the reduced version of ring A substituted cyclopropyl amide (**62**) and 4-fluoro benzylamide (**63**) showed decreased activity in both assays. This is most likely due to

3-methoxyphenyl or 3-trifluoromethoxyphenyl amide-containing compounds being the optimal fit in the space-filling pocket, which spans the interface between the two Ku subunits. We have also observed a better binding affinity for these compounds in computational studies compared to aliphatic or benzyl amides.

2.3.6 Replacement of phenyl carboxylic acid with a bioisosteric moiety to improve the metabolic stability and cellular permeability. The carboxylic acid functional group sometimes has limited utilization in drug discovery due to its limited passive diffusion across biological membranes (cellular permeability) and metabolic instability.[43,44] Therefore, for the final step of optimization, we assessed how bioisosteric modification of the carboxylic acid of phenyl ring C impacts inhibitory activity. Initially, we assessed the activity of 4-phenyl substituted sulfonamides as 3-phenyl substituted sulfonamides building blocks were not easily available. The phenyl sulfonamides **67–69** showed decreased Ku inhibitory and DNA-PK activities compared to their predecessor compounds containing phenyl carboxylic acids. 3-Methoxyphenyl amide containing phenyl sulfonamide **70**, which has a double bond reduced between the furan and pyrazolone rings, showed a 1–2.5-fold increase in Ku inhibitory and DNA-PK activities than compound **67**, aligning with our previous inhibition trend observed for other reduced compounds **53** (**149**), **55**, **57–58**, and **61** (**322**).

Overall, we observed that 3- or *meta*-substituted phenyl acids show better activity than 4- or *para*-substituted phenyl acids. During our earlier studies, we observed a decrease in Ku activity even with ethyl ester-containing compounds. Subsequently, the importance of the carboxylic acid was assessed by replacing it with a nitrile group (**74**), and we observed complete abolition of Ku inhibitory activity.

Tetrazole is widely utilized as a bioisostere for carboxylic acid in drug development, as it is metabolically stable to many biological transformations.[45] The tetrazoles with a double bond (**75**) and a reduced double bond (**76**) showed more potent Ku and DNA PK inhibitory activities than carboxylic acid or sulfonamide-containing compounds. In fact, molecular docking revealed a tighter binding affinity for the tetrazole moiety compared to the carboxylic acid moiety with the Ku protein, primarily due to its interactions with Arg368 [see ref. 27].

2.4 SAR analysis

The structure–activity relationship derived from the current study of Ku-DBi's is summarized in Fig. 3A. Collectively, extending ring A towards the space-filling hydrophobic pocket of the Ku heterodimer dramatically improved the activity. The substituted phenylamides showed better potency than benzylamides and alkylamides. Among all ring A substitutions, 3-trimethoxyphenyl and 3-trifluoromethoxy phenylamide are the optimal fit in the space-filling pocket and are critical to maintaining both Ku and DNA-PK inhibitory activities.
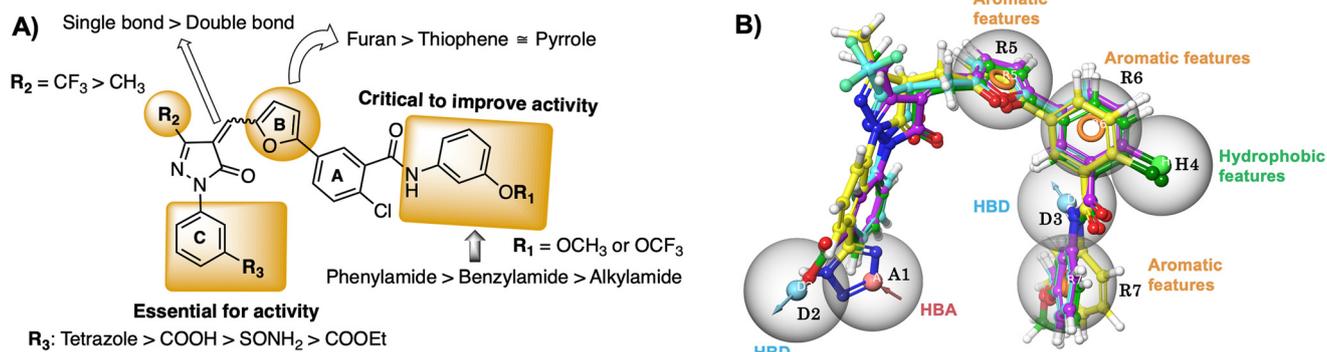
Fig. 3 A) SAR analysis based on Ku inhibitory and DNA-PK activities. B) Seven-feature ligand-based pharmacophore model (ADDHRRR) superimposed on **35** (**68**) (magenta carbons), **53** (**149**) (green carbons), **61** (**322**) (cyan carbons), and **76** (**245**) (yellow carbons). Features are shown as an orange sphere (hydrogen bond acceptor/HBA), blue spheres (hydrogen bond donors/HBD), green spheres (hydrophobic features), and orange rings (aromatic features). 2 Å tolerances are shown (light grey spheres) for HBA, HBD, hydrophobic features and three aromatic ring systems/features.

The central furan ring B can be replaced with either thiophene or pyrrole, which show comparable potency. However, the thiophene ring is toxic to normal cells, and the pyrrole ring does not significantly improve cellular activities. The reduction of the double bond to a single bond typically results in a 2- to 3-fold increase in potency for all compounds under multiple assay conditions. The replacement of the methyl group with trifluoromethyl shows a significant improvement in DNA-PK potency compared to Ku inhibitory activity. The *meta* or 3-substituted acid group of ring C is essential for activity. Among all acids, tetrazole shows better potency in both assays than carboxylic acid, sulfonamide, and ethyl ester.

2.5 Ligand-based pharmacophore modeling

On the basis of the SAR studies presented within this paper, a seven-feature three-dimensional ligand-based pharmacophore model (Fig. 3B) was developed and validated using Phase software (Schrödinger release 2024-2: Phase, Schrödinger, LLC, New York, NY).[46] A training set composed of 40 compounds listed in Table 1 was used to generate several pharmacophore hypotheses. The Phase software employs a unified pharmacophore perception algorithm to generate pharmacophore hypotheses by aligning the pharmacophore features (hydrogen bond acceptor, hydrogen bond donor, hydrophobic group, negative ionizable, positive ionizable, and aromatic ring) across multiple conformations of a training set of known active compounds. During pharmacophore model generation for KuDBis, conformational sampling, enumeration of chiral and *E/Z* isomers, prediction of ionization states, and tautomer generation were carried out using LigPrep prior to Phase modeling, thereby eliminating the need for manual ligand alignment and ensuring comprehensive representation of all relevant chemical forms. The resulting pharmacophore hypotheses were ranked using the Phase HypoScore scoring function, which incorporates internal validation metrics to

assess the quality of each model. As shown in Fig. 3B, a seven-feature pharmacophore model was constructed by merging the top-ranking five-point model with additional features from another high-ranking model. During model generation, both *E/Z* isomers of compound **35** (**68**) and the *R*- and *S*-stereoisomers of compounds **53** (**149**), **61** (**322**), and **76** (**245**) were evaluated. The final model was derived from the *Z*-isomer of **35** (**68**) and the *S*-isomers of **53** (**149**), **61** (**322**), and **76** (**245**), which collectively produced the highest-ranking pharmacophore hypothesis. The selected pharmacophore hypothesis comprises two hydrogen bond donors, one hydrophobic feature, and three aromatic ring features for compounds **35** (**68**), **53** (**149**), and **61** (**322**). For compound **76** (**245**), the hypothesis includes one hydrogen bond acceptor, one hydrogen bond donor, one hydrophobic feature, and three aromatic ring features, corresponding to the ADDHRRR feature pattern. Pharmacophore features represent the structural attributes of ligands involved in receptor binding; however, they do not always pinpoint the specific interactions that are critical for ligand–protein recognition. The compound series investigated shares common structural features, including a carboxylic acid- or bioisostere-substituted phenylpyrazolidinone core, a heteroaromatic ring, and a 2-substituted aromatic ring. Systematic SAR studies based on our rational design strategy were employed to evaluate their impact on Ku and DNA-PK inhibitory activity. Compounds exhibiting better activity consistently aligned with the full pharmacophore model, particularly matching the hydrogen bond donor or acceptor, hydrophobic, and aromatic features critical for anchoring to the Ku70/80 binding interface. Less active analogs lacked proper alignment with these features, indicating their importance for molecular recognition. This misalignment likely reduced their ability to engage essential residues in the Ku70/80 interface, resulting in diminished inhibitory activity. Together, the SAR and pharmacophore analyses highlight the essential role of hydrogen bond donors/acceptors, a hydrophobic moiety, and an aromatic scaffold for Ku

Table 2 *In silico* OPERA-predicted physicochemical and ADME-related properties of lead compounds

Physiochemical and ADME properties	35 (68)	53 (149)	61 (322)	76 (245)	Recommended range
MolWeight	555.97	557.14	611.11	581.16	100 to 1000 Da
TopoPolSurfAir	121.44	121.44	121.44	138.6	<140 Å^2 (ideal < 90 Å^2)
LogP_pred	3.08	2.98	3.51	1.42	1 to 3.5
LogWS_pred	−6.61	−6.64	−4.76	−5.0	$>−4.0$, ideally $>−2.0$
pKa_a_pred	5.01	6.43	6.63	9.02	~3.5 to 7.5
LogD55_pred	2.47	2.93	3.48	1.42	~1 to 3.5
LogD74_pred	0.69	1.97	2.67	1.41	~1.0 to 3.5
CACO$_2$_pred	−4.86	−4.86	−6.36	−6.11	$>−5.0 \log$ (cm s^{-1})
LogKM_pred	0.09	0.13	0.16	−0.31	$>−2.0$
BioDeg_LogHalfLife_pred	0.87	0.87	0.87	1.57	<1.0
Clint_pred	15.52	32.62	3.69	9.16	<30 μL min^{-1} mg^{-1} (ideal <10)
Overall drug likeness score and ranking	0.564	0.591	0.740	0.192	—
	Rank 3	Rank 2	Rank 1	Rank 4	

inhibition. These insights will guide further optimization of potency and selectivity in this chemical series.

2.6 *In silico* prediction of physicochemical and drug-likeness properties of lead Ku-DBi's

To evaluate the physicochemical and drug-likeness of lead Ku-DBi's, we used the OPERA (Open (Quantitative) Structure–Activity/Property Relationship App) suite of QSAR models.[47,48] The OPERA models are built on curated experimental data and provide validated predictions for a broad range of molecular descriptors relevant to drug discovery. SMILES representations of lead compounds 35 (68), 53 (149), 61 (322), and 76 (245) were used as input to predict key physicochemical and ADME-related properties (Table 2). The predicted molecular weight (MolWeight) and topological polar surface area (TopoPolSurfAir) were within the acceptable range for drug-like molecules, indicating favorable size and polarity consistent with drug-likeness. Predicted LogP_pred and LogD74_pred values indicated a well-balanced lipophilicity profile at both neutral and physiological pH. While LogWS_pred values predicted low aqueous solubility across the series, this aligns with the solubility challenges observed during our biological studies. The predicted acid dissociation constants (pKa_a_pred) were within the optimal range for compounds 35 (68), 53 (149), and 61 (322), indicating partial ionization of acidic functional groups at physiological pH. In contrast, compound 76 (245) exhibited a less favorable pK_a. Additionally, LogD55_pred values helped characterize lipophilicity under mildly acidic conditions, which may be relevant in tumor microenvironments. Predicted Caco-2 permeability (CACO2_pred) values suggested good intestinal permeability for compounds 35 (68) and 53 (149), but poor permeability for 61 (322) and 76 (245). In terms of metabolic and environmental stability, the LogKM_pred and Clint_pred values indicated favorable metabolic turnover, while BioDeg_LogHalfLife_pred values pointed to moderate to high biodegradability, supporting the environmental acceptability of these compounds. Among the series, compound 61 (322) demonstrated the most favorable

combination of physicochemical and drug-likeness properties. These findings, combined with insights from SAR analysis and pharmacophore modeling, support the continued development of this series as a promising platform for potent and drug-like Ku–DNA binding inhibitors.

Overall, we identified compounds 35 (68), 53 (149), 61 (322), and 76 (245) as our lead compounds through extensive SAR studies as they specifically block Ku–DNA binding interactions and inhibit DNA-PK kinase activity. Earlier, we reported that these Ku-DBi's have a high specificity against a series of protein kinases, inhibit *in vitro* NHEJ, and cellular NHEJ, and potentiate the cellular activity of radiomimetic agents and IR.[27] We also showed the utility of our lead compound, 76 (245), in a CRISPR gene-editing model by inhibiting NHEJ and activating homologous recombination to increase the efficiency of gene insertion. Very recently, we demonstrated that our lead compound, 76 (245), potentiates the cellular effects of bleomycin and IR through p53 phosphorylation, mediated by the activation of the ATM pathway.[31] Our Ku-DBi's impact DSB repair and DDR signaling through a novel mechanism of action and thus represent a promising anticancer therapeutic strategy in combination with DNA DSB-inducing agents.

2.7 Biophysical analysis

Earlier, we showed that our lead compound, 76 (245), directly interacts with the Ku70/80 protein through a gel-based thermal-shift assay (TSA).[27] We further quantitatively assessed the interactions between the Ku protein and our four lead Ku-DBi's by microscale thermophoresis (MST) and nano Differential Scanning Fluorometry (nanoDSF) analysis.[32,49]

2.7.1 Microscale thermophoresis (MST). In an effort to identify a direct interaction between our Ku-DBi's and Ku70–Ku80 protein, we assessed the interaction between Ku70–Ku80 protein and Ku-DBi's 35 (68), 53 (149), 61 (322), and 76 (245) by microscale thermophoresis-based approach, which quantify the direct interaction between our compounds and Ku in 10 min and the results are presented in Fig. 4. We
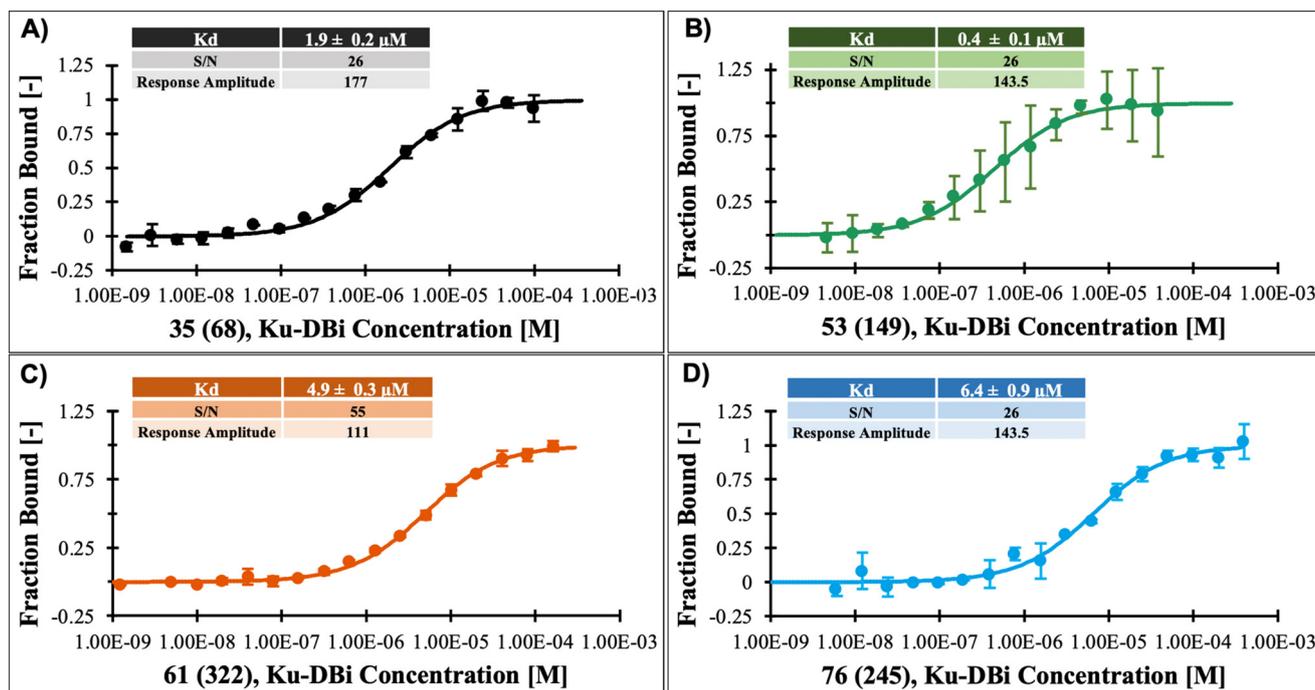
Fig. 4 Interaction between Ku-DBi's A) **35** (**68**), B) **53** (**149**), C) **61** (**322**) and D) **76** (**245**) with Ku70–Ku80 measured by MST (Microscale Thermophoresis). The estimated bound fraction is plotted as a function of Ku-DBi's concentration. Error bars represent standard deviation (SD); $n = 2$.

identified that our Ku-DBi's interact more strongly with Ku, with Kd values ranging from 0.4 to 6.4 μM, consistent with the IC_{50} values obtained from the EMSA analysis. We assessed the ligand-induced fluorescence-change specificity using the SDS-denaturation test (SD-test) (Fig. S4). Fig. S4 shows the thermophoretic property of the fluorescently labeled Ku proteins in the presence or absence of Ku-DBi. Since the ligand-induced fluorescence changes exceeded ±20% of the average, we conducted the SD-test to assess their specificity. This assessment is used to distinguish between direct protein interactions and non-specific effects, such as protein loss, aggregation, adsorption, or spectral interference. The MST signal is clearly attributed to a specific binding phenomenon, as shown in Fig. S4.

2.7.2 nano Differential Scanning Fluorometry (nanoDSF). We also assessed the interaction between our Ku-DBi's and Ku70–Ku80 protein by nano Differential Scanning Fluorimetry (nanoDSF) to determine protein thermal stability and aggregation with or without our Ku-DBi's. NanoDSF utilizes the intrinsic fluorescence of aromatic residues of the protein and avoids the possible competition of an inhibitor with the dye used in classical TSA. The data presented in Fig. 5 demonstrates that concentration-dependent induction of a shift in thermal stability with compound **53** (**149**). In the presence of our Ku-DBi's, the thermal stability of the protein was changed by 2 °C, and the aggregation temperature by 4 °C at 25 μM. The impact of our other Ku-DBi's, **35** (**68**) and **76** (**245**), on the thermostability and aggregation propensity of Ku70–Ku80

are presented in Fig. S5 and S6. These data reveal that our Ku-DBi's directly interact with Ku and are consistent with our previous data with the compound **76** (**245**), in which a gel-based thermal shift assay was used to conclude direct Ku-DBi–Ku interactions.[33]

3. Conclusion

Several DNA-PK inhibitors are currently in preclinical and clinical trials. The therapeutic window and potential for drug resistance with DNA-PK inhibitors remain a concern, as demonstrated by many other kinase targets, which have an active site mutation that abrogates inhibitor binding affinity. Targeting early critical events of the NHEJ pathway and DDR by utilizing Ku-DBi is a potential strategy to overcome the resistance phenomenon associated with DNA-PK inhibitors. To develop potent and effective Ku-DBi's, we designed, synthesized, and evaluated a series of 4-substituted phenylpyrazolidinone derivatives. Consequently, a total of 38 novel compounds were synthesized and evaluated for their ability to inhibit Ku–DNA interactions and DNA-PK activity. As anticipated, the extensive SAR analysis enhanced the inhibitory potency of Ku and the DNA-PK inhibitory activity of several compounds. The substitutions on ring A and C are critical in maintaining these inhibitors' Ku potency and DNA-PK activity. We also explored biosisosteric replacements of the carboxylic acid and methyl group, which proved to be an effective strategy to improve potency, suggesting that these Ku-DBi's are promising candidates for further optimization.
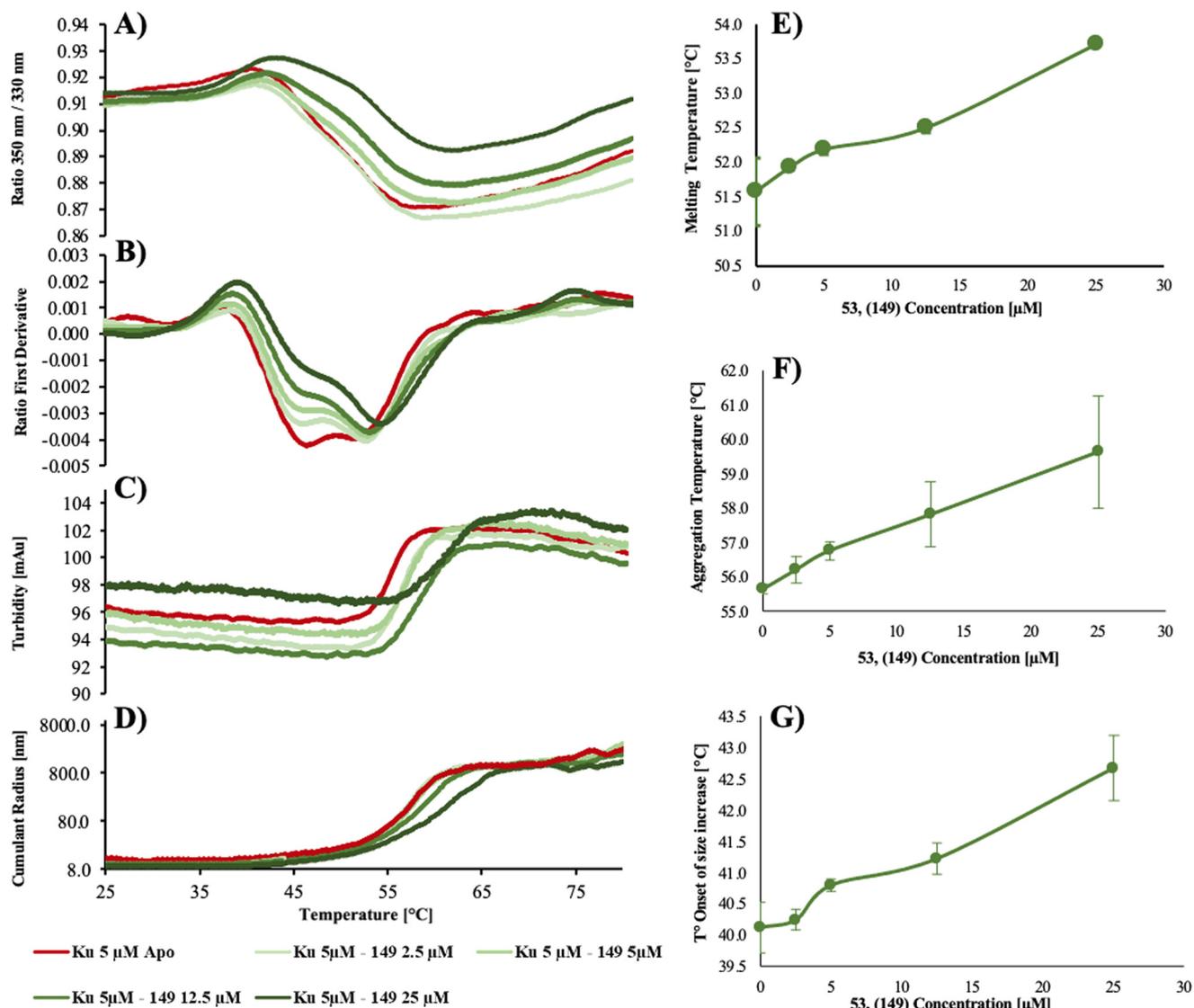

Fig. 5 Impact of Ku-DBi, **53** (**149**) on the thermostability and aggregation propensity of Ku70–80. A) Ratio of intrinsic fluorescence at 350 nm divided by 330 nm, B) first derivative of the ratio, C) turbidity measurement, D) cumulant radius measured by DLS as a function of temperature, E) plot of second melting temperature (Tm) of Ku70/80 as a function of ligand concentration, F) aggregation temperature (Tagg) determined from turbidity measurement as a function of ligand concentration, G) onset temperature of size increase measured by DLS as function of ligand concentration. Error bars represent standard deviation (SD); $n = 2$.

The lead compounds were also demonstrated to bind with high affinities to the Ku70–Ku80 protein as measured by MST and nanoDSF assays, indicating their target engagement. The Ku-DBi developed in this report could represent the potential to develop more potent and drug-like inhibitors as anticancer therapeutics in combination with DNA DSB-inducing agents.

4. Experimental section

4.1 General

All chemicals used for synthesis were purchased from Aldrich, Alfa Aesar, Acros, Fisher Scientific, AK Scientific and Combi-Blocks Chemical Co. (USA) and used without further purification. Anhydrous solvents were obtained from Fisher Scientific or Aldrich and used directly. All reactions involving air- or moisture-sensitive reagents were performed under a nitrogen atmosphere. ^{1}H NMR spectra were recorded at 300 MHz, 400 MHz and 500 MHz using Bruker AV NMR spectrometer. ^{13}C NMR spectra were recorded at 75 MHz, 101 MHz and 125 MHz using Bruker AV NMR spectrometer. The chemical shifts were reported as δ ppm relative to TMS, using the residual solvent peak as the reference unless otherwise noted. All coupling constants (J) are given in hertz. Data are reported as follows: chemical shift, multiplicity (s = singlet, d = doublet, t = triplet, q = quartet, br = broad, m = multiplet), number of protons and coupling constants. Thin layer chromatography was performed using Merck silica gel 60

F-254 thin layer plates, which were developed using one of the following techniques: UV fluorescence (254 nm), alkaline potassium permanganate solution (0.5% w/v) or ninhydrin (0.2% w/v) and iodine vapors. Automated flash column chromatography was carried out on prepacked silica cartridges using the indicated solvent system on Biotage Isolera chromatography system. Target compounds 35–63, 67–70 and 74–76 were crystallized in ethanol, solid was collected, washed with EtOAc and then hot solutions of 20–30% EtOAc in hexanes to afford red to orange solids. If necessary, the products were purified with automated flash column chromatography. The chemical purity of target compounds was ≥95% determined by HPLC coupled to electrospray ionization mass spectrometry (LC/ESI-MS) analysis. LC-MS analyses and compounds purity data were obtained using an Agilent 6130 Quadrupole LC-MS connected to an Agilent 1200 HPLC system and both instruments were connected to an Agilent diode array detector. A C-18 reversed phase column (Vydac monomeric/Phenomenex/Kinetex 2.6 μM XB-C18, 50 × 4.6 mm) was used as stationary phase, water and methanol/acetonitrile (both containing 0.1 to 0.25% TFA) was used as mobile phase (gradient: 0–100% methanol, flow 0.8 mL min^{-1}, run time 15 min), and UV absorbance at the fixed wavelength of 254 nm and positive and negative ESI-MS data were recorded. The retention time and corresponding ESI-MS data were used as an identity of molecules. HRMS data were obtained using Waters/Macromass LCT electrospray ionization (ESI) on a time of flight (TOF) mass spectrometer at the Mass Spectrometry Facility at Indiana University Chemistry Department (http://msf.chem.indiana.edu).

4.2 General procedure for the synthesis of target compounds 35–63, 67–70 and 74–76

Synthesis of 3-(3-methyl-5-oxo-4,5-dihydro-1H-pyrazol-1-yl)benzoic acid (4a). Ethyl acetoacetate 2 (0.25 mL, 1.2 equiv.) was added to a solution of 3-hydrazinobenzoic acid 1a (250 mg, 1 equiv.) in glacial acetic acid (4 mL) under an argon atmosphere. After addition, the reaction mixture was heated at reflux with stirring for 12 h. Once the reaction was allowed to cool to room temperature, the reaction mixture was concentrated *in vacuo* resulting in the formation of a precipitate. The solid was filtered and washed with 5% MeOH in DCM (two times) and then two times with DCM to obtain 4a as an off-white solid (262 mg, 73% yield, requires no further purification). TLC: 4% MeOH in DCM, R_f = 0.42; visualized with UV. ^{1}H NMR (500 MHz, DMSO-d$_6$): δ 13.22 (brs, 1H, COOH), 8.36 (s, 1H), 8.05 (d, 1H, J = 8.5 Hz), 7.94 (d, 1H, J = 8.0 Hz), 7.70 (t, 1H, J = 8.0 and 16 Hz), 5.97 (s, 1H), 2.45 (s, 3H, CH$_3$). ^{13}C NMR (125 MHz, DMSO-d$_6$): δ 166.48, 158.79, 154.09, 150.10, 144.90, 136.81, 132.15, 129.96, 127.57, 124.16, 120.66, 104.64, 102.19, 19.12, 14.25. HRMS (ESI): calcd for C$_{11}$H$_{11}$N$_2$O$_3$ [M + H]$^+$ m/z = 219.0770, found 219.0768.

Synthesis of 4-(3-methyl-5-oxo-4,5-dihydro-1H-pyrazol-1-yl)benzoic acid (4b). 4b was prepared by an above-described procedure using 4-hydrazinobenzoic acid hydrochloride 1b (400 mg) as a starting material. Off-white solid (352 mg, 76% yield, requires no further purification). TLC: 4% MeOH in DCM, R_f = 0.42; visualized with UV. ^{1}H NMR (300 MHz, DMSO-d$_6$): δ 12.87 (brs, 1H, COOH), 7.98 (d, 2H, J = 8.8 Hz), 7.88 (d, 2H, J = 8.4 Hz), 5.38 (s, 1H), 2.12 (s, 3H, CH$_3$). ^{13}C NMR (75 MHz, DMSO-d$_6$) δ 172.17, 170.56, 167.32, 159.86, 150.25, 142.66, 142.06, 130.80, 126.86, 126.46, 119.33, 117.49, 117.34, 43.61, 14.45. HRMS (ESI): calcd for C$_{11}$H$_9$N$_2$O$_3$ [M–H]$^-$ m/z = 217.0613, found 217.0619.

Synthesis of 3-(5-oxo-3-(trifluoromethyl)-4,5-dihydro-1H-pyrazol-1-yl)benzoic acid (4c). Compound 4c was prepared by an above-described procedure using 3-hydrazinobenzoic acid 1a (250 mg, 1 equiv.) and ethyl 4,4,4-trifluoroacetoacetate 3 (0.288 mL, 1.2 equiv.) as starting materials. Light brown color solid (348 mg, 78% yield, requires no further purification). TLC: 4% MeOH in DCM, R_f = 0.46; visualized with UV. ^{1}H NMR (300 MHz, DMSO-d$_6$): δ 13.03 (brs, 1H, COOH), 8.30 (s, 1H), 8.03 (d, 1H, J = 8.13 Hz), 7.94 (d, 1H, J = 7.74 Hz), 7.66–7.61 (t, 1H, J = 7.95 and 15.87 Hz), 5.96 (s, 1H). ^{13}C NMR (75 MHz, DMSO-d$_6$): δ 167.06, 154.56, 138.44, 132.23, 130.09, 128.15, 126.35, 122.72, 86.27. MS (ESI) m/z = 271.1 [M–H]$^-$.

Synthesis of ethyl 3-(3-methyl-5-oxo-4,5-dihydro-1H-pyrazol-1-yl)benzoate (5a). To a stirred suspension of 3-(3-methyl-5-oxo-4,5-dihydro-1H-pyrazol-1-yl)benzoic acid 4a (250 mg) in anhydrous ethanol (4 mL) was added a catalytic amount of concentrated sulfuric acid (0.3 mL) slowly under an argon atmosphere. The reaction mixture was refluxed for 12 h, and then it was allowed to cool to room temperature. The solvent was removed under vacuum, and the obtained residue was dissolved in ethyl acetate and washed successively with saturated NaHCO$_3$ (2 × 10 mL), water, and brine solution. The organic layer was dried over Na$_2$SO$_4$ and concentrated under reduced pressure. The crude residue was purified by Biotage automated flash column chromatography using 0–50% EtOAc in hexanes as the eluent to furnish ethyl 3-(3-methyl-5-oxo-4,5-dihydro-1H-pyrazol-1-yl)benzoate 5a as a red oil (214 mg, 76% yield). TLC: 45% EtOAc in hexanes, R_f = 0.44; visualized with UV. ^{1}H NMR (300 MHz, CDCl$_3$): δ 8.41 (s, 1H), 8.05 (d, 1H, J = 8.2 Hz), 7.78 (d, 1H, J = 8.0 Hz), 7.38 (t, 1H, J = 7.95 and 15.99 Hz), 4.35–4.28 (q, 2H, OCH$_2$), 3.37 (s, 2H, CH$_2$), 2.11 (s, 3H, CH$_3$), 1.33 (t, 3H, J = 7.11 and 14.25 Hz, CH$_3$). ^{13}C NMR (75 MHz, CDCl$_3$): δ 170.70, 166.14, 156.84, 138.18, 131.22, 128.82, 125.77, 122.69, 119.46, 61.10, 43.02, 16.93, 14.29. MS (ESI) m/z = 247.1 [M + H]$^+$.

Synthesis of ethyl 4-(3-methyl-5-oxo-4,5-dihydro-1H-pyrazol-1-yl)benzoate (5b). Compound 5b was prepared by an above-described procedure using 4b (250 mg) as a starting material. White solid (225 mg, 80% yield). TLC: 40% EtOAc in hexanes, R_f = 0.44; visualized with UV. ^{1}H NMR (300 MHz, CDCl$_3$): δ 8.05 (d, 2H, J = 8.97 Hz), 8.01 (d, 2H, J = 8.94 Hz), 4.40–4.33 (q, 2H, OCH$_2$), 3.46 (s, 2H, CH$_2$), 2.22 (s, 3H, CH$_3$), 1.39 (t, 3H, J = 7.11 and 14.25 Hz, CH$_3$). ^{13}C NMR (75 MHz, CDCl$_3$): δ 170.78, 166.18, 156.89, 141.69,

130.54, 126.42, 117.61, 60.90, 43.17, 17.09, 14.36. MS (ESI) m/z = 247.1 [M + H]$^+$.

Synthesis of ethyl 3-(5-oxo-3-(trifluoromethyl)-4,5-dihydro-1H-pyrazol-1-yl)benzoate (5c). Compound **5c** was prepared by an above-described procedure using **4c** (300 mg) as a starting material. Off-white solid (268 mg, 81% yield). TLC: 50% EtOAc in hexanes, R_f = 0.48; visualized with UV. ^{1}H NMR (300 MHz, CDCl$_3$): δ 10.26 (brs, 1H, OH), 8.49 (s, 1H), 8.03–7.99 (m, 2H), 7.57–7.52 (t, 1H, J = 8.01 and 15.99 Hz), 5.87 (s, 1H), 4.53–4.45 (q, 2H, OCH$_2$), 1.47 (t, 3H, J = 7.14 and 14.28 Hz, CH$_3$). ^{13}C NMR (75 MHz, CDCl$_3$): δ 167.90, 152.81, 138.30, 130.37, 129.52, 128.23, 127.38, 122.76, 86.75, 62.41, 14.29. MS (ESI) m/z = 301.1 [M + H]$^+$.

Synthesis of 2-chloro-5-(5-formylfuran-2-yl)benzoic acid (8a). A solution of K$_2$CO$_3$ (1.18 g, 3 equiv.) in water (5 mL) was added to a mixture of 5-bromo-2-furaldehyde **6a** (500 mg, 1 equiv.) and 4-chloro-3-carboxyphenylboronic acid **7** (687 mg, 1.2 equiv.) in toluene/ethanol (1 : 1, v/v, 25 mL). The mixture was degassed with argon for 5 min, and then Pd(PPh$_3$)$_4$ (165 mg, 0.05 equiv.) was added. The reaction mixture was stirred at 90 °C for 15 h. The reaction mixture was cooled to room temperature, filtered through Celite, and washed with water (2 × 10 mL). The pH of the solution was adjusted to 1–2 by addition of 6 N HCl solution. The precipitated reaction mixture was extracted with dichloromethane (3 × 50 mL); the combined organic fractions were washed with brine, dried over anhydrous Na$_2$SO$_4$, and concentrated under reduced pressure. The crude product was triturated with 20–30% EtOAc in hexanes (2 times), and solid was filtered to afford 2-chloro-5-(5-formylfuran-2-yl)benzoic acid **8a** (637 mg, 89% yield) as an off-white solid. TLC: 60% EtOAc in hexanes, R_f = 0.40; visualized with UV and KMnO$_4$ solution. ^{1}H NMR (300 MHz, DMSO-d$_6$): δ 13.74 (brs, 1H, COOH), 9.63 (s, 1H, CHO), 8.23 (d, 1H, J = 2.22 Hz), 8.01 (dd, 1H, J = 2.28 and 8.43 Hz), 7.70 (d, 1H, J = 8.34 Hz), 7.67 (d, 1H, J = 2.85 Hz), 7.45 (d, 1H, J = 3.75 Hz). ^{13}C NMR (75 MHz, DMSO-d$_6$): δ 178.64, 166.63, 156.44, 152.47, 132.93, 132.78, 132.13, 129.00, 128.10, 127.23, 110.56. MS (ESI) m/z = 249.0 [M–H]$^-$.

Synthesis of 2-chloro-5-(5-formylthiophen-2-yl)benzoic acid (8b). Compound **8b** was prepared by an above-described procedure using 5-bromothiophene-2-carbaldehyde **6b** (250 mg, 1 equiv.) and 4-chloro-3-carboxyphenylboronic acid **7** (1.2 equiv.) as starting materials. Yellow solid (271 mg, 78% yield). TLC: 60% EtOAC in hexane, R_f = 0.44; visualized with UV. ^{1}H NMR (300 MHz, DMSO-d$_6$): δ 13.63 (brs, 1H, COOH), 9.94 (s, 1H, CHO), 8.14 (d, J = 3.54 Hz, 1H), 8.07 (d, J = 3.93 Hz, 1H), 7.94 (dd, J = 9.04, 2.75 Hz, 1H), 7.86 (d, J = 3.93 Hz, 1H), 7.66 (d, J = 8.25 Hz, 1H). ^{13}C NMR (75 MHz, DMSO-d$_6$): δ 184.7, 166.6, 150.3, 143.2, 139.6, 133.0, 132.6, 132.0, 131.9, 130.2, 128.2, 126.9. MS (ESI) m/z = 266.1 [M–H]$^-$.

Synthesis of 2-chloro-5-(5-formyl-1H-pyrrol-2-yl)benzoic acid (8c). Compound **8c** was prepared by an above-described procedure for the preparation of compound **8a** using 5-bromo-1H-pyrrole-2-carbaldehyde **6c** (250 mg, 1 equiv.) and 4-chloro-3-carboxyphenylboronic acid **7** (1.2 equiv.) as starting

materials. Light yellow solid (429 mg, 60% yield). TLC: 10% EtOAC in hexane, R_f = 0.2; visualized with UV. ^{1}H NMR (400 MHz, DMSO-d$_6$): δ 13.52 (brs, 1H, COOH), 12.61 (s, 1H, NH), 9.52 (s, 1H, CHO), 8.31 (s, 1H), 8.02 (d, J = 8.44 Hz, 1H), 7.58 (d, J = 8.48 Hz, 1H), 7.07 (s, 1H), 6.88 (s, 1H). MS (ESI) m/z = 249.1 [M–H]$^-$.

Synthesis of (Z)-2-chloro-5-(5-((1-(3-(ethoxycarbonyl)phenyl)-3-methyl-5-oxo-1H-pyrazol-4(5H)ylidene)methyl)furan-2-yl)benzoic acid (9). Ethyl 3-(3-methyl-5-oxo-4,5-dihydro-1H-pyrazol-1-yl)benzoate **5a** (200 mg, 1 equiv.) and 2-chloro-5-(5-formylfuran-2-yl)benzoic acid **8a** (203 g, 1 equiv.) were dissolved in glacial acetic acid (10 mL). The reaction mixture was heated at reflux with stirring for 3 h. Solvent was removed in vacuo, and solid was suspended in EtOH, filtered, washed with EtOH, EtOAc, and DCM (2 times each) to obtain **9** as a red solid (311 mg, 80% yield, requires no further purification). TLC: 5% MeOH in DCM, R_f = 0.45; visualized with UV. Major Z-isomer data: ^{1}H NMR (300 MHz, DMSO-d$_6$) δ 13.75 (brs, 1H, COOH), 8.63 (d, 1H, J = 3.87 Hz), 8.48 (t, 1H, J = 1.86 and 3.69 Hz), 8.27 (d, 1H, J = 2.22 Hz), 8.19 (d, 1H, J = 7.08 Hz), 8.01 (dd, 1H, J = 2.22 and 8.43 Hz), 7.76–7.64 (m, 3H), 7.56–7.51 (m, 2H), 4.36–4.29 (q, 2H, OCH$_2$), 2.64 (s, 0.29H, minor isomer, CH$_3$), 2.32 (s, 2.71H, major isomer, CH$_3$), 1.33 (t, 3H, J = 7.08 and 14.16 Hz, CH$_3$). ^{13}C NMR (75 MHz, DMSO-d$_6$): δ 166.59, 165.88, 162.11, 157.65, 151.64, 150.82, 138.96, 133.15, 132.67, 131.11, 130.91, 130.08, 129.77, 128.96, 127.84, 127.26, 125.17, 122.41, 121.60, 118.43, 112.91, 61.38, 14.65, 13.29. MS (ESI) m/z = 477.1 [M–H]$^-$.

Synthesis of (Z)-2-chloro-5-(5-((1-(3-(ethoxycarbonyl)phenyl)-3-methyl-5-oxo-1,5-dihydro-4H-pyrazol-4-ylidene)methyl)thiophen-2-yl)benzoic acid (10). Compound **10** was prepared by an above-described procedure for the preparation of compound **9** using **5a** (250 mg, 1 equiv.) and **8b** (1 equiv.) as starting materials. Red solid (382 mg, 86% yield). TLC: 5% MeOH in DCM, R_f = 0.48; visualized with UV. Single Z-isomer data: ^{1}H NMR (300 MHz, DMSO-d$_6$): δ 12.87 (brs, 1H), 8.41 (brs 1H), 8.18 (d, J = 9.07 Hz, 1H), 8.09–8.03 (m, 2H), 7.96 (s, 2H), 7.87 (dd, J = 8.59 and 2.39 Hz, 1H), 7.75 (d, J = 4.29 Hz, 1H), 7.69 (d, J = 6.68 Hz, 1H), 7.56–7.47 (m, 2H), 4.32 (q, J = 7.28 Hz, 2H, OCH$_2$), 2.26 (s, 3H, CH$_3$, single Z isomer), 1.33 (t, J = 7.28 Hz, 3H, CH$_3$). ^{13}C NMR (75 MHz, DMSO-d$_6$): δ 172.5, 166.5, 165.9, 162.3, 153.3, 151.5, 144.6, 138.8, 138.2, 136.6, 132.8, 132.4, 132.1, 130.8, 130.1, 129.6, 128.3, 126.3, 125.0, 122.2, 121.1, 118.2, 61.3, 21.5, 14.6. MS (ESI) m/z = 494.1 [M–H]$^-$.

Synthesis of (Z)-2-chloro-5-(5-((1-(4-(ethoxycarbonyl)phenyl)-3-methyl-5-oxo-1,5-dihydro-4H-pyrazol-4-ylidene)methyl)furan-2-yl)benzoic acid (11). Compound **11** was prepared by an above-described procedure using **5b** (200 mg, 1 equiv.) and **8a** (202 mg, 1 equiv.) as starting materials. Red solid (294 mg, 87% yield). TLC: 5% MeOH in DCM, R_f = 0.48; visualized with UV. Major Z-isomer data: ^{1}H NMR (300 MHz, DMSO-d$_6$) δ 13.72 (brs, 1H, COOH), 8.62 (d, 1H, J = 3.84 Hz), 8.33 (d, 1H, J = 2.19 Hz), 8.15–7.90 (m, 5H), 7.79 (s, 1H), 7.71 (d, 1H, J = 8.49 Hz), 7.58 (d, 1H, J = 3.84 Hz), 4.33–4.26 (q, 2H, OCH$_2$), 2.68 (s, 0.51H, minor isomer, CH$_3$), 2.34 (s,

2.49H, major isomer, CH_3), 1.32 (t, 3H, J = 7.11 and 14.19 Hz, CH_3). ^{13}C NMR (75 MHz, DMSO-d$_6$): δ 166.60, 165.69, 162.41, 157.81, 152.26, 150.83, 142.42, 133.23, 132.70, 132.18, 130.71, 129.03, 127.87, 127.35, 125.42, 121.39, 117.39, 112.97, 61.01, 14.67, 13.35. MS (ESI) m/z = 477.1 [M–H]$^-$.

Synthesis of (Z)-2-chloro-5-(5-((1-(4-(ethoxycarbonyl)phenyl)-3-methyl-5-oxo-1,5-dihydro-4H-pyrazol-4-ylidene)methyl)thiophen-2-yl)benzoic acid (12). Compound **12** was prepared by an above-described procedure for the preparation of compound **9** using **5b** (250 mg, 1 equiv.) and **8b** (1 equiv.) as starting materials. Red solid (84% yield). TLC: 5% MeOH in DCM, R_f = 0.52; visualized with UV. Single Z-isomer data: ^{1}H NMR (300 MHz, DMSO-d$_6$) δ ^{1}H NMR (300 MHz, DMSO-d$_6$): δ 13.75 (brs, 1H), 8.17–8.16 (m, 3H), 8.14–8.10 (m, 2H), 8.03–7.97 (m, 3H), 7.90 (d, J = 4.0 Hz, 1H), 7.66 (d, J = 8.44 Hz, 1H), 4.31 (q, J = 5.23 Hz, 2H, OCH_2), 2.35 (s, 3H, CH_3, single Z isomer), 1.32 (t, 3H, J = 7.09 and 14.15 Hz, CH_3). ^{13}C NMR (75 MHz, DMSO-d$_6$): δ 166.6, 165.7, 162.8, 153.6, 152.4, 145.1, 142.3, 138.9, 136.6, 132.9, 132.8, 132.2, 132.1, 130.8, 130.2, 128.4, 126.7, 125.4, 121.0, 117.3, 61.0, 14.7, 13.3. MS (ESI) m/z = 494.1 [M–H]$^-$.

Synthesis of (Z)-2-chloro-5-(5-((1-(3-(ethoxycarbonyl)phenyl)-5-oxo-3-(trifluoromethyl)-1,5-dihydro-4H-pyrazol-4-ylidene)methyl)furan-2-yl)benzoic acid (13). Compound **13** was prepared by an above-described procedure for the preparation of compound **9** using **5c** (250 mg, 1 equiv.) and **8a** (208 mg, 1 equiv.) as starting materials. Red solid (397 mg, 88% yield). TLC: 5% MeOH in DCM, R_f = 0.5; visualized with UV. Major Z-isomer data: ^{1}H NMR (300 MHz, DMSO-d$_6$): δ 13.73 (brs, 1H, COOH), 8.73 (s, 1H), 8.40 (d, 2H, J = 19.05 Hz), 8.11 (t, 2H, J = 9 and 17.7 Hz), 7.82 (d, 1H, J = 7.77 Hz), 7.74 (s, 1H), 7.69–7.57 (m, 3H), 4.36–4.29 (q, 2H, OCH_2), 1.36 (t, 3H, J = 7.08 and 14.19 Hz, CH_3). ^{13}C NMR (75 MHz, DMSO-d$_6$): δ 166.56, 165.58, 161.24, 160.38, 150.71, 138.10, 133.99, 132.98, 131.73, 131.08, 130.02, 129.46, 127.88, 127.29, 126.76, 123.83, 119.75, 114.40, 114.08, 61.52, 14.60. MS (ESI) m/z = 531.1 [M–H]$^-$.

Synthesis of (Z)-2-chloro-5-(5-((1-(3-(ethoxycarbonyl)phenyl)-3-methyl-5-oxo-1,5-dihydro-4H-pyrazol-4-ylidene)methyl)-1H-pyrrol-2-yl)benzoic acid (14). Compound **14** was prepared by an above-described procedure for the preparation of compound **9** using **5a** (200 mg, 1 equiv.) and **8c** (203 mg, 1 equiv.) as starting materials. Red solid (362 mg, 58% yield). TLC: 10% MeOH in DCM, R_f = 0.3; visualized with UV. Single Z-isomer data: ^{1}H NMR (300 MHz, DMSO-d$_6$): δ 14.4 (s, 1H, NH), 13.8 (brs, 1H), 8.51 (s, 1H), 8.36–8.29 (m, 1H), 8.16–7.99 (m, 1H), 7.72–7.89 (m, 3H), 7.70–7.56 (m, 2H), 7.31 (brs, 1H), 7.23–7.16 (m, 1H), 4.36 (q, 2H, OCH_2), 2.32 (s, 1H, CH_3, single Z isomer), 1.91 (s, 1H), 1.35 (t, 3H, J = 7.12 Hz). ^{13}C NMR (75 MHz, DMSO-d$_6$): δ 171.9, 166.6, 166.5, 165.3, 163.6, 151.7, 140.2, 138.5, 136.8, 134.3, 134.0, 133.06, 131.9, 131.5, 131.4, 131.1, 130.5, 130.0, 129.3, 128.5, 128.4, 127.4, 126.6, 125.1, 122.9, 119.0, 116.1, 113.2, 60.9, 55.9, 21.0, 18.5, 14.14, 12.67. MS (ESI) m/z = 477.1 [M–H]$^-$.

Synthesis of (Z)-5-(5-((1-(3-carboxyphenyl)-3-methyl-5-oxo-1,5-dihydro-4H-pyrazol-4-ylidene)methyl)thiophen-2-yl)-2-chlorobenzoic acid (15). To a stirred suspension of compound **10** (150 mg) in THF : MeOH (2 : 1, v/v, 10 mL) was added 2 N NaOH (1 mL) solution. The reaction mixture was stirred at room temperature for 6 h. Solvent was removed in vacuo and residue was acidified to pH 2–3 using 20% citric acid solution. The product was extracted with EtOAc (3 × 15 mL). The combined organic extracts were washed with brine, dried over Na$_2$SO$_4$ and concentrated under reduced pressure. The product was crystallized in EtOAc and triturated with 30% EtOAc in hexanes to afford **15** (120 mg, 85% yield) as an orange solid. Single Z isomer data: ^{1}H NMR (300 MHz, DMSO-d$_6$): δ 13.29 (brs, 2H, 2COOH), 8.33 (s, 1H), 8.20–8.01 (m, 2H), 7.89 (d, J = 1.59 Hz, 1H), 7.82–7.76 (m, 1H), 7.73–7.69 (m, 1H), 7.60–7.42 (m, 3H), 6.79 (d, J = 2.35 Hz, 1H), 2.36 (s, 3H, CH_3, single Z isomer). ^{13}C NMR (75 MHz, DMSO-d$_6$): δ 167.5, 167.2, 166.8, 147.1, 139.4, 133.4, 132.4, 132.0, 131.7, 130.2, 129.9, 129.0, 126.8, 126.3, 125.1, 124.6, 121.1, 30.1. MS (ESI) m/z = 466.0 [M–H]$^-$.

Synthesis of (Z)-5-(5-((1-(3-carboxyphenyl)-5-oxo-3-(trifluoromethyl)-1,5-dihydro-4H-pyrazol-4-ylidene)methyl)furan-2-yl)-2-chlorobenzoic acid (16). Acid **16** was prepared by an above-described procedure using **13** (100 mg) as starting material. Red solid (74 mg, 78% yield). Major Z isomer data: ^{1}H NMR (300 MHz, DMSO-d$_6$): δ 13.44 (brs, 2H, 2COOH), 8.73 (s, 1H), 8.38 (s, 1H), 8.29 (s, 1H), 8.06–8.02 (t, 2H, J = 7.05 and 13.5 Hz), 7.81 (d, 1H, J = 7.65 Hz), 7.72 (s, 1H), 7.66–7.53 (m, 3H). ^{13}C NMR (75 MHz, DMSO-d$_6$): δ 167.18, 166.52, 161.19, 160.32, 150.69, 139.93, 139.44, 138.00, 133.98, 132.88, 132.02, 130.38, 129.80, 129.42, 127.88, 127.24, 126.93, 123.43, 122.04, 120.03, 118.45, 114.42, 114.03. MS (ESI) m/z = 504.0 [M–H]$^-$.

General synthesis of amides 17–34

(Z)-Ethyl 3-(4-((5-(4-chloro-3-((3-methoxyphenyl)carbamoyl)phenyl)furan-2-yl)methylene)-3-methyl-5-oxo-4,5-dihydro-1H-pyrazol-1-yl)benzoate (17). To a solution of compound **9** (300 mg, 1 equiv.) in dry DMF (6 mL) were added EDCI·HCl (180 mg, 1.5 equiv.), HOBt (127 mg 1.5 equiv.), and DIPEA (0.16 mL, 1.5 equiv.), and the mixture was stirred for 30 min at room temperature under an argon atmosphere. m-Anisidine (73 μL, 1.05 equiv.) and DIPEA (0.16 mL, 1.5 equiv.) were added to the reaction mixture. The reaction mixture was stirred at room temperature for 18 h. The reaction mixture was poured into water and extracted with EtOAc (3 × 20 mL). The combined organic extracts were washed with saturated NaHCO$_3$ (2 × 10 mL), brine, dried over Na$_2$SO$_4$, and concentrated under reduced pressure. The product was purified by flash chromatography and triturated with mixture of EtOAc in hexanes (2–3 times) to afford **17** (267 mg, 73% yield) as a red solid. TLC: 3% MeOH in EtOAc, R_f = 0.47; visualized with UV. Major Z-isomer data: ^{1}H NMR (300 MHz, DMSO-d$_6$): δ 10.64 (s, 1H, CONH), 8.65 (d, 1H, J = 3.81 Hz), 8.52 (t, 1H, J = 1.83 and 3.63 Hz), 8.22–8.14 (m, 2H), 8.06 (dd, 1H, J = 2.16 and 8.46 Hz), 7.81–7.70 (m, 3H), 7.64–7.53 (m, 2H), 7.43 (s, 1H), 7.29–7.27 (m, 2H), 6.74–6.70 (m, 1H), 4.37–

4.30 (q, 2H, OCH$_2$), 3.75 (s, 3H, OCH$_3$), 2.70 (s, 0.58H; minor isomer, CH$_3$), 2.33 (s, 2.42H; major isomer, CH$_3$), 1.33 (t, 3H, J = 7.11 and 14.19 Hz, CH$_3$). ^{13}C NMR (75 MHz, DMSO-d$_6$): δ 165.91, 164.69, 162.20, 160.01, 157.96, 151.75, 150.82, 140.40, 139.00, 138.22, 131.78, 131.52, 131.21, 130.66, 127.96, 125.69, 125.28, 121.63, 118.58, 112.32, 109.89, 105.83, 61.42, 55.51, 14.66, 13.30. MS (ESI) m/z = 584.1 [M + H]$^+$. HRMS (ESI): calcd for C$_{32}$H$_{26}$N$_3$O$_6$Cl [M]$^+$ m/z = 583.1510, found 583.1520, HPLC purity: 96.56%.

Compounds **18–34** were synthesized using the above synthetic procedure described for the preparation of amide **17** using appropriate starting materials. Each compound was purified by flash chromatography and triturated with the mixture of EtOAc in hexanes (2–3 times) to afford the desired compound.

Ethyl (Z)-3-(4-((5-(4-chloro-3-((3,4-dimethoxyphenyl)carbamoyl)phenyl)furan-2-yl)methylene)-3-methyl-5-oxo-4,5-dihydro-1H-pyrazol-1-yl)benzoate (18). Compound **9** (180 mg, 1 equiv.) and 3,4-dimethoxyphenyl amine (1.05 equiv.) used as starting materials. Red solid (261 mg, 68% yield). TLC: 3% MeOH in EtOAc, R$_f$ = 0.54; visualized with UV. Major Z-isomer data: 1H NMR (300 MHz, DMSO-d$_6$): δ 10.52 (s, 1H, CONH), 8.67 (d, 1H, J = 3.72 Hz), 8.56–8.50 (m, 1H), 8.27–8.14 (m, 2H), 8.06–7.94 (m, 1H), 7.82–7.73 (m, 3H), 7.64–7.54 (m, 2H), 7.48–7.44 (m, 1H), 7.29–7.26 (dd, 1H, J = 2.16 and 8.67 Hz), 6.97–6.94 (d, 1H, J = 8.82 Hz), 4.38–4.31 (q, 2H, OCH$_2$), 3.75 (s, 6H, diOCH$_3$), 2.72 (s, 0.59H; minor isomer, CH$_3$), 2.34 (s, 2.41H; major isomer, CH$_3$), 1.34 (t, 3H, J = 7.08 and 14.16 Hz, CH$_3$); ^{13}C NMR (75 MHz, DMSO-d$_6$): δ 165.92, 164.21, 162.21, 158.01, 151.75, 150.81, 150.35, 149.00, 148.71, 145.79, 138.01, 138.83, 138.36, 138.22, 132.85, 131.84, 131.59, 131.19, 131.01, 130.18, 129.88, 128.01, 127.92, 127.38, 127.05, 125.72, 125.28, 122.59, 121.60, 118.58, 118.32, 112.93, 112.44, 111.97, 104.97, 61.43, 56.17, 55.84, 55.38, 14.66, 13.30. MS (ESI) m/z = 614.1 [M + H]$^+$; HRMS (ESI): calcd for C$_{33}$H$_{29}$N$_3$O$_7$Cl [M + H]$^+$ m/z = 614.1694, found 614.1696, HPLC purity: 95.23%.

Ethyl (Z)-3-(4-((5-(3-(benzylcarbamoyl)-4-chlorophenyl)furan-2-yl)methylene)-3-methyl-5-oxo-4,5-dihydro-1H-pyrazol-1-yl)benzoate (19). Compound **9** (215 mg, 1 equiv.) and benzyl amine (1.05 equiv.) used as starting materials. Red solid (78% yield). TLC: 3% MeOH in DCM, R$_f$ = 0.49; visualized with UV. Major Z-isomer data: ^{1}H NMR (300 MHz, DMSO-d$_6$): δ 9.17–9.06 (m, 1H), 8.55–8.52 (m, 1H), 8.27–8.20 (m, 1H), 8.03–7.92 (m, 1H), 7.81–7.75 (m, 1H), 7.70–7.68 (m, 1H), 7.64–7.58 (m, 2H), 7.47–7.22 (m, 7H), 4.51–4.44 (m, 2H, NHCH$_2$), 4.38–4.29 (q, 2H, OCH$_2$), 2.66 (s, 0.38H; minor isomer, CH$_3$), 2.35 (s, 2.62H; major isomer, CH$_3$), 1.34 (t, J = 7.09 Hz, 3H, CH$_3$). ^{13}C NMR (75 MHz, DMSO-d$_6$): δ 166.6, 166.29, 166.24, 165.9, 162.2, 158.1, 154.9, 151.8, 150.0, 149.2, 146.8, 141.3, 138.1, 137.7, 131.5, 130.6, 128.8, 127.7, 119.6, 118.6, 112.8, 100.2, 61.4, 61.1, 49.0, 14.6, 13.4. MS (ESI) m/z = 568.1 [M + H]$^+$, HPLC purity: 97.11%.

Ethyl (Z)-3-(4-((5-(4-chloro-3-((2-chlorobenzyl)carbamoyl)phenyl)furan-2-yl)methylene)-3-methyl-5-oxo-4,5-dihydro-1H-pyrazol-1-yl)benzoate (20). Compound **9** (260 mg, 1 equiv.) and 2-chlorobenzyl amine (1.05 equiv.) used as starting

materials. Red solid (69% yield). TLC: 3% MeOH in DCM, R$_f$ = 0.43; visualized with UV. Major Z-isomer data: ^{1}H NMR (300 MHz, DMSO-d$_6$): δ 9.13 (t, J = 6.04 Hz, 1H), 8.66 (d, J = 4.26 Hz, 1H), 8.55–8.51 (m, 1H), 8.23–8.20 (m, 1H), 8.08–8.00 (m, 2H), 7.82–7.69 (m, 3H), 7.63–7.47 (m, 4H), 7.41–7.29 (m, 2H), 4.56 (d, J = 6.41 Hz, 2H, NHCH$_2$), 4.34 (q, J = 7.69 Hz, 2H, OCH$_2$), 2.69 (s, 0.66H; minor isomer, CH$_3$), 2.35 (s, 2.34H; major isomer, CH$_3$),1.34 (t, J = 7.27 Hz, 3H, CH$_3$). ^{13}C NMR (75 MHz, DMSO-d$_6$): δ 166.4, 165.9, 162.2, 158.0, 151.7, 150.0, 139.0, 138.0, 136.1, 132.5, 131.5, 131.1, 131.0, 130.2, 129.9, 129.6, 129.4, 127.7, 125.6, 122.6, 121.5, 118.6, 112.9, 61.4, 14.6, 13.3. MS (ESI) m/z = 602.1 [M + H]$^+$, HPLC purity: 98.03%.

Ethyl (Z)-3-(4-((5-(4-chloro-3-((cyclohexylmethyl)carbamoyl)phenyl)furan-2-yl)methylene)-3-methyl-5-oxo-4,5-dihydro-1H-pyrazol-1-yl)benzoate (21). Compound **9** (200 mg, 1 equiv.) and cyclohexylmethyl amine (1.05 equiv.) used as starting materials. Red solid (81% yield). TLC: 3% MeOH in DCM, R$_f$ = 0.51; visualized with UV. Major Z-isomer data: ^{1}H NMR (300 MHz, DMSO-d$_6$): δ 8.65 (d, J = 3.79 Hz, 1H), 8.60–8.52 (m, 2H), 8.24–8.20 (m, 1H), 8.01–7.92 (m, 2H), 7.83–7.76 (m, 2H), 7.70–7.64 (m, 1H), 7.62–7.56 (m, 2H), 4.35 (q, J = 7.06 Hz, 2H, OCH$_2$), 3.11 (t, J = 8.07 Hz, 2H), 2.72 (s, 0.63H; minor isomer, CH$_3$), 2.35 (s, 2.37H; major isomer, CH$_3$),1.79–1.63 (m, 5H), 1.34 (t, J = 7.06 Hz, 3H, CH$_3$), 1.18–1.10 (m, 2H), 1.00–0.89 (m, 2H). ^{13}C NMR (75 MHz, DMSO-d$_6$): δ 166.1, 162.2, 158.1, 151.8, 150.7, 139.0, 131.4, 131.0, 130.2, 129.9, 127.7, 127.0, 125.3, 122.6, 121.5, 118.6, 112.8, 61.4, 45.8, 37.8, 30.9, 26.5, 25.8, 14.6, 13.3. MS (ESI) m/z = 574.1 [M + H]$^+$, HPLC purity: 95.42%.

Ethyl (Z)-3-(4-((5-(4-chloro-3-((3-methoxyphenyl)carbamoyl)phenyl)thiophen-2-yl)methylene)-3-methyl-5-oxo-4,5-dihydro-1H-pyrazol-1-yl)benzoate (22). Compound **10** (200 mg, 1 equiv.) and m-anisidine (1.05 equiv.) used as starting materials. Red solid (75% yield). TLC: 3% MeOH in EtOAc, R$_f$ = 0.49; visualized with UV. Single Z isomer data: ^{1}H NMR (300 MHz, DMSO-d$_6$): δ 10.68 (s, 1H, CONH), 8.21–8.19 (d, 2H), 8.16–8.13 (d, 2H), 8.08–7.98 (m, 3H), 7.96–7.91 (m, 2H), 7.71 (d, J = 8.84 Hz, 1H), 7.47–7.41 (m, 1H), 7.30–7.28 (m, 2H), 6.93–6.70 (m, 1H), 4.32 (q, J = 6.71 Hz, 2H, OCH$_2$), 3.78 (s, 3H, OCH$_3$), 2.38 (s, 3H, CH$_3$, single Z isomer), 1.33 (t, J = 5.61 Hz, 3H, CH$_3$). MS (ESI) m/z = 600.1 [M + H]$^+$, HPLC purity: 96.67%.

Ethyl (Z)-4-(4-((5-(4-chloro-3-((3-methoxyphenyl)carbamoyl)phenyl)thiophen-2-yl)methylene)-3-methyl-5-oxo-4,5-dihydro-1H-pyrazol-1-yl)benzoate (23). Compound **12** (200 mg, 1 equiv.) and m-anisidine (1.05 equiv.) used as starting materials. Red solid (73% yield). TLC: 3% MeOH in DCM, R$_f$ = 0.52; visualized with UV. Single Z-isomer data: ^{1}H NMR (300 MHz, DMSO-d$_6$): δ 10.64 (s, 1H, CONH), 8.19–8.18 (m, 2H), 8.13–8.10 (m, 2H), 8.06–8.0 (m, 3H), 7.94–7.93 (m, 2H), 7.69 (d, J = 8.81 Hz, 1H), 7.45–7.44 (m, 1H), 7.29–7.27 (m, 2H), 6.94–6.70 (m, 1H), 4.30 (q, J = 6.62 Hz, 2H, OCH$_2$), 3.76 (s, 3H, OCH$_3$), 2.35 (s, 3H, CH$_3$, single Z isomer), 1.31 (t, J = 5.51 Hz, 3H, CH$_3$). ^{13}C NMR (75 MHz, DMSO-d$_6$): δ 165.7, 164.6, 162.8, 160.0, 158.5, 154.0, 152.0, 145.1, 142.3, 140.4,

138.9, 138.2, 136.6, 132.2, 131.3, 130.8, 130.1, 128.9, 126.7, 125.4, 121.0, 118.2, 117.3, 112.3, 109.9, 107.2, 105.8, 101.8, 99.7, 61.0, 55.5, 14.7, 13.3. MS (ESI) m/z = 600.1 [M + H]$^+$, HPLC purity: 98.46%.

Ethyl (Z)-3-(4-((5-(4-chloro-3-((cyclopropylmethyl) carbamoyl)phenyl)thiophen-2-yl)methylene)-3-methyl-5-oxo-4,5-dihydro-1H-pyrazol-1-yl)benzoate (24). Compound **10** (220 mg, 1 equiv.) and cyclopropylmethyl amine (1.05 equiv.) used as starting materials. Red solid (79% yield). TLC: 3% MeOH in DCM, R_f = 0.49; visualized with UV. Single Z-isomer data: ^{1}H NMR (300 MHz, DMSO-d$_6$) δ 8.59–8.54 (m, 1H), 8.41 (s, 1H), 8.08–8.05 (d, 1H, J = 10.53 Hz), 7.79–7.75 (d, 2H, J = 10.09 Hz), 7.60–7.49 (m, 3H), 7.42–7.39 (m, 2H), 6.74 (s, 1H), 4.21–4.17 (q, 2H, OCH$_2$), 3.12–3.09 (m, 2H, NHCH$_2$), 2.32 (s, 3H, CH$_3$, single Z isomer), 1.32 (t, 3H, J = 7.4 and 14.5 Hz, CH$_3$), 0.99–0.96 (m, 1H, CH), 0.40–0.37 (m, 2H, CH$_2$), 0.21–0.18 (m, 2H, CH$_2$). MS (ESI) m/z = 548.1 [M + H]$^+$, HPLC purity: 95.01%.

Ethyl (Z)-3-(4-((5-(4-chloro-3-((4-fluorobenzyl)carbamoyl) phenyl)thiophen-2-yl)methylene)-3-methyl-5-oxo-4,5-dihydro-1H-pyrazol-1-yl)benzoate (25). Compound **10** (180 mg, 1 equiv.) and 4-fluorobenzyl amine (1.05 equiv.) used as starting materials. Red solid (78% yield). TLC: 3% MeOH in DCM, R_f = 0.49; visualized with UV. Single Z-isomer data: ^{1}H NMR (300 MHz, DMSO-d$_6$) δ 9.13 (t, J = 6.33 Hz, 1H), 8.09–7.96 (m, 3H), 7.96–7.91 (m, 3H), 7.72 (d, J = 8.10 Hz, 1H), 7.62–7.59 (m, 2H), 7.4–7.39 (m, 3H), 7.19–7.15 (m, 2H), 4.49 (d, J = 6.39 Hz, 2H, NHCH$_2$), 4.31 (q, J = 6.8 Hz, 2H, OCH$_2$), 2.34 (s, 3H, CH$_3$, single Z isomer), 1.32 (t, J = 5.61 Hz, 3H, CH$_3$). MS (ESI) m/z = 602.1 [M + H]$^+$, HPLC purity: 95.01%.

Ethyl (Z)-3-(4-((5-(4-chloro-3-((3-methoxyphenyl)carbamoyl) phenyl)-1H-pyrrol-2-yl)methylene)-3-methyl-5-oxo-4,5-dihydro-1H-pyrazol-1-yl)benzoate (26). Compound **14** (230 mg, 1 equiv.) and m-anisidine (1.05 equiv.) used as starting materials. Red solid (198 mg, 65% yield). TLC: 5% MeOH in DCM, R_f = 0.47; visualized with UV. Single Z-isomer data: ^{1}H NMR (400 MHz, DMSO-d$_6$): δ 14.5 (brs, 1H, NH), 10.63 (s, 1H), 8.54 (s, 1H), 8.30 (d, 1H, J = 8.12 Hz), 8.14–7.98 (m, 1H), 7.94–7.71 (m, 4H), 7.63–7.52 (m, 1H), 7.49–7.16 (m, 5H), 6.80–6.63 (m, 1H), 4.33 (q, 2H, OCH$_2$), 3.83–3.63 (m, 3H), 2.34 (s, 3H, CH$_3$, single Z isomer), 1.33 (t, 3H, J = 7.12 Hz, CH$_3$). ^{13}C NMR (101 MHz, DMSO-d_6): δ 165.3, 164.4, 164.2, 163.6, 159.9, 159.4, 151.7, 140.2, 140.0, 139.9, 138.5, 137.8, 137.3, 136.9, 134.1, 131.9, 130.8, 130.5, 130.3, 130.2, 129.8, 129.5, 129.4, 129.3, 128.9, 128.7, 127.9, 127.0, 126.5, 125.4, 125.1, 122.9, 119.0, 116.1, 113.4, 111.8, 109.3, 109.2, 105.3, 60.8, 54.9, 54.8, 14.0, 12.6. MS (ESI) m/z = 583.1 [M + H]$^+$, HPLC purity: 95.73%.

Ethyl (Z)-3-(4-((5-(4-chloro-3-((3-(trifluoromethoxy)phenyl) carbamoyl)phenyl)-1H-pyrrol-2-yl)methylene)-3-methyl-5-oxo-4,5-dihydro-1H-pyrazol-1-yl)benzoate (27). Compound **14** (190 mg, 1 equiv.) and 3-(trifluoromethoxy)aniline (1.05 equiv.) used as starting materials. Red solid (306 mg, 68% yield). TLC: 5% MeOH in DCM, R_f = 0.5; visualized with UV. Single Z-isomer data: ^{1}H NMR (400 MHz, DMSO-d$_6$): δ 14.49 (brs, 1H, NH), 11.0 (s, 1H), 8.64–8.44 (m, 1H), 8.38–8.21 (m, 1H),

8.13 (s, 1H), 8.04–7.86 (m, 2H), 7.86–7.45 (m, 6H), 7.31 (s, 1H), 7.21–7.02 (m, 1H), 4.45–4.18 (q, 2H, OCH$_2$), 2.34 (s, 3H, CH$_3$, single Z isomer), 1.47–1.19 (t, 3H, J = 7.10 Hz, CH$_3$). ^{13}C NMR (101 MHz, DMSO-d$_6$): δ 165.38, 165.33, 164.6, 163.6, 151.8, 148.4, 140.3, 140.1, 138.5, 138.3, 137.3, 131.9, 130.9, 130.6, 130.5, 130.3, 129.3, 128.8, 126.6, 125.6, 125.2, 123.0, 119.0, 118.2, 116.2, 116.0, 60.8, 54.8, 14.14, 14.0, 12.6. MS (ESI) m/z = 637.1 [M + H]$^+$, HPLC purity: 95.32%.

Ethyl (Z)-4-(4-((5-(4-chloro-3-((3-methoxyphenyl)carbamoyl) phenyl)furan-2-yl)methylene)-3-methyl-5-oxo-4,5-dihydro-1H-pyrazol-1-yl)benzoate (28). Compound **11** (225 mg, 1 equiv.) and m-anisidine (1.05 equiv.) used as starting materials. Dark Red solid (272 mg, 67% yield). TLC: 3% MeOH in EtOAc, R_f = 0.49; visualized with UV. Major Z-isomer data: ^{1}H NMR (300 MHz, DMSO-d$_6$): δ 10.66 (s, 1H, CONH), 8.60 (d, 1H, J = 3.0 Hz), 8.20 (d, 1H, J = 1.5 Hz), 8.14–7.94 (m, 5H), 7.82–7.73 (m, 2H), 7.63–7.54 (m, 1H), 7.45–7.39 (m/brs, 1H), 7.29–7.23 (m, 2H), 6.74–6.69 (m, 1H), 4.32–4.26 (q, 2H, OCH$_2$), 3.75 (s, 3H, OCH$_3$), 2.70 (s, 0.72H; minor isomer, CH$_3$), 2.32 (s, 2.31H; major isomer, CH$_3$), 1.32 (t, 3H, J = 7.05 and 14.04 Hz, CH$_3$). ^{13}C NMR (75 MHz, DMSO-d$_6$): δ 165.70, 164.69, 162.43, 160.01, 158.07, 152.30, 150.79, 150.44, 142.44, 140.41, 138.20, 131.58, 131.22, 130.74, 130.16, 129.06, 127.92, 125.76, 125.46, 121.36, 117.42, 112.97, 112.31, 109.89, 105.82, 61.04, 55.51, 55.38, 54.95, 14.69, 13.34. MS (ESI) m/z = 584.1 [M + H]$^+$; HRMS (ESI): calcd for $C_{30}H_{21}N_3O_6Cl$ [M–H]$^-$ m/z = 584.1588, found 584.1596, HPLC purity: 98.07%.

Ethyl (Z)-4-(4-((5-(4-chloro-3-((3-methoxybenzyl)carbamoyl) phenyl)furan-2-yl)methylene)-3-methyl-5-oxo-4,5-dihydro-1H-pyrazol-1-yl)benzoate (29). Compound **11** (195 mg, 1 equiv.) and 3-methoxybenzyl amine (1.05 equiv.) used as starting materials. Red solid (81% yield). TLC: 3% MeOH in DCM, R_f = 0.49; visualized with UV. Major Z-isomer data: ^{1}H NMR (300 MHz, DMSO-d$_6$): δ 9.16 (t, J = 7.92 and 8.08 Hz, 1H), 8.64 (s, 1H), 8.13–8.08 (t, J = 11.96 and 7.36 Hz, 2H), 8.04–7.92 (m, 4H), 7.79 (s, 1H), 7.71–7.68 (d, J = 11.12 Hz, 1H), 7.62–7.59 (m, 1H), 7.30–7.24 (m, 1H), 6.97–6.96 (m, 2H), 6.85–6.82 (m, 1H), 4.49 (d, J = 7.88 Hz, 2H, NHCH$_2$), 4.47–4.27 (q, 2H, OCH$_2$), 3.75 (s, 3H, OCH$_3$), 2.67 (s, 0.74H; minor isomer, CH$_3$), 2.35 (s, 2.26H; major isomer, CH$_3$), 1.34 (t, 3H, J = 7.08 and 14.16 Hz, CH$_3$); ^{13}C NMR (75 MHz, DMSO-d$_6$): δ 166.23, 166.11, 165.72, 165.31, 162.48, 159.78, 158.19, 152.35, 150.79, 150.31, 142.45, 140.99, 140.93, 138.29, 138.11, 131.83, 131.17, 130.78, 130.36, 128.20, 127.82, 127.37, 125.54, 121.33, 119.88, 119.62, 117.49, 117.28, 113.39, 112.93, 112.76, 61.05, 55.44, 42.96, 4.69, 13.36. MS (ESI) m/z = 598.1 [M + H]$^+$, HPLC purity: 96.81%.

Ethyl (Z)-4-(4-((5-(3-(benzylcarbamoyl)-4-chlorophenyl) furan-2-yl)methylene)-3-methyl-5-oxo-4,5-dihydro-1H-pyrazol-1-yl)benzoate (30). Compound **11** (170 mg, 1 equiv.) and benzyl amine (1.05 equiv.) used as starting materials. Red solid (72% yield). TLC: 3% MeOH in DCM, R_f = 0.48; visualized with UV. Major Z-isomer data: ^{1}H NMR (300 MHz, DMSO-d$_6$): δ 9.15 (t, J = 6.40 Hz, 1H), 8.62 (d, J = 3.94 Hz, 1H), 8.15–8.06 (m, 2H), 8.04–7.97 (m, 3H), 7.81–7.77 (m, 1H), 7.68 (d, J = 8.81 Hz, 1H), 7.61–7.57 (m, 1H), 7.42–7.24 (m,

4H), 4.50 (d, J = 6.42 Hz, 2H, NHCH_2), 4.30 (q, J = 5.62 Hz, 2H, OCH_2), 2.65 (s, 0.50H; minor isomer, CH_3), 2.34 (s, 2.50H; major isomer, CH_3), 1.35 (t, J = 8.06 Hz, 3H, CH_3). ^{13}C NMR (75 MHz, DMSO-d$_6$): δ 166.2, 165.7, 162.4, 158.6, 158.1, 152.3, 150.7, 149.1, 142.4, 139.3, 138.0, 131.6, 130.7, 130.3, 128.8, 127.7, 127.3, 125.5, 121.2, 117.4, 112.9, 61.0, 43.0, 14.6, 13.4. MS (ESI) m/z = 568.1 [M + H]$^+$, HPLC purity: 96.11%.

Ethyl **(*Z*)-4-(4-((5-(4-chloro-3-((pyridin-3-ylmethyl)carbamoyl)phenyl)furan-2-yl)methylene)-3-methyl-5-oxo-4,5-dihydro-1*H*-pyrazol-1-yl)benzoate (31).** Compound **11** (170 mg, 1 equiv.) and pyridin-3-ylmethanamine (1.05 equiv.) used as starting materials. Red solid (82% yield). TLC: 3% MeOH in DCM, R_f = 0.52; visualized with UV. Major *Z*-isomer data: ^{1}H NMR (300 MHz, DMSO-d$_6$): δ 9.30 (t, J = 6.0 Hz, 1H), 8.62 (s, 1H), 8.49 (dd, J = 1.54, 3.48 Hz, 1H), 8.15–7.99 (m, 5H), 7.92–7.89 (m, 1H), 7.84–7.76 (m, 2H), 7.70–7.67 (m, 1H), 7.63–7.60 (m, 1H), 7.42–7.37 (m, 1H), 4.52 (d, J = 5.38 Hz, 2H, NHCH_2), 4.29 (q, J = 6.65 Hz, 2H, OCH_2), 2.66 (s, 0.41H; minor isomer, CH_3), 2.34 (s, 2.59H; major isomer, CH_3), 1.31 (t, J = 7.64 Hz, 3H, CH_3). ^{13}C NMR (75 MHz, DMSO-d$_6$): δ 166.7, 159.3, 149.9, 149.3, 145.5, 136.1, 131.0, 124.7, 119.0, 101.2, 61.5, 15.4, 14.2. MS (ESI) m/z = 569.1 [M + H]$^+$, HPLC purity: 95.37%.

Ethyl (*Z*)-3-(4-((5-(4-chloro-3-((3-methoxyphenyl)carbamoyl)phenyl)furan-2-yl)methylene)-5-oxo-3-(trifluoromethyl)-4,5-dihydro-1*H*-pyrazol-1-yl)benzoate (32). Compound **13** (180 mg, 1 equiv.) and *m*-anisidine (1.05 equiv.) used as starting materials. Red solid (269 mg, 75% yield). TLC: 3% MeOH in DCM, R_f = 0.52; visualized with UV. Major *Z*-isomer: ^{1}H NMR (300 MHz, DMSO-d$_6$) δ 10.53 (brs, 1H, CONH), 8.48 (t, 1H, J = 1.83 and 3.66 Hz), 8.22–8.19 (d, 2H, J = 7.55 Hz), 7.84–7.80 (d, 2H, J = 7.77 Hz), 7.75 (d, 1H, J = 1.95 Hz), 7.66–7.52 (m, 3H), 7.40 (brs, 1H), 7.28–7.23 (m, 2H), 7.03 (d, 1H, J = 3.33 Hz), 6.71–6.67 (m, 1H), 4.38–4.30 (q, 2H, OCH_2), 3.74 (s, 3H, OCH_3), 1.34 (t, 3H, J = 7.11 and 14.19 Hz, CH_3). ^{13}C NMR (75 MHz, DMSO-d$_6$): δ 165.83, 165.07, 159.97, 158.76, 157.58, 155.94, 150.10, 140.48, 139.86, 137.78, 130.94, 130.78, 129.80, 126.56, 125.51, 124.37, 121.30, 112.32, 109.83, 105.81, 98.53, 61.46, 55.46, 14.64. MS (ESI) m/z = 638.1 [M + H]$^+$. HRMS (ESI): calcd for C$_{32}$H$_{23}$F$_3$N$_3$O$_6$ClNa [M + Na]$^+$ m/z = 660.1125, found 660.1128, HPLC purity: 98.04%.

Ethyl (*Z*)-3-(4-((5-(4-chloro-3-((cyclopropylmethyl)carbamoyl)phenyl)furan-2-yl)methylene)-5-oxo-3-(trifluoromethyl)-4,5-dihydro-1*H*-pyrazol-1-yl)benzoate (33). Compound **13** (140 mg, 1 equiv.) and cyclopropylmethyl amine (1.05 equiv.) used as starting materials. Brown solid (86% yield). TLC: 3% MeOH in DCM, R_f = 0.46; visualized with UV. Major *Z*-isomer data: ^{1}H NMR (300 MHz, DMSO-d$_6$): 8.78–8.73 (t, J = 5.80 Hz and 11.12, 1H), 8.67 (s, 1H), 8.45–8.41 (m, 1H), 8.10–8.06 (m, 3H), 7.83–7.79 (m, 1H), 7.71–7.56 (m, 4H), 4.28–4.23 (q, 2H, OCH_2), 3.20–3.15 (m, 2H, NHCH_2), 1.31 (t, 3H, J = 7.3 and 14.12 Hz, CH_3). 1.01–0.98 (m, 1H, CH), 0.42–0.38 (m, 2H, CH_2), 0.22–0.18 (m, 2H, CH_2). MS (ESI) m/z = 586.1 [M + H]$^+$, HPLC purity: 97.23%.

Ethyl (*Z*)-3-(4-((5-(4-chloro-3-((4-fluorobenzyl)carbamoyl)phenyl)furan-2-yl)methylene)-5-oxo-3-(trifluoromethyl)-4,5-

dihydro-1*H*-pyrazol-1-yl)benzoate (34). Compound **13** (140 mg, 1 equiv.) and 4-fluorobenzyl amine (1.05 equiv.) used as starting materials. Red solid (84% yield). TLC: 3% MeOH in DCM, R_f = 0.49; visualized with UV. Major *Z*-isomer data: ^{1}H NMR (300 MHz, DMSO-d$_6$): δ 9.07 (t, J = 5.55 Hz, 1H), 8.75 (s, 1H), 8.46–8.41 (m, 1H), 8.11–8.08 (m, 3H), 7.82–7.84 (m, 2H), 7.75–7.68 (m, 2H), 7.58 (t, J = 7.05 Hz, 1H), 7.41–7.37 (m, 2H), 7.21–7.17 (m, 2H), 4.43 (d, J = 6.38 Hz, 2H, NHCH_2). MS (ESI) m/z = 640.1 [M + H]$^+$, HPLC purity: 96.89%.

General synthesis of target compounds 35–52

Synthesis of (*Z*)-3-(4-((5-(4-chloro-3-((3-methoxyphenyl)carbamoyl)phenyl)furan-2-yl)methylene)-3-methyl-5-oxo-4,5-dihydro-1*H*-pyrazol-1-yl)benzoic acid (35/68). To a stirred suspension of ester **17** (250 mg, 1 equiv.) in THF/EtOH/H$_2$O (4 : 2 : 1, 7 mL) was added LiOH (117 mg, 10 equiv.). The reaction mixture was stirred at room temperature for 12 h. Solvent was removed *in vacuo*, and residue was acidified to pH 2–3 using 20% citric acid solution. The product was extracted with EtOAc (3 × 20 mL). The combined organic extracts were washed with brine, dried over Na$_2$SO$_4$, and concentrated under reduced pressure. The product was crystallized in 5% EtOH in EtOAc, and solid was collected, washed with EtOAc and then hot solutions of 20–30% EtOAc in hexanes to afford target compound **35** (164 mg, 69% yield) as a red solid. Major *Z*-isomer data: ^{1}H NMR (300 MHz, DMSO-d$_6$): δ 13.13 (brs, 1H, COOH), 10.66 (s, 1H, CONH), 8.69 (d, 1H, J = 3.16 Hz), 8.55 (t, 1H, J = 1.95 and 3.5 Hz), 8.31–8.19 (m, 2H), 8.08–7.97 (m, 1H), 7.80–7.70 (m, 3H), 7.65–7.55 (m, 2H), 7.43 (s, 1H), 7.29–7.28 (m, 2H), 6.74–6.71 (m, 1H), 3.76 (s, 3H, OCH_3), 2.73 (s, 0.69H; minor isomer, CH_3), 2.34 (s, 2.31H; major isomer, CH_3). ^{13}C NMR (101 MHz, DMSO-d$_6$): δ 166.98, 164.17, 161.71, 159.52, 158.88, 157.42, 151.14, 150.34, 149.89, 139.89, 138.42, 137.73, 131.44, 131.02, 130.71, 129.62, 129.17, 127.47, 127.38, 126.95, 125.19, 124.97, 121.78, 121.23, 118.47, 112.41, 111.85, 109.40, 105.37, 52.02, 12.77. MS (ESI) m/z = 554.1 [M–H]$^-$. HRMS (ESI): calcd for C$_{30}$H$_{21}$N$_3$O$_6$Cl [M–H]$^-$ m/z = 554.1119, found 554.1122. HPLC purity: 97.72%.

Target Compounds **36–52** were synthesized by the synthetic procedure described above for the preparation of compound **35** using appropriate starting materials. Each compound was crystallized in EtOH, solid was collected, washed with EtOAc and then hot solutions of 20–30% EtOAc in hexanes to afford the desired final compound. If necessary, the products were purified using 2–5% MeOH in DCM (1% AcOH in DCM) solvent system on automated flash column chromatography.

(*Z*)-3-(4-((5-(4-Chloro-3-((3,4-dimethoxyphenyl)carbamoyl)phenyl)furan-2-yl)methylene)-3-methyl-5-oxo-4,5-dihydro-1*H*-pyrazol-1-yl)benzoic acid (36). Compound **18** (120 mg, 1 equiv.) used as starting material. Red solid (67% yield). Major *Z*-isomer data: ^{1}H NMR (300 MHz, DMSO-d$_6$): δ 13.14 (brs, 1H, COOH), 10.52 (s, 1H, CONH), 8.70 (d, 1H, J = 3.75 Hz), 8.56–8.51 (m, 1H), 8.28–8.15 (m, 2H), 8.08–7.95 (m, 1H),

7.80–7.74 (m, 3H), 7.65–7.55 (m, 2H), 7.47–7.43 (m, 1H), 7.30–7.27 (m, 1H), 6.97–6.94 (m, 1H), 3.75 and 3.74 (s, 6H, diOCH$_3$), 2.74 (s, 0.49H; minor isomer, CH$_3$), 2.35 (s, 2.50H; major isomer, CH$_3$). ^{13}C NMR (75 MHz, DMSO-d$_6$): δ 167.51, 164.22, 164.69, 162.22, 157.99, 151.70, 150.84, 149.00, 145.79, 138.93, 138.37, 131.93, 131.58, 130.46, 129.74, 127.94, 127.39, 125.73, 125.43, 122.30, 121.71, 118.96, 112.44, 111.98, 104.97, 105.83, 56.17, 55.84, 13.3. MS (ESI) m/z = 584.1 [M–H]$^-$; HRMS (ESI): calcd for C$_{31}$H$_{23}$N$_3$O$_7$Cl [M–H]$^-$ m/z = 584.1225, found 584.1229. HPLC purity: 95.07%.

(Z)-3-(4-((5-(3-(Benzylcarbamoyl)-4-chlorophenyl)furan-2-yl)methylene)-3-methyl-5-oxo-4,5-dihydro-1H-pyrazol-1-yl)benzoic acid (37). Compound **19** (130 mg, 1 equiv.) used as starting material. Red solid (79% yield). Major Z-isomer data: ^{1}H NMR (300 MHz, DMSO-d$_6$): δ 13.17 (brs, 1H, COOH), 9.07–9.03 (m, 1H), 8.33 (s, 1H), 8.03 (d, J = 8.75 Hz, 1H), 7.80–7.77 (m, 2H), 7.69–7.58 (m, 2H), 7.55–7.47 (m, 2H), 7.36–7.24 (m, 6H), 4.45–4.43 (m, 2H, NHCH$_2$), 2.70 (s, 0.67H; minor isomer, CH$_3$), 2.35 (s, 2.33H; major isomer, CH$_3$). ^{13}C NMR (75 MHz, DMSO-d$_6$): δ 167.3, 166.6, 150.3, 147.1, 139.4, 137.8, 131.9, 130.6, 129.7, 129.1, 128.7, 127.6, 127.3, 124.6, 123.3, 121.0, 108.6, 55.3, 13.3. MS (ESI) m/z = 539.1 [M–H]$^-$, HPLC purity: 97.02%.

(Z)-3-(4-((5-(4-Chloro-3-((2-chlorobenzyl)carbamoyl)phenyl)furan-2-yl)methylene)-3-methyl-5-oxo-4,5-dihydro-1H-pyrazol-1-yl)benzoic acid (38). Compound **20** (100 mg, 1 equiv.) used as starting material. Red solid (67% yield). Major Z-isomer data: ^{1}H NMR (300 MHz, DMSO-d$_6$): δ 13.14 (brs, 1H, COOH), 9.12–9.09 (m, 1H), 8.32 (s, 1H), 8.02 (d, J = 8.31 Hz, 1H), 8.03–8.02 (m, 1H), 7.92–7.78 (m, 2H), 7.70–7.62 (m, 2H), 7.59–7.47 (m, 4H), 7.41–7.33 (m, 3H), 7.06–6.99 (m, 1H), 4.51 (s, 2H, NHCH$_2$), 2.71 (s, 0.17H; minor isomer, CH$_3$), 2.36 (s, 2.83H; major isomer, CH$_3$). ^{13}C NMR (75 MHz, DMSO-d$_6$): δ 167.7, 167.4, 155.6, 153.7, 151.7, 150.5, 138.0, 136.4, 132.7, 132.2, 130.9, 130.0, 129.8, 129.5, 129.4, 128.6, 127.8, 121.2, 109.2, 109.4, 55.5, 13.3. MS (ESI) m/z = 573.1 [M–H]$^-$, HPLC purity: 95.12%.

(Z)-3-(4-((5-(4-Chloro-3-((cyclohexylmethyl)carbamoyl)phenyl)furan-2-yl)methylene)-3-methyl-5-oxo-4,5-dihydro-1H-pyrazol-1-yl)benzoic acid (39). Compound **21** (100 mg, 1 equiv.) used as starting material. Red solid (70% yield). Major Z-isomer data: ^{1}H NMR (300 MHz, DMSO-d$_6$): δ 13.13 (brs, 1H, COOH), 8.67 (d, J = 4.66 Hz, 1H), 8.59–8.47 (m, 2H), 8.19 (d, J = 7.20 Hz, 1H), 8.04–7.92 (m, 2H), 7.83–7.74 (m, 2H), 7.70–7.66 (m, 1H), 7.62–7.54 (m, 2H), 3.12–3.08 (m, 2H), 2.72 (s, 0.43H; minor isomer, CH$_3$), 2.35 (s, 2.57H; major isomer, CH$_3$), 2.32–2.29 (m, 1H), 1.79–1.63 (m, 5H), 1.22–1.18 (m, 3H), 1.0–0.9 (m, 2H). ^{13}C NMR (75 MHz, DMSO-d$_6$): δ 167.5, 166.1, 162.2, 158.1, 151.7, 150.7, 138.9, 131.9, 131.4, 131.0, 130.2, 129.7, 128.0, 127.7, 127.0, 125.4, 122.3, 121.6, 118.9, 112.8, 45.8, 37.8, 30.9, 26.5, 25.8, 13.3. MS (ESI) m/z = 545.1 [M–H]$^-$, HPLC purity: 98.67%.

(Z)-3-(4-((5-(4-Chloro-3-((3-methoxyphenyl)carbamoyl)phenyl)thiophen-2-yl)methylene)-3-methyl-5-oxo-4,5-dihydro-1H-pyrazol-1-yl)benzoic acid (40). Compound **22** (120 mg, 1 equiv.) used as starting material. Red solid (84% yield). Single

Z-isomer data: ^{1}H NMR (300 MHz, DMSO-d$_6$): δ 10.63 (s, 1H, CONH), 8.57 (t, J = 3.51 Hz, 1H), 8.19–8.15 (m, 3H), 8.07–8.02 (m, 1H), 7.97–7.92 (m, 2H), 7.76–7.66 (m, 2H), 7.55 (t, J = 8.18 Hz, 1H), 7.44–7.43 (m, 1H), 7.29–7.27 (m, 2H), 6.74–6.70 (m, 1H), 3.75 (s, 3H, OCH$_3$), 2.34 (s, 3H, CH$_3$, single Z isomer). ^{13}C NMR (75 MHz, DMSO-d$_6$): δ 167.5, 164.4, 162.5, 159.9, 153.8, 151.8, 145.0, 140.4, 138.8, 138.7, 138.1, 136.6, 132.2, 131.8, 131.2, 130.1, 129.8, 128.9, 126.7, 125.4, 122.1, 121.2, 118.7, 112.4, 109.9, 105.8, 55.5, 13.3. MS (ESI) m/z = 571.1 [M–H]$^-$, HPLC purity: 96.14%.

(Z)-4-(4-((5-(4-Chloro-3-((3-methoxyphenyl)carbamoyl)phenyl)thiophen-2-yl)methylene)-3-methyl-5-oxo-4,5-dihydro-1H-pyrazol-1-yl)benzoic acid (41). Compound **23** (105 mg, 1 equiv.) used as starting material. Red solid (81% yield). Single Z-isomer data: ^{1}H NMR (300 MHz, DMSO-d$_6$): δ 12.87 (brs, 1H, COOH), 10.64 (s, 1H, CONH), 8.19–8.14 (m, 2H), 8.12–7.90 (m, 7H), 7.70 (d, J = 8.39 Hz, 1H), 7.45 (s, 1H), 7.29–7.24 (m, 2H), 6.73–6.70 (m, 1H), 3.76 (s, 3H, OCH$_3$), 2.35 (s, 3H, CH$_3$, single Z isomer). ^{13}C NMR (75 MHz, DMSO-d$_6$): δ 167.3, 165.7, 164.6, 162.8, 160.0, 153.9, 152.3, 145.1, 142.1, 140.4, 138.9, 138.2, 136.7, 132.2, 131.3, 131.0, 130.8, 130.1, 128.9, 126.7, 126.4, 125.4, 121.0, 117.3, 112.3, 109.9, 105.8, 55.5, 13.3. MS (ESI) m/z = 571.1 [M–H]$^-$, HPLC purity: 99.05%.

(Z)-3-(4-((5-(4-Chloro-3-((cyclopropylmethyl)carbamoyl)phenyl)thiophen-2-yl)methylene)-3-methyl-5-oxo-4,5-dihydro-1H-pyrazol-1-yl)benzoic acid (42). Compound **24** (100 mg, 1 equiv.) used as starting material. Yellow solid (64% yield). Single Z-isomer data: ^{1}H NMR (300 MHz, DMSO-d$_6$): δ 13.11 (brs, 1H, COOH), 8.58–8.54 (m, 1H), 8.39 (s, 1H), 8.09–8.06 (d, 1H, J = 10.52 Hz), 7.76–7.74 (d, 2H, J = 10.08 Hz), 7.61–7.51 (m, 3H), 7.44–7.37 (m, 2H), 6.76 (s, 1H), 3.13–3.09 (m, 2H, NHCH$_2$), 2.31 (s, 3H, CH$_3$, single Z isomer), 1.00–0.97 (m, 1H, CH), 0.41–0.39 (m, 2H, CH$_2$), 0.22–0.20 (m, 2H, CH$_2$). ^{13}C NMR (75 MHz, DMSO-d$_6$): δ 167.43, 166.19, 146.94, 139.53, 138.00, 133.42, 131.88, 131.37, 130.67, 129.68, 128.68, 127.19, 125.96, 125.20, 124.27, 120.77, 43.56, 11.13, 9.02, 3.63. MS (ESI) m/z = 519.1 [M–H]$^-$, HPLC purity: 96.09%.

(Z)-3-(4-((5-(4-Chloro-3-((4-fluorobenzyl)carbamoyl)phenyl)thiophen-2-yl)methylene)-3-methyl-5-oxo-4,5-dihydro-1H-pyrazol-1-yl)benzoic acid (43). Compound **25** (105 mg, 1 equiv.) used as starting material. Red solid (73% yield). Single Z-isomer data: ^{1}H NMR (300 MHz, DMSO-d$_6$): δ 13.1 (brs, 1H, COOH), 9.16 (t, J = 6.34 Hz, 1H), 8.5 (brs, 1H), 8.20–8.19 (m, 3H), 7.94–7.92 (m, 3H), 7.76 (d, J = 7.99 Hz, 1H), 7.65–7.55 (m, 2H), 7.46–7.41 (m, 3H), 7.22–7.16 (m, 2H), 4.49 (d, J = 6.39 Hz, 2H, NHCH$_2$), 2.36 (s, 3H, CH$_3$, single Z isomer). ^{13}C NMR (75 MHz, DMSO-d$_6$): δ 167.5, 166.1, 163.3, 162.5, 160.1, 153.9, 151.8, 145.0, 138.9, 138.0, 136.6, 135.6, 132.1, 131.9, 131.3, 129.8, 128.8, 126.6, 125.5, 122.2, 121.2, 118.7, 115.6, 115.4, 42.3, 13.3. MS (ESI) m/z = 573.1 [M–H]$^-$, HPLC purity: 95.37%.

(Z)-3-(4-((5-(4-Chloro-3-((3-methoxyphenyl)carbamoyl)phenyl)-1H-pyrrol-2-yl)methylene)-3-methyl-5-oxo-4,5-dihydro-1H-pyrazol-1-yl)benzoic acid (44). Compound **26** (150 mg, 1 equiv.) used as starting material. Red solid (79% yield). Single Z-isomer data: ^{1}H NMR (400 MHz, DMSO-d$_6$): δ 14.51 (brs,

1H), 13.10 (brs, 1H, COOH), 10.63 (s, 1H, CONH), 8.47 (s, 1H), 8.31 (d, J = 9.43 Hz, 1H), 8.10 (d, J = 2.06 Hz, 1H), 7.90–7.88 (m, 1H), 7.18–7.78 (m, 3H), 7.56 (t, J = 8.92, 16.73 Hz, 1H), 7.43 (s, 1H), 7.32–7.25 (m, 4H), 6.74–6.71 (m, 1H), 3.76 (s, 3H, OCH_3), 2.35 (s, 3H, CH_3, single Z isomer). ^{13}C NMR (101 MHz, DMSO-d_6): δ 166.95, 164.28, 163.65, 159.54, 151.77, 140.24, 139.95, 138.46, 137.89, 134.22, 131.95, 131.56, 130.95, 130.41, 129.64, 129.20, 128.82, 126.44, 125.74, 125.52, 122.86, 119.59, 116.31, 113.54, 111.91, 109.41, 105.41, 55.03, 12.71. MS (ESI) m/z = 554.1 [M–H]$^-$, HPLC purity: 98.02%.

(Z)-3-(4-((5-(4-Chloro-3-((3-(trifluoromethoxy)phenyl) carbamoyl)phenyl)-1H-pyrrol-2-yl)methylene)-3-methyl-5-oxo-4,5-dihydro-1H-pyrazol-1-yl)benzoic acid (45). Compound **27** (150 mg, 1 equiv.) used as starting material. Red solid (71% yield). ^{1}H NMR (400 MHz, DMSO-d_6): δ 14.52 (brs, 1H), 13.13 (brs, 1H, COOH), 10.96 (s, 1H, CONH), 8.47 (s, 1H), 8.30 (d, J = 7.82 Hz, 1H), 8.17 (d, J = 2.69 Hz, 1H), 7.91–7.89 (m, 2H), 7.84–7.78 (m, 3H), 7.67 (d, J = 8.40 Hz, 1H), 7.58–7.50 (m, 3H), 7.32 (s, 1H), 7.14 (d, J = 8.40 Hz, 1H), 2.35 (s, 3H, CH_3). ^{13}C NMR (101 MHz, DMSO-d_6): δ 166.96, 164.63, 148.49, 140.36, 140.12, 137.40, 131.02, 130.67, 130.33, 129.14, 128.90, 125.91, 118.22, 116.05, 113.54, 111.60, 12.71. MS (ESI) m/z = 608.1 [M–H]$^-$, HPLC purity: 94.87%.

(Z)-4-(4-((5-(4-Chloro-3-((3-methoxyphenyl)carbamoyl) phenyl)furan-2-yl)methylene)-3-methyl-5-oxo-4,5-dihydro-1H-pyrazol-1-yl)benzoic acid (46). Compound **28** (160 mg, 1 equiv.) used as starting material. Red solid (71% yield). Major Z-isomer data: ^{1}H NMR (300 MHz, DMSO-d_6): δ 12.86 (brs, 1H, COOH), 10.55 (s, 1H, CONH), 8.14–7.96 (m, 4H), 7.95–7.85 (m, 3H), 7.83–7.75 (m, 1H), 7.73–7.66 (m, 1H), 7.61–7.54 (m, 1H), 7.47–7.40 (m, 1H), 7.32–7.23 (m, 2H), 6.75–6.67 (m, 1H), 3.74 (s, 3H, OCH_3), 2.74 (s, 0.24H; minor isomer, CH_3), 2.35 (s, 2.87H; major isomer, CH_3); ^{13}C NMR (75 MHz, DMSO-d_6): δ 167.21, 165.10, 164.66, 162.20, 159.98, 157.91, 150.39, 140.46, 137.86, 132.01, 131.58, 130.86, 130.07, 129.92, 128.42, 127.51, 125.52, 123.55, 122.26, 119.96, 119.68, 112.32, 109.79, 105.80, 55.47, 13.36. MS (ESI) m/z = 554.1 [M–H]$^-$; HRMS (ESI): calcd for $C_{30}H_{21}N_3O_6Cl$ [M–H]$^-$ m/z = 554.1119, found 554.1122. HPLC purity: 96.34%.

(Z)-4-(4-((5-(4-Chloro-3-((3-methoxybenzyl)carbamoyl) phenyl)furan-2-yl)methylene)-3-methyl-5-oxo-4,5-dihydro-1H-pyrazol-1-yl)benzoic acid (47). Compound **29** (140 mg, 1 equiv.) used as starting material. Brown solid (66% yield). Major Z-isomer data: ^{1}H NMR (300 MHz, DMSO-d_6): δ 12.87 (brs, 1H, COOH), 9.13 (t, J = 5.56 Hz, 1H), 8.10–7.89 (m, 6H), 7.82–7.75 (m, 1H), 7.70 (d, J = 8.54 Hz, 1H), 7.62–7.56 (m, 1H), 7.32–7.24 (m, 1H), 6.97–6.96 (m, 2H), 6.88–6.82 (m, 1H), 4.84 (d, J = 6.61 Hz, 2H), 3.75 (s, 3H, OCH_3), 2.67 (s, 0.59H; minor isomer, CH_3), 2.34 (s, 2.41H; major isomer, CH_3). ^{13}C NMR (75 MHz, DMSO-d_6): δ 167.3, 166.2, 162.4, 159.7, 158.1, 152.2, 150.8, 142.2, 140.9, 138.2, 131.1, 130.9, 129.8, 127.8, 127.3, 126.4, 125.5, 121.4, 119.8, 117.4, 113.1, 112.9, 55.4, 42.9, 13.3. MS (ESI) m/z = 569.1 [M–H]$^-$, HPLC purity: 98.06%.

(Z)-4-(4-((5-(3-(Benzylcarbamoyl)-4-chlorophenyl)furan-2-yl) methylene)-3-methyl-5-oxo-4,5-dihydro-1H-pyrazol-1-yl) benzoic acid (48). Compound **30** (130 mg, 1 equiv.) used as

starting material. Brown solid (72% yield). Major Z-isomer data: ^{1}H NMR (300 MHz, DMSO-d_6): δ 12.87 (brs, 1H, COOH), 9.16–9.08 (m, 1H), 8.10–7.86 (m, 6H), 7.82–7.74 (m, 1H), 7.69 (d, J = 8.05 Hz, 1H), 7.62–7.53 (m, 1H), 7.46–7.16 (m, 6H), 4.50 (d, J = 6.09 Hz, 2H, NHCH_2), 2.66 (s, 0.29H; minor isomer, CH_3), 2.34 (s, 2.71H; major isomer, CH_3). ^{13}C NMR (75 MHz, DMSO-d_6): δ 167.3, 166.3, 162.4, 158.1, 152.3, 150.8, 150.3, 142.4, 139.3, 138.2, 131.6, 130.9, 128.8, 127.7, 127.3, 126.4, 125.5, 121.3, 117.4, 112.9, 43.0, 13.3. MS (ESI) m/z = 539.1 [M–H]$^-$, HPLC purity: 96.13%.

(Z)-4-(4-((5-(4-Chloro-3-((pyridin-3-ylmethyl)carbamoyl) phenyl)furan-2-yl)methylene)-3-methyl-5-oxo-4,5-dihydro-1H-pyrazol-1-yl)benzoic acid (49). Compound **31** (140 mg, 1 equiv.) used as starting material. Brown solid (70% yield). Major Z-isomer data: ^{1}H NMR (300 MHz, DMSO-d_6): δ 12.82 (brs, 1H, COOH), 9.30 (t, 2H, J = 5.88 and 11.58 Hz), 8.73–8.64 (m, 2H), 8.59 (s, 1H), 8.14–7.83 (m, 7H), 7.73–7.42 (m, 4H), 4.58 (d, 2H, J = 5.7 Hz, NHCH_2), 2.73 (s, 0.48H; minor isomer, CH_3), 2.35 (s, 2.52H; major isomer, CH_3). ^{13}C NMR (75 MHz, DMSO): δ 174.99, 171.76, 167.31, 167.20, 166.81, 166.46, 162.45, 158.10, 152.24, 150.82, 150.36, 147.29, 147.01, 146.65, 142.20, 141.22, 137.92, 137.45, 136.17, 135.94, 131.57, 130.95, 129.81, 127.89, 127.48, 126.48, 125.60, 124.84, 123.45, 121.44, 119.73, 117.48, 112.97, 43.12, 13.38. MS (ESI) m/z = 540.1 [M–H]$^-$, HPLC purity: 95.67%.

(Z)-3-(4-((5-(4-Chloro-3-((3-methoxyphenyl)carbamoyl) phenyl)furan-2-yl)methylene)-5-oxo-3-(trifluoromethyl)-4,5-dihydro-1H-pyrazol-1-yl)benzoic acid (50). Compound **32** (190 mg, 1 equiv.) used as starting material. Red solid (69% yield). Major Z-isomer data: ^{1}H NMR (300 MHz, DMSO): δ 10.56 (brs, 1H, CONH), 8.49 (s, 1H), 8.20–8.17 (d, 2H, J = 7.5 Hz), 7.85–7.79 (d, 2H, J = 7.62 Hz), 7.75 (d, 1H, J = 1.68 Hz), 7.66–7.51 (m, 3H), 7.41 (brs, 1H), 7.28–7.23 (m, 2H), 7.03 (d, 1H, J = 3.36 Hz), 6.71–6.68 (m, 1H), 3.74 (s, 3H, OCH_3). ^{13}C NMR (75 MHz, DMSO): δ 175.00, 171.76, 167.39, 165.08, 159.97, 158.74, 156.00, 149.48, 140.49, 139.80, 137.78, 131.82, 130.06, 129.97, 127.99, 126.69, 125.26, 124.40, 123.51, 121.57, 112.32, 109.84, 108.65, 105.75, 98.53, 55.46. MS (ESI) m/z = 608.1 [M–H]$^-$. HRMS (ESI): calcd for $C_{30}H_{18}F_3N_3O_6Cl$ [M–H]$^-$ m/z = 608.0836, found 608.0833, HPLC purity: 97.21%.

(Z)-3-(4-((5-(4-Chloro-3-((cyclopropylmethyl)carbamoyl) phenyl)furan-2-yl)methylene)-5-oxo-3-(trifluoromethyl)-4,5-dihydro-1H-pyrazol-1-yl)benzoic acid (51). Compound **33** (100 mg, 1 equiv.) used as starting material. Brown solid (67% yield). Major Z-isomer data: ^{1}H NMR (300 MHz, DMSO-d_6): δ 13.21 (brs, 1H, COOH), 8.80 (s, 1H), 8.71–8.67 (t, J = 5.55 Hz and 11.07, 1H), 8.48–8.45 (m, 1H), 8.13–8.08 (m, 3H), 7.87–7.85 (m, 1H), 7.74–7.53 (m, 4H), 3.18–3.14 (m, 2H, NHCH_2), 1.03–0.97 (m, 1H, CH), 0.45-0.41 (m, 2H, CH_2), 0.25–0.21 (m, 2H, CH_2). ^{13}C NMR (75 MHz, DMSO): δ 167.55, 167.39, 167.22, 165.90, 161.42, 160.82, 150,76, 140.11, 138.75, 138.10, 132.52, 132.12, 131.86, 131.12, 130.55, 129.99, 129.64, 127.81, 127.27, 127.13, 126.15, 120.44, 114.43, 113.99, 43.72, 11.14, 3.74. MS (ESI) m/z = 557.1 [M–H]$^-$, HPLC purity: 96.02%.

(Z)-3-(4-((5-(4-Chloro-3-((4-fluorobenzyl)carbamoyl)phenyl) furan-2-yl)methylene)-5-oxo-3-(trifluoromethyl)-4,5-dihydro-

1*H*-pyrazol-1-yl)benzoic acid (**52**). Compound **34** (100 mg, 1 equiv.) used as starting material. Red solid (72% yield). Major Z-isomer data: ^{1}H NMR (300 MHz, DMSO-d$_6$): δ 13.23 (brs, 1H, *COOH*), 9.16 (t, *J* = 5.66 Hz, 1H), 8.81 (s, 1H), 8.50 8.46 (m, 1H), 8.16–8.05 (m, 3H), 7.88–7.86 (m, 2H), 7.79–7.70 (m, 2H), 7.63 (t, *J* = 6.95 Hz, 1H), 7.45–7.41 (m, 2H), 7.24–7.14 (m, 2H), 4.48 (d, *J* = 6.38 Hz, 2H, NH*CH*$_2$). ^{13}C NMR (75 MHz, DMSO-d$_6$): δ 167.2, 166.1, 163.3, 161.3, 160.7, 160.1, 150.7, 138.3, 138.0, 135.5, 132.5, 132.3, 131.1, 130.7, 129.8, 129.7, 128.6, 127.9, 127.3, 127.1, 126.1, 123.8, 115.6, 115.3, 114.4, 114.0, 42.3. MS (ESI) *m/z* = 611.1 [M–H]$^-$, HPLC purity: 94.78%.

General synthesis of target compounds 53–63

Synthesis of 3-(4-((5-(4-chloro-3-((3-methoxyphenyl)carbamoyl)phenyl)furan-2-yl)methyl)-3-methyl-5-oxo-4,5-dihydro-1*H*-pyrazol-1-yl)benzoic acid (53/149). To a suspension of **35** (100 mg, 1 equiv.) in anhydrous methanol (5 mL) at 0 °C was added sodium borohydride (20 mg, 3 equiv.) in portions. During addition gas evolution was observed, and the color of the solution changed from dark red to yellowish orange. The resulting solution was stirred at room temperature for 1.5 h. Solvent was removed *in vacuo* and the residue was acidified to pH 2–3 using 20% citric acid solution. The product was extracted with EtOAc (3 × 15 mL). The combined organic extracts were washed with brine, dried over Na$_2$SO$_4$, and concentrated under reduced pressure. The product was crystallized in 2% EtOH in EtOAc, solid was collected, washed with EtOAc and then hot solutions of 20–30% EtOAc in hexanes to afford target compound **53/149** (66 mg, 66% yield) as a red solid. ^{1}H NMR (400 MHz, DMSO-d$_6$): δ 13.00 (brs, 1H, *COOH*), 10.54 (s, 1H, *CONH*), 8.32 (s, 1H), 8.01 (s, 1H), 7.81 (s, 1H), 7.75–7.69 (m, 2H), 7.59–7.52 (m, 2H), 7.41 (s, 1H), 7.26–7.23 (m, 2H), 7.01 (d, *J* = 3.37 Hz, 1H), 6.71–6.69 (m, 1H), 6.17 (s, 1H), 3.74 (m, 2H, CH$_2$), 3.74 (s, *OCH$_3$*), 2.17 (m, 3H, *CH$_3$*). MS (ESI) *m/z* = 610.1 [M–H]$^-$. HRMS (ESI): calcd for C$_{30}$H$_{21}$F$_3$N$_3$O$_6$ClNa [M + Na]$^+$ *m/z* = 634.0969, found 634.09670. HPLC purity: 96.18%.

Target compounds **54–63** were synthesized by the above synthetic procedure described for the preparation of compound **53** using either sodium borohydride protocol or Pd/C hydrogenation protocol with corresponding starting materials. Each compound was crystallized in EtOH, solid was collected, washed with EtOAc and then hot solutions of 20–30% EtOAc in hexanes to afford the desired final compound. If necessary, the products were purified using 2–5% MeOH in DCM (1% AcOH in DCM) solvent system on automated flash column chromatography.

3-(4-((5-(4-Chloro-3-((3,4-dimethoxyphenyl)carbamoyl)phenyl)furan-2-yl)methyl)-3-methyl-5-oxo-4,5-dihydro-1*H*-pyrazol-1-yl)benzoic acid (54). Compound **36** (80 mg, one equiv.) used as starting material. Red solid (70% yield). ^{1}H NMR (300 MHz, DMSO-d$_6$): δ 10.43 (s, 1H, *CONH*), 8.31 (s, 1H), 8.02 (t, *J* = 7.65 and 15 Hz, 1H), 7.80–7.73 (m, 3H), 7.59–7.54 (m, 2H), 7.44–7.40 (m, 2H), 7.27–7.23 (m, 2H), 6.94 (d, *J*

= 8.55 Hz, 1H), 3.73 (s, 6H, di*OCH$_3$*), 2.17 (m, 3H, *CH$_3$*). MS (ESI) *m/z* = 587.1 [M–H]$^-$. HPLC purity: 95.48%.

4-(4-((5-(4-Chloro-3-((3-methoxyphenyl)carbamoyl)phenyl)furan-2-yl)methyl)-3-methyl-5-oxo-4,5-dihydro-1*H*-pyrazol-1-yl)benzoic acid (55). Compound **46** (80 mg, 1 equiv.) used as starting material. Red solid (68% yield). ^{1}H NMR (300 MHz, DMSO-d$_6$): δ 12.91 (brs, 1H, *COOH*), 10.67 (s, 1H, CO*NH*), 8.22 (s, 1H), 8.11–7.76 (m, 7H), 7.67 (m, 1H), 7.47–7.41 (m, 1H), 7.33–7.25 (m, 2H), 6.75–6.70 (m, 1H), 3.76 (s, 3H, *OCH$_3$*), 2.17 (m, 3H, *CH$_3$*). ^{13}C NMR (75 MHz, DMSO-d$_6$): δ 167.31, 166.54, 163.21, 159.97, 158.06, 153.11, 150.82, 141.23, 140.91, 130.87, 130.16, 130.08, 117.45, 112.31, 109.84, 107.21, 105.79, 55.47, 31.16, 13.36. MS (ESI) *m/z* = 557.1 [M–H]$^-$. HPLC purity: 95.23%.

4-(4-((5-(4-Chloro-3-((3-methoxybenzyl)carbamoyl)phenyl)furan-2-yl)methyl)-3-methyl-5-oxo-4,5-dihydro-1*H*-pyrazol-1-yl)benzoic acid (56). Compound **47** (95 mg, 1 equiv.) used as starting material. Brown solid (65% yield). ^{1}H NMR (300 MHz, DMSO-d$_6$): δ 12.80 (brs, 1H, *COOH*), 9.14 (t, *J* = 5.65 and 11.12 Hz, 1H), 8.11–7.81 (m, 5H), 7.30–7.52 (m, 2H), 7.29–7.23 (m, 2H), 7.08–6.83 (m, 4H), 4.47 (s, 2H, NH*CH$_2$*), 3.75 (s, 3H, *OCH$_3$*), 1.98 (m, 3H, *CH$_3$*). MS (ESI) *m/z* = 571.1 [M–H]$^-$. HPLC purity: 95.12%.

3-(4-((5-(4-Chloro-3-((3-methoxyphenyl)carbamoyl)phenyl)thiophen-2-yl)methyl)-3-methyl-5-oxo-4,5-dihydro-1*H*-pyrazol-1-yl)benzoic acid (57). Compound **40** (65 mg, 1 equiv.) used as starting material. Brown solid (71% yield). ^{1}H NMR (300 MHz, DMSO-d$_6$): δ 10.51 (s, 1H, CO*NH*), 8.33 (s, 1H), 8.03–8.00 (d, 1H, *J* = 8.16 Hz), 7.80–7.72 (m, 2H), 7.65–7.63 (t, 1H, *J* = 2.64 and 5.1 Hz), 7.59–7.49 (m, 3H), 7.46–7.44 (t, 1H, *J* = 3.3 and 6.69 Hz), 7.39 (s, 1H), 7.26–7.22 (m, 2H), 6.73–6.69 (m, 1H), 3.73 (s, 3H, *OCH$_3$*), 2.25 (m, 3H, *CH$_3$*). MS (ESI) *m/z* = 573.1 [M–H]$^-$. HPLC purity: 96.65%.

4-(4-((5-(4-Chloro-3-((3-methoxyphenyl)carbamoyl)phenyl)thiophen-2-yl)methyl)-3-methyl-5-oxo-4,5-dihydro-1*H*-pyrazol-1-yl)benzoic acid (58). Compound **41** (50 mg, 1 equiv.) used as starting material. Red solid (69% yield). ^{1}H NMR (300 MHz, DMSO-d$_6$): δ 12.88 (brs, 1H, *COOH*), 10.53 (s, 1H, CO*NH*), 8.03–7.98 (m, 2H), 7.95–7.89 (m, 2H), 7.76 (d, *J* = 2.17 Hz, 1H), 7.68–7.64 (m, 1H), 7.53 (d, *J* = 8.59 Hz, 1H), 7.47–7.41 (m, 2H), 7.26–7.21 (m, 2H), 6.91 (d, *J* = 3.61 Hz, 1H), 6.71–6.67 (m, 1H), 3.79 (m, 2H, CH$_2$), 3.74 (s, 3H, *OCH$_3$*), 2.17 (m, 3H, *CH$_3$*). ^{13}C NMR (75 MHz, DMSO-d$_6$): δ 167.2, 165.7, 164.9, 159.9, 140.5, 139.3, 137.8, 133.5, 130.8, 130.7, 130.0, 128.6, 127.5, 126.4, 125.2, 112.3, 109.7, 105.8, 55.48, 22.63, 14.68. MS (ESI) *m/z* = 573.1 [M–H]$^-$. HPLC purity: 98.07%.

3-(4-((5-(4-Chloro-3-((cyclopropylmethyl)carbamoyl)phenyl)thiophen-2-yl)methyl)-3-methyl-5-oxo-4,5-dihydro-1*H*-pyrazol-1-yl)benzoic acid (59). Compound **42** (60 mg, 1 equiv.) used as starting material. Red solid (76% yield). ^{1}H NMR (300 MHz, DMSO-d$_6$): δ 13.02 (brs, 1H, *COOH*), 8.68–8.62 (t, 1H, *J* = 5.4 and 11.15 Hz), 8.42 (s, 1H), 8.09–8.06 (m, 2H), 7.82 (s, 2H), 7.72–7.62 (m, 2H), 6.82 (m, 1H), 6.67–6.59 (m, 1H), 3.20–3.17 (t, 2H, *J* = 6.15 Hz, NH*CH$_2$*), 2.18 (m, 3H, *CH$_3$*), 1.02–0.98 (m, 1H, *CH*), 0.45–0.40 (m, 2H, *CH$_2$*), 0.24–0.19 (m, 2H, *CH$_2$*). ^{13}C NMR (75 MHz, DMSO-d$_6$): 171.76, 167.55, 167.27, 166.23,

139.85, 138.09, 136.62, 133.30, 132.06, 130.69, 129.92, 128.80, 127.29, 125.26, 124.97, 121.06, 43.56, 13.36. MS (ESI) m/z = 521.1 [M–H]⁻. HPLC purity: 97.54%.

3-(4-((5-(4-Chloro-3-(((4-fluorobenzyl)carbamoyl)phenyl) thiophen-2-yl)methyl)-3-methyl-5-oxo-4,5-dihydro-1H-pyrazol-1-yl)benzoic acid (60). Compound **43** (60 mg, 1 equiv.) used as starting material. Red solid (77% yield). ^{1}H NMR (300 MHz, DMSO-d$_6$): δ 10.52 (s, 1H, CONH), 8.05–7.98 (m, 2H), 7.88–7.97 (m, 2H), 7.75 (d, J = 7.8 Hz, 1H), 7.65–7.55 (m, 2H), 7.46–7.41 (m, 2H), 7.22–7.16 (m, 2H), 6.88 (d, J = 5.1 Hz, 1H), 6.67–6.61 (m, 1H), 4.49 (d, J = 6.45 Hz, 2H, NHCH$_2$), 2.36 (s, 3H, CH$_3$). ^{13}C NMR (75 MHz, DMSO-d$_6$): δ 167.42, 166.44, 163.27, 160.06, 139.34, 137.66, 135.65, 133.39, 131.97, 130.76, 129.77, 129.66, 128.75, 127.39, 126.37, 125.28, 125.15, 115.64, 115.36, 42.26, 22.67. MS (ESI) m/z = 575.1 [M–H]⁻. HPLC purity: 96.07%.

3-(4-((5-(4-Chloro-3-((3-methoxyphenyl)carbamoyl)phenyl) furan-2-yl)methyl)-5-oxo-3-(trifluoromethyl)-4,5-dihydro-1H-pyrazol-1-yl)benzoic acid (61/322). Compound **50** (100 mg, 1 equiv.) used as starting material. Red solid (63 mg, 70% yield), ^{1}H NMR (300 MHz, DMSO-d$_6$): δ 10.54 (brs, 1H, CONH), 8.49 (s, 1H), 8.20–8.17 (d, 1H, J = 8.34 Hz), 7.93–7.75 (m, 3H), 7.67–7.51 (m, 3H), 7.41 (s, 1H), 7.26 (m, 2H), 6.73–7.68 (m, 1H), 6.32–6.31 (d, 1H), 3.74 (s, 3H, OCH$_3$), 3.70 (m, 2H, CH$_2$), 2.79 (q, 1H, CH). ^{13}C NMR (75 MHz, DMSO-d$_6$): δ 175.00, 171.76, 167.39, 165.08, 159.96, 158.74, 156.00, 149.98, 140.49, 139.79, 137.78, 131.82, 130.05, 129.97, 128.36, 126.68, 125.09, 124.40, 124.40, 123.51, 121.57, 112.32, 109.83, 108.78, 105.75, 98.53, 72.90, 55.46, 43.13, 28.30. MS (ESI) m/z = 556.1 [M–H]⁻. HRMS (ESI): calcd for C$_{30}$H$_{23}$N$_3$O$_6$Cl [M–H]⁻ m/z = 556.1275, found 556.1279. HPLC purity: 98.34%.

3-(4-((5-(4-Chloro-3-((cyclopropylmethyl)carbamoyl)phenyl) furan-2-yl)methyl)-5-oxo-3-(trifluoromethyl)-4,5-dihydro-1H-pyrazol-1-yl)benzoic acid (62). Compound **51** (60 mg, 1 equiv.) used as starting material. Brown solid (70% yield), ^{1}H NMR (300 MHz, DMSO-d$_6$): δ 13.06 (brs, 1H, COOH), 8.71–8.68 (t, 1H, J = 5.61 and 11.19 Hz), 8.46 (s, 1H), 8.12–8.09 (m, 2H), 7.89 (s, 2H), 7.77–7.64 (m, 4H), 3.19–3.15 (t, 2H, J = 6.12 Hz, NHCH$_2$), 2.78–2.62 (q, 2H, CH$_2$), 1.02–0.98 (m, 1H, CH), 0.48–0.42 (m, 2H, CH$_2$), 0.27–0.22 (m, 2H, CH$_2$). ^{13}C NMR (75 MHz, DMSO-d$_6$): δ 175.00, 171.76, 167.39, 167.23, 165.91, 160.83, 150.77, 138.77, 138.11, 132.52, 132.13, 130.01, 127.82, 127.28, 127.14, 126.17, 123.97, 120.47, 114.45, 114.00, 72.89, 43.72, 43.13, 11.14, 3.74. MS (ESI) m/z = 559.1 [M–H]⁻. HPLC purity: 95.43%.

3-(4-((5-(4-Chloro-3-((4-fluorobenzyl)carbamoyl)phenyl) furan-2-yl)methyl)-5-oxo-3-(trifluoromethyl)-4,5-dihydro-1H-pyrazol-1-yl)benzoic acid (63). Compound **52** (65 mg, 1 equiv.) used as starting material. Red solid (69% yield), ^{1}H NMR (300 MHz, DMSO-d$_6$): δ 13.09 (brs, 1H, COOH), 9.18–1.14 (t, 1H, J = 5.64 and 11.76 Hz), 8.47 (s, 1H), 8.19–8.11 (m, 2H), 7.88 (s, 2H), 7.76–7.57 (m, 4H), 7.45–7.37 (m, 2H), 7.20–7.14 (m, 2H), 4.49 (d, 2H, J = 6.09 Hz, NHCH$_2$), 2.78–2.62 (q, 2H, CH$_2$). ^{13}C NMR (75 MHz, DMSO-d$_6$): δ 174.99, 171.76, 167.23, 166.14, 161.43, 160.73, 160.10, 150.78, 138.34, 138.10, 135.48, 132.52, 130.02, 129.86, 129.61, 127.36, 126.25, 123.98, 120.47,

115.66, 114.52, 114.06, 72.89, 43.13, 42.35. MS (ESI) m/z = 613.1 [M–H]⁻. HPLC purity: 98.03%.

Synthesis of target compounds 67–70

Synthesis of 4-(3-methyl-5-oxo-4,5-dihydro-1H-pyrazol-1-yl) benzenesulfonamide (65). Compound **65** was synthesized following the procedure described for the preparation of compound **4a**, using 4-hydrazineylbenzenesulfonamide **64** (250 mg, 1 equiv.) and ethyl acetoacetate **2** (1.2 equiv.) as starting materials. White solid (74% yield). ^{1}H NMR (300 MHz, DMSO-d$_6$): δ 7.94–7.91 (d, 2H, J = 9.06 Hz), 7.87–7.84 (d, 2H, J = 9.06 Hz), 5.40 (s, 1H), 2.13 (s, 3H, CH$_3$). ^{13}C NMR (75 MHz, DMSO-d$_6$): δ 172.18, 150.16, 140.56, 140.21, 127.31, 119.76, 117.66, 89.70, 43.62, 14.84.

Synthesis of (Z)-2-chloro-5-(5-((3-methyl-5-oxo-1-(4-sulfamoylphenyl)-1,5-dihydro-4H-pyrazol-4-ylidene)methyl) furan-2-yl)benzoic acid (66). Compound **66** was synthesized following the synthetic procedure described for the preparation of compound **9**, using 4-(3-methyl-5-oxo-4,5-dihydro-1H-pyrazol-1-yl)benzenesulfonamide **65** (250 mg, 1 equiv.) and 2-chloro-5-(5-formylfuran-2-yl)benzoic acid **8a** (0.25 mL, 1.2 equiv.) as starting materials. Red solid (81% yield). Major Z-isomer data: ^{1}H NMR (300 MHz, DMSO-d$_6$): δ 8.61 (d, J = 3.87 Hz, 1H), 8.32 (d, J = 2.23 Hz, 1H), 8.14–8.11 (m, 2H), 7.93–7.88 (m, 3H), 7.75 (s, 1H), 7.67 (d, J = 7.85 Hz, 1H), 7.57 (d, J = 4.24 Hz, 1H), 7.35 (brs, 2H), 2.69 (s, 0.18H; minor isomer, CH$_3$), 2.33 (s, 2.82H; major isomer, CH$_3$). ^{13}C NMR (75 MHz, DMSO-d$_6$): δ 172.5, 166.5, 162.3, 157.8, 152.1, 150.8, 141.1, 139.6, 133.2, 132.6, 132.1, 130.2, 129.0, 128.0, 127.8, 127.7, 127.3, 127.2, 121.3, 117.7, 112.9, 21.5. MS (ESI) m/z = 484.1 [M–H]⁻.

Compounds **67–69** were synthesized following the synthetic procedure described for the preparation of amide **17** using appropriate starting materials. Each compound was triturated with the mixture of EtOAc in hexanes (2–3 times) to afford the desired compound. If necessary, the products were purified using 2–5% MeOH in DCM (1% AcOH in DCM) solvent system on automated flash column chromatography.

(Z)-2-Chloro-N-(3-methoxyphenyl)-5-(5-((3-methyl-5-oxo-1-(4-sulfamoylphenyl)-1,5-dihydro-4H-pyrazol-4-ylidene)methyl) furan-2-yl)benzamide (67). Compound **66** (150 mg, 1 equiv.) and m-anisidine (1.05 equiv.) used as starting materials. Red solid (68% yield). TLC: 6% MeOH in DCM, R_f = 0.49; visualized with UV. Major Z-isomer data: ^{1}H NMR (300 MHz, DMSO-d$_6$): δ 10.66 (s, 1H, CONH), 8.64 (d, J = 5.96 Hz, 1H), 8.20 (d, 1H, J = 2.1 Hz), 8.15–8.06 (m, 3H), 7.90 (dd, J = 8.85 and 2.34 Hz, 2H), 7.82 (s, 1H), 7.79–7.75 (d, 1H, J = 8.46 Hz), 7.66–7.59 (d, 1H, J = 3.9 Hz), 7.45–7.43 (m, 1H), 7.34 (s, 2H), 7.29–7.28 (m, 2H), 6.75–6.71 (m, 1H), 3.76 (s, 1H, OCH$_3$), 2.74 (s, 0.32H; minor isomer, CH$_3$), 2.34 (s, 2.78H; major isomer, CH$_3$). ^{13}C NMR (75 MHz, DMSO-d$_6$): δ 165.2, 1623.4, 160.0, 158.1, 152.2, 150.8, 150.3, 141.1, 140.3, 139.7, 138.2, 131.8, 131.2, 130.4, 130.1, 127.9, 127.3, 125.7, 121.3, 119.7, 117.7, 113.0, 112.3, 109.8, 105.8, 55.5, 13.3. MS (ESI) m/z = 590.1 [M–H]⁻. HPLC purity: 94.96%.

(Z)-2-Chloro-N-(cyclopropylmethyl)-5-(5-((3-methyl-5-oxo-1-(4-sulfamoylphenyl)-1,5-dihydro-4H-pyrazol-4-ylidene)methyl)furan-2-yl)benzamide (68). Compound 66 (100 mg, 1 equiv.) and cyclopropylmethyl amine (1.05 equiv.) used as starting materials. Red solid (77% yield). TLC: 6% MeOH in DCM, R_f = 0.46; visualized with UV. Major Z-isomer data: ^{1}H NMR (300 MHz, DMSO-d$_6$): δ 8.71–8.67 (t, J = 5.55 and 11.28 Hz, 1H), 8.63 (d, J = 3.57 Hz, 1H), 8.16–8.11 (m, 2H), 8.02–7.98 (m, 2H), 7.90–7.87 (m, 2H), 7.82 (s, 1H), 7.70–7.67 (m, 1H), 7.63–7.62 (d, J = 3.96 Hz, 1H), 7.34 (s, 2H), 3.19–3.15 (t, 2H, NHCH$_2$), 2.74 (s, 0.41H; minor isomer, CH$_3$), 2.35 (s, 2.59H; major isomer, CH$_3$), 1.05–0.99 (m, 1H, CH), 0.49–0.43 (m, 2H, CH$_2$), 0.28–0.23 (m, 2H, CH$_2$). ^{13}C NMR (75 MHz, DMSO-d$_6$): δ 166.01, 162.44, 158.30, 152.30, 150.78, 141.16, 139.74138.65, 131.10, 130.43, 128.27, 127.74, 127.40, 127.19, 125.48, 121.28, 117.78, 112.87, 43.70, 13.38, 11.30, 3.73. MS (ESI) m/z = 538.1 [M–H]$^-$. HPLC purity: 97.24%.

(Z)-2-Chloro-N-(4-fluorobenzyl)-5-(5-((3-methyl-5-oxo-1-(4-sulfamoylphenyl)-1,5-dihydro-4H-pyrazol-4-ylidene)methyl)furan-2-yl)benzamide (69). Compound 66 (65 mg, 1 equiv.) and 4-fluorobenzyl amine (1.05 equiv.) used as starting materials. Red solid (83% yield). TLC: 10% MeOH in DCM, R_f = 0.51; visualized with UV. Major Z-isomer data: ^{1}H NMR (300 MHz, DMSO-d$_6$): 9.18–9.14 (t, J = 5.97 and 11.82 Hz, 1H), 8.66 (d, 1H, J = 3.66 Hz), 8.16–8.11 (m, 2H), 8.04 (s, 1H), 7.91–7.88 (m, 2H), 7.83–7.80 (m, 1H), 7.72–7.69 (m, 1H), 7.64–7.60 (m, 1H), 7.47–7.41 (m, 2H), 7.36–7.32 (m, 2H), 7.23–7.16 (m, 3H), 4.49 (d, 2H, J = 3.66 Hz, NHCH$_2$), 2.68 (s, 0.55H; minor isomer, CH$_3$), 2.36 (s, 2.49H; major isomer, CH$_3$). ^{13}C NMR (75 MHz, DMSO-d$_6$): δ 169.59, 166.23, 163.32, 162.46, 158.52, 158.21, 152.31, 150.82, 143.49, 141.15, 139.76, 138.24, 135.56, 131.78, 130.61, 130.48, 130.27, 129.72, 129.61, 128.20, 127.31, 126.84, 125.56, 121.34, 117.80, 115.70, 115.41, 112.96, 42.36, 13.46. MS (ESI) m/z = 594.1 [M–H]$^-$. HPLC purity: 95.72%.

Synthesis of 2-chloro-N-(3-methoxyphenyl)-5-(5-((3-methyl-5-oxo-1-(4-sulfamoylphenyl)-4,5-dihydro-1H-pyrazol-4-yl)methyl)furan-2-yl)benzamide (70). Compound 70 was synthesized following the synthetic procedure described for the preparation of compound 53 (149), using (Z)-2-chloro-N-(3-methoxyphenyl)-5-(5-((3-methyl-5-oxo-1-(4-sulfamoylphenyl)-1,5-dihydro-4H-pyrazol-4-ylidene)methyl)furan-2-yl)benzamide 67 (45 mg, 1 equiv.) as starting material. Red solid (77% yield). TLC: 10% MeOH in DCM, R_f = 0.48; visualized with UV. ^{1}H NMR (300 MHz, DMSO-d$_6$): 10.57 (s, 1H, CONH), 7.94–7.80 (m, 5H), 7.71–7.80 (d, 1H, J = 2.13 Hz), 7.59–7.56 (d, 1H, J = 8.49 Hz), 7.45–7.36 (m, 3H), 7.29–7.23 (m, 2H), 7.01–7.00 (d, 1H, J = 3.24 Hz), 6.73–6.68 (m, 1H), 6.19–6.18 (d, 1H, J = 3.18 Hz), 3.74 (s, 3H, OCH$_3$), 3.74–3.71 (m, 2H), 2.17 (s, 3H, CH$_3$). ^{13}C NMR (75 MHz, DMSO-d$_6$): δ 165.14, 159.97, 155.20, 150.31, 140.43, 137.80, 130.76, 130.13, 129.89, 128.37, 127.23, 125.46, 123.45, 112.34, 109.82, 108.83, 108.68, 105.84, 55.94, 21.13. MS (ESI) m/z = 592.1 [M–H]$^-$. HPLC purity: 98.21%.

Synthesis of target compounds 74–76

Synthesis of 3-(3-methyl-5-oxo-4,5-dihydro-1H-pyrazol-1-yl)benzonitrile (72). Compound 72 was synthesized by an above synthetic procedure described for the preparation of intermediate 4a using 3-hydrazinylbenzonitrile 71 (200 mg, 1 equiv.) and ethyl acetoacetate 2 (0.228 mL, 1.2 equiv.) as starting materials. Off-white solid (363 mg, 88% yield, requires no further purification). TLC: 40% EtOAc in hexanes, R_f = 0.51; visualized with UV. ^{1}H NMR (300 MHz, DMSO-d$_6$): δ 8.20 (s, 1H), 8.01 (d, 1H, J = 8.4 Hz), 7.99–7.97 (m, 1H), 7.65–7.62 (m, 1H), 5.37 (s, 1H), 2.13 (s, 3H, CH$_3$). MS (ESI) m/z = 200.1 [M + H]$^+$.

Synthesis of (Z)-2-chloro-5-(5-((1-(3-cyanophenyl)-3-methyl-5-oxo-1,5-dihydro-4H-pyrazol-4-ylidene)methyl)furan-2-yl)benzoic acid (73). Compound 73 was synthesized by an above synthetic procedure described for the preparation of intermediate 9 using compound 72 (170 mg, 1 equiv.) and 2-chloro-5-(5-formylfuran-2-yl)benzoic acid 8a (214 mg, 1 equiv.) as starting materials. Red solid (305 mg, 83% yield). Major Z-isomer data: ^{1}H NMR (300 MHz, DMSO-d$_6$): δ 8.58 (d, 1H, J = 3.84 Hz), 8.23 (s, 1H), 8.18–8.14 (m, 2H), 7.98–7.95 (dd, 1H, J = 2.22 and 8.4 Hz), 7.75 (s, 1H), 7.59–7.54 (m, 4H), 2.61 (s, 0.45H; minor isomer, CH$_3$), 2.30 (s, 2.55H; major isomer, CH$_3$). ^{13}C NMR (75 MHz, DMSO-d$_6$): δ 166.41, 162.18, 157.90, 152.06, 150.75, 139.14, 133.44, 131.25, 130.79, 128.89, 127.94, 127.57, 127.08, 122.24, 120.56, 118.98, 112.14, 13.31. MS (ESI) m/z = 430.1 [M–H]$^-$.

Synthesis of (Z)-2-chloro-5-(5-((1-(3-cyanophenyl)-3-methyl-5-oxo-1,5-dihydro-4H-pyrazol-4-ylidene)methyl)furan-2-yl)-N-(3-methoxyphenyl)benzamide (74). Compound 74 was prepared by an above synthetic procedure described for the preparation of amide 17 using compound 73 (180 mg) as a starting material. Red solid (172 mg, 77% yield). TLC: 4% MeOH in DCM, R_f = 0.49; visualized with UV. Major Z-isomer data: Major Z-isomer data: ^{1}H NMR (300 MHz, DMSO-d$_6$): δ 10.65 (s, 1H, CONH), 8.63 (brs, 1H), 8.31–8.15 (m, 3H), 8.07–8.04 (dd/m, 1H), 7.83–7.74 (m, 2H), 7.66–7.61 (m, 3H), 7.43 (s, 1H), 7.29 (brs, 2H), 6.32 (m, 1H), 3.76 (s, 3H, OCH$_3$), 2.71 (s, 0.51H; minor isomer, CH$_3$), 2.33 (s, 2.49H; major isomer, CH$_3$). ^{13}C NMR (75 MHz, DMSO-d$_6$): δ 170.82, 164.69162.34, 160.01, 158.19, 152.22, 150.80, 140.39, 139.23, 138.22, 131.62, 130.93, 130.16, 128.30, 127.90, 125.74, 122.51, 121.22, 120.82, 118.99, 112.32, 112.24, 109.90, 105.82, 55.51, 13.32. MS (ESI) m/z = 537.1 [M + H]$^+$. HPLC purity: 98.43%.

Synthesis of (Z)-5-(5-((1-(3-(1H-tetrazol-5-yl)phenyl)-3-methyl-5-oxo-1,5-dihydro-4H-pyrazol-4-ylidene)methyl)furan-2-yl)-2-chloro-N-(3-methoxyphenyl)benzamide (75). To a solution of nitrile 74 (150 mg, 1 equiv.) in anhydrous DMF (7.5 mL) was added sodium azide (54 mg, 3 equiv.) and then NH$_4$Cl (45 mg, 3 equiv.). The reaction mixture was heated at 130 °C for 24 h. After cooling the reaction mixture, it was poured into 40–50 mL cold water and then acidified with 1 N HCl to pH ~ 2. The precipitated solid was collected by filtration, washed with water 2–3 times. The crude product was crystallized in EtOH/EtOAc mixture (1 : 9), solid was collected, washed with EtOAc and then hot solutions of 20–30% EtOAc in hexanes to afford tetrazole 75 (100 mg, 62% yield) as a red solid. Major Z-isomer data: ^{1}H NMR (300 MHz, DMSO-d$_6$): δ 10.65 (s, 1H, CONH), 8.64 (d, 1H, J = 3.66 Hz),

8.32 (s, 1H), 8.28–8.21 (m, 2H), 8.08–8.02 (d, 1H, J = 8.43 Hz), 7.84 (s, 1H), 7.77–7.74 (d, 1H, J = 8.49 Hz), 7.65–7.62 (m, 3H), 7.43 (brs, 1H), 7.29–7.25 (m, 2H), 6.74–6.70 (m, 1H), 3.76 (s, 3H, OCH_3), 2.71 (s, 0.58H; minor isomer, CH_3), 2.33 (s, 2.42H; major isomer, CH_3). ^{13}C NMR (75 MHz, DMSO-d$_6$): δ 164.68, 162.35, 160.01, 158.19, 152.23, 150.80, 140.39, 139.24, 138.24, 131.62, 130.94, 130.54, 130.16, 128.16, 127.50, 125.75, 122.53, 121.23, 120.84, 118.99, 113.04, 112.32, 112.25, 109.90, 105.82, 55.51, 13.34. MS (ESI) m/z = 580.1 [M + H]$^+$. HRMS (ESI): calcd for $C_{30}H_{23}N_7O_4Cl$ [M + H]$^+$ m/z = 580.1500, found 580.1496. HPLC purity: 95.77%.

Synthesis of 5-(5-((1-(3-(1*H*-tetrazol-5-yl)phenyl)-3-methyl-5-oxo-4,5-dihydro-1*H*-pyrazol-4-yl)methyl)furan-2-yl)-2-chloro-*N*-(3-methoxyphenyl)benzamide 76 (245). Compound **76** (**245**) was prepared by an above reduction procedure described for the preparation of compound **53** using compound **75** (70 mg) as a starting material. The product was crystallized in 5% EtOH in EtOAc, solid was collected, washed with EtOAc and then hot solutions of 20–30% EtOAc in hexanes to afford target compound **245** (49 mg, 70% yield) as a red solid. ^{1}H NMR (300 MHz, DMSO-d$_6$): δ 10.54 (s, 1H, NH), 8.59–8.57 (t, 1H, J = 5.16 and 10.5 Hz), 8.28 (s, 1H), 8.05–8.03 (d, 1H, J = 7.8 Hz), 7.74–7.77 (m, 2H), 7.67–7.41 (m, 3H), 7.26–7.24 (brs, 2H), 6.99–6.98 (d, 1H, J = 3.24 Hz), 6.73–6.69 (m, 1H), 6.31–6.30 (d, 1H, J = 3.03 Hz), 3.75 (s, 3H, OCH_3), 1.98 (m, 3H, CH_3). ^{13}C NMR (75 MHz, DMSO-d$_6$): δ 166.22, 165.09, 159.97, 158.66, 156.17, 149.95, 140.49, 139.59, 137.79, 135.90, 130.77, 130.06, 129.12, 128.33, 125.27, 124.66, 123.87, 123.47, 120.26, 112.32, 109.84, 108.61, 105.75, 55.47, 22.63, 14.68. MS (ESI) m/z = 582.1 [M + H]$^+$. HRMS (ESI): calcd for $C_{30}H_{25}N_7O_4Cl$ [M + H]$^+$ m/z = 582.1657, found 582.1661. HPLC purity: 97.56%.

4.3 Pharmacophore modeling

Small molecule preparation and pharmacophore modeling were performed using Maestro version 14.0.134 (Schrödinger, LLC).[46] Ligand structures were prepared using the LigPrep module with default parameters, including generation of ionization states at physiological pH (7.0 ± 2.0), retention of specified chiralities, and generation of relevant tautomers and protonation states. To gain insights into the SAR of the 4-substituted phenylpyrazolidinone series, ligand-based pharmacophore modeling was carried out using the Phase module. Conformational sampling was performed with a target of 50 low-energy conformers per ligand, and all output conformers were energy-minimized. Both E/Z geometric isomers and R/S stereoisomers of the training set compounds were included to comprehensively capture stereochemical diversity. Pharmacophore hypotheses were generated using Phase's common pharmacophore perception algorithm, which identifies shared chemical features such as hydrogen bond acceptors/HBA (A), hydrogen bond donors/HBD (D), hydrophobic groups (H), aromatic rings (R), and ionizable groups (positive [P] and negative [N]) based on conformational alignment of known active ligands. No

custom feature definitions were applied. The hypotheses were constrained to contain five to seven pharmacophoric features, with a requirement of at least one or two hydrogen bond acceptors or donors to reflect the prevalence of acidic functional groups (*e.g.*, carboxylic acids and tetrazoles) in the active compounds. The top ten scoring pharmacophore models were ranked using the Phase HypoScore function, which considers alignment quality, feature overlap, and coverage across the training set.

4.4 Prediction of physicochemical and ADME-related profiles using OPERA QSAR models

To assess the physicochemical and drug-likeness profiles of lead Ku–DNA binding inhibitors (Ku-DBi's), we employed the OPERA (Open [Quantitative] Structure–Activity/Property Relationship App) suite of validated QSAR models developed by the U.S. EPA.[47,48] OPERA is built on curated experimental datasets and provides predictive models for a broad range of molecular descriptors relevant to drug discovery and environmental risk assessment. All predictions were performed using OPERA's default settings, and each output included an applicability domain (AD) score, which reflects the confidence in the prediction based on chemical similarity to the model's training set. The predicted values were evaluated against widely accepted drug-likeness thresholds, such as Lipinski's rule of five, TPSA limits, and aqueous solubility cutoffs, to assess the developability of the compounds.

To enable multi-parametric ranking, all predicted descriptors were scaled using min–max normalization to transform values into a [0–1] range, ensuring comparability across variables with different units and scales. Each descriptor was assigned a weight based on its relative importance to drug-likeness and ADME (Absorption, Distribution, Metabolism, and Excretion) properties. Properties where higher values are favorable such as LogP_pred, LogWS_pred, LogD55_pred, LogD74_pred, and CACO2_pred were assigned positive weights, while those where lower values are preferred such as MolWeight, TopoPolSurfAir, Clint_pred, and LogVP_pred which received negative weights. Parameters such as pKa_a_pred is considered of moderate relevance and assigned intermediate weights.

For each compound, a composite drug-likeness score was calculated using the weighted sum of normalized values:

$$\text{Score} = \sum I = 1n(\text{Normalized Value } i \times \text{Weight } i)\text{Score} = I = 1\sum n(\text{Normalized Value } i \times \text{Weight } i)$$

This scoring system reflects the overall favorability of each compound across all selected descriptors. Compounds were then ranked based on their composite scores, where a higher score indicates greater drug-likeness and ADME-favorability.

4.5 Protein purification and preparation

For biochemical analysis, the Ku70/80 heterodimer was purified from baculovirus-infected SF9 cells and DNA-PKcs

was purified from HeLa cells or HEK 293 cells, as described previously.[50]

For biophysical analyses, full-length Ku heterodimer was expressed in and purified from Sf21 insect cells using a multiBac expression system as previously described.[51,52] Protein labeling was achieved following buffer exchange using an Amicon 50 kDa cutoff concentrator into PBS (10 mM phosphate buffer, pH 7.4, 2.7 mM KCl, 137 mM NaCl) supplemented with 0.005% Tween-20.

4.6 Biochemical activity assays

EMSA (electrophoretic mobility shift assays) were used to assess Ku–DNA binding activity and the effect of potential inhibitors. Assays were conducted using purified Ku and a [^{32}P]-labeled 30-bp duplex DNA substrate. The DNA substrate was prepared by annealing 5′-[^{32}P]-CCCTATCCTTTCCGCG TCCTTACTTCCCC-3′ to its complementary strand. Reactions were performed in a final volume of 20 μL, containing 1× NEB buffer 3 (New England Biolabs) and 1 mM DTT. Purified Ku was pre-incubated with increasing concentrations of each compound for 20 min at room temperature before addition to the EMSA reaction mixture containing 300 fmol DNA substrate. Reaction mixtures were incubated for an additional 20 min at room temperature, and products were separated by electrophoresis on a 6% non-denaturing polyacrylamide gel. Gels were then transferred to a piece of Whatman paper, and exposed to a phosphor screen cassette. Imaging was performed using a PhosphorImager scanner. The scans were quantified using ImageQuant software (Molecular Dynamics) as we have described previously.[50,53]

DNA-PK Phosphorylation Kinase assays were used to assess the DNA-PK catalytic activity of our inhibitors. DNA-PK catalytic activity was evaluated by measuring the DNA-dependent transfer of [^{32}P] from ATP to a synthetic p53-based peptide substrate as described previously.[50,53] For these assays, the same 30 bp duplex DNA used in the EMSA experiments above was employed, but without the [^{32}P] label. Briefly, kinase assays were performed in a final volume of 20 μL, containing 20 mM Tris-HCl, pH 7.5, 8 mM MgCl$_2$, 1 mM DTT, 5% glycerol, and 500 μM p53 peptide. Compounds were pre-incubated with DNA-PKcs/Ku for 15 min at room temperature, and the reaction was initiated by the addition of an ATP-DNA mix containing 0.5 μCi γ-^{32}P-ATP, 125 μM ATP, and 5 nM DNA. The DNA-PK phosphorylation assays were performed at 37 °C for 15 min and stopped with 30% acetic acid. Reaction products were spotted on P81-filter paper that was then washed five times for 5 min each in 15% acetic acid, then once in 100% methanol, and allowed to dry. Filters were exposed to PhosphorImager screen and analyzed using ImageQuant software (Molecular Dynamics).

Inhibitor titration assays (both EMSA and DNA-PK) were performed in triplicate, and data were fit to standard binding curves using GraphPad Prism to calculate IC$_{50}$ values.

4.7 Biophysical analysis

4.7.1 Microscale thermophoresis (MST). Ku heterodimer was labeled using the Monolith NT™ Protein Labeling Kit RED-NHS (2nd generation amine reactive, NanoTemper Technologies GmbH, MO-L011, München, Germany), following the manufacturer's protocol. Ku-DBi powder was resuspended in 100% DMSO, and the concentration was adjusted to 50 mM after UV absorbance measurement (absorbance at 417 nm with an extension coefficient equal to 15.2 mM^{-1} cm^{-1}). The ligand stock solution was sonicated in an ultrasonic bath before preparations of the dilution series. The MST and Differential Scanning Fluorometry (DSF) assays contain 5% DMSO to fit the DMSO concentration at the highest ligand concentration (200 μM). The labeled protein (5 nM) was incubated with ligand 3392 ranging from 98 nM to 200 μM in a 12-point 1:1 dilution series. Protein–ligand solutions were incubated for 30 min at room temperature before MST measurements, which were performed in triplicate. Proteins were transferred to capillaries (Monolith NT. Automated Premium Capillary Chips), and binding was analyzed with a Monolith NT. Automated pico-RED device using MO. Control Software with nano-red excitation, LED light adjusted to 20% excitation power, and infrared laser (MST power) set to medium. The dissociation constants (Kd or K_D) were determined with MO. Binding Affinity software (NanoTemper Technologies GmbH, v1.6) using the single-site fit binding mode (referred to as K_D binding mode in the software).

4.7.2 nano Differential Scanning Fluorometry (nanoDSF). The thermostability and aggregation propensity of Ku was assessed using a Prometheus Panta nanoDSF instrument (NanoTemper Technologies GmbH, München, Germany). High sensitivity capillaries were filled with Ku (10 μL each, experiments in triplicate) at a concentration of 5 μM into the instrument. We titrated against Ku-DBi's covering a concentration ranging from 0 to 25 μM with measurements collected at a 1 °C per minute scan rate from 25 to 95 °C. Thermal unfolding was assessed by the increase in intrinsic tryptophan fluorescence detected at 350 and 330 nm following excitation at 280 nm. Inflection points in the thermal denaturation curves were identified using the first derivatives of the ratio r = fluorescence (350 nm)/fluorescence (330 nm). We measured dynamic light scattering (DLS) and turbidity throughout the heating ramp using back reflection to characterize protein aggregation. We determined aggregation temperatures using turbidity variations and increases in particle sizes.

Author contributions

N. D. K., J. D. G. and N. S. G. synthesized and characterized novel Ku-DBi's, contributed to original writing, review and editing of the manuscript; P. V.-C., T. L. V., and P. L. M.-M. performed biochemical and biological analysis of Ku-DBi's, contributed to review and editing of the manuscript; K. B. A. G. performed MST and NanoDSF experiments, contributed to

review and editing of the manuscript; J. E. performed pharmacophore modeling; J.-B. C. participated in the design and analysis of biophysical studies, contributed to review and editing of the manuscript; N. S. G. and J. J. T. designed and conceptualized SAR strategy, chemistry and biology of the project, supervised all the project activities, contributed to original writing, review and editing of the manuscript. All authors contributed essential portions of the manuscript, reviewed and approved the final manuscript.

Conflicts of interest

Author Karim Ben Ali Gacem was employed by the company Sanofi. J. J. Turchi is a co-founder and CSO of NERx Biosciences. Navnath S. Gavande and John J. Turchi have patent # WO2017205503 issued to Indiana University School of Medicine. If there are other authors, they declare that they have no known competing financial interests or personal relationships that could have appeared to influence the work reported in this paper. All other authors declare no potential conflicts of interest.

Data availability

Supplementary information: *E/Z* isomer determination, Thermophoretic property of Ku-DBi's, Thermostability and aggregation propensity of Ku-DBi's, Copy of ^{1}H NMR and ^{13}C NMR of final compounds. See DOI: **https://doi.org/10.1039/D5MD00263J**.

The data supporting this article have been included as part of the SI. Further inquiries can be directed to the corresponding authors.

Acknowledgements

References

1 R. Huang and P.-K. Zhou, *Signal Transduction Targeted Ther.*, 2021, **6**, 254.

2 J. M. Kelm, A. Samarbakhsh, A. Pillai, P. S. VanderVere-Carozza, H. Aruri, D. S. Pandey, K. S. Pawelczak, J. J. Turchi and N. S. Gavande, *Front. Oncol.*, 2022, **12**, 850883.

3 R. Scully, A. Panday, R. Elango and N. A. Willis, *Nat. Rev. Mol. Cell Biol.*, 2019, **20**, 698–714.

4 B. M. Stinson and J. J. Loparo, *Annu. Rev. Biochem.*, 2021, **90**, 137–164.

5 N. S. Gavande, P. S. VanderVere-Carozza, H. D. Hinshaw, S. I. Jalal, C. R. Sears and K. S. Pawelczak, *et al.*, *Pharmacol. Ther.*, 2016, **160**, 65–83.

6 A. Sfeir and L. S. Symington, *Trends Biochem. Sci.*, 2015, **40**, 701–714.

7 D. A. Ramsden, J. Carvajal-Garcia and G. P. Gupta, *Nat. Rev. Mol. Cell Biol.*, 2021, **23**, 125–140.

8 R. Bhargava, D. O. Onyango and J. M. Stark, *Trends Genet.*, 2016, **32**, 566–575.

9 K. Karanam, R. Kafri, A. Loewer and G. Lahav, *Mol. Cell*, 2012, **47**, 320–329.

10 H. H. Y. Chang, N. R. Pannunzio, N. Adachi and M. R. Lieber, *Nat. Rev. Mol. Cell Biol.*, 2017, **18**, 495–506.

11 M. R. Lieber, *Annu. Rev. Biochem.*, 2010, **79**, 181–211.

12 S. Zahid, M. Seif El Dahan, F. Iehl, P. Fernandez-Varela, M. H. Le Du and V. Ropars, *et al.*, *Int. J. Mol. Sci.*, 2021, **22**, 1–23.

13 S. Abbasi, G. Parmer, R. D. Kelly, N. Balasuriya and C. Schild-Poulter, *Cell. Mol. Life Sci.*, 2021, **78**, 4589–4613.

14 G. Damia, *Mutat. Res.*, 2020, **821**, 111692.

15 D. Davidson, L. Amrein, L. Panasci and R. Aloyz, *Front. Pharmacol.*, 2013, **4**, 5.

16 A. O. Agboola, *et al.*, *Pathol., Res. Pract.*, 2017, **213**, 27–33.

17 J. F. Goodwin and K. E. Knudsen, *Cancer Discovery*, 2014, **4**, 1126–1139.

18 E. Dylgjeri and K. E. Knudsen, *Cancer Res.*, 2021, **82**, 523–533.

19 S. Hu, Z. Hui, F. Lirussi, C. Garrido, X.-Y. Ye and T. Xie, *Expert Opin. Ther. Pat.*, 2021, **31**, 435–452.

20 B. Cheng, Y. Shi, C. Shao, S. Wang, Z. Su, J. Liu, Y. Zhou, X. Fei, W. Pan and J. Chen, *J. Med. Chem.*, 2024, **67**, 6253–6267.

21 Y. Matsumoto, *Int. J. Mol. Sci.*, 2022, **23**, 4264.

22 T. M. Gilmer, C.-H. Lai and K. Guo, *et al.*, *Mol. Cancer Ther.*, 2024, **23**, 751–765.

23 M. Fiorillo, B. Ozsvari, F. Sotgia and M. P. Lisanti, *Front. Oncol.*, 2021, **11**, 740720.

24 M. Samuels, J. Falkenius, V. Bar-Ad and J. Dunst, *et al.*, *Int. J. Radiat. Oncol., Biol., Phys.*, 2024, **118**, 743–756.

25 K. Liu, X. Yuan, T. Yang, D. Deng and Y. Chen, *et al.*, *J. Med. Chem.*, 2024, **67**, 245–271.

26 J. L. Zhao, E. S. Antonarakis, H. H. Cheng, D. J. George, R. Aggarwal, E. Riedel, T. Sumiyoshi, J. D. Schonhoft, A. Anderson and N. Mao, *et al.*, *Br. J. Cancer*, 2024, **130**, 53–62.

27 N. S. Gavande, P. S. VanderVere-Carozza, K. S. Pawelczak, P. Mendoza-Munoz, T. L. Vernon and L. A. Hanakahi, *et al.*, *Nucleic Acids Res.*, 2020, **48**, 11536–11550.

28 K. S. Pawelczak, N. S. Gavande, P. S. VanderVere-Carozza and J. J. Turchi, *ACS Chem. Biol.*, 2018, **13**, 389–396.

29 E. Weterings, A. C. Gallegos, L. N. Dominick, L. S. Cooke, T. N. Bartels and J. Vagner, *et al.*, *DNA Repair*, 2016, **43**, 98–106.

30 X. Chen, C. Chen, C. Luo, J. Liu and Z. Lin, *Eur. J. Pharmacol.*, 2024, **975**, 176647.

31 P. L. Mendoza-Munoz, N. S. Gavande, P. S. VanderVere-Carozza, K. S. Pawelczak, J. R. Dynlacht, J. E. Garrett and J. J. Turchi, *NAR Cancer*, 2023, **5**, zcad003.

32 P. L. Mendoza-Munoz, N. D. Kushwaha, D. Chauhan, K. B. Ali Gacem, J. E. Garrett, J. R. Dynlacht, J.-B. Charbonnier, N. S. Gavande and J. J. Turchi, *Cancers*, 2024, **16**, 3286.

33 J. R. Walker, R. A. Corpina and J. Goldberg, *Nature*, 2001, **412**, 607–614.

34 V. Kumar, C.-K. Chang, K.-P. Tan, Y.-S. Jung, S.-H. Chen, Y.-S. E. Cheng and P.-H. Liang, *Org. Lett.*, 2014, **16**, 5060–5063.

35 F. Moreau, N. Desroy and J. M. Genevard, *Bioorg. Med. Chem. Lett.*, 2008, **18**, 4022–4026.

36 N. S. Gavande, P. VanderVere-Carozza, A. K. Mishra, T. L. Vernon, K. S. Pawelczak and J. J. Turchi, *J. Med. Chem.*, 2017, **60**, 8055–8070.

37 L. Sun, N. Tran, F. Tang, H. App, P. Hirth, G. McMahon and C. Tang, *J. Med. Chem.*, 1998, **41**, 2588–2603.

38 D. Gramec, L. P. Masic and M. S. Dolenc, *Chem. Res. Toxicol.*, 2014, **27**, 1344–1358.

39 C. K. Jaladanki, N. Taxak, R. A. Varikoti and P. V. Bharatam, *Chem. Res. Toxicol.*, 2015, **28**, 2364–2376.

40 A. Abula, Z. Xu, Z. Zhu, C. Peng, Z. Chen, W. Zhu and H. Aisa, *J. Chem. Inf. Model.*, 2020, **60**, 6242–6250.

41 N. Sheikhi, M. Bahraminejad, M. Saeedi and S. S. Mirfazli, *Eur. J. Med. Chem.*, 2023, **260**, 115758.

42 Q. Zhang, W. Yin, X. Chen and A. Zhou, *et al.*, *J. Med. Chem.*, 2025, **68**, 706–718.

43 C. Ballatore, D. M. Huryn and A. B. Smith III, *ChemMedChem*, 2013, **8**, 385–395.

44 P. Lassalas, B. Gay, C. Lasfargeas and M. J. James, *et al.*, *J. Med. Chem.*, 2016, **59**, 3183–3203.

45 A. Hall, M. Chatzopoulou and J. Frost, *Bioorg. Med. Chem.*, 2024, **104**, 117653.

46 *Schrödinger Release 2024-2: Phase*, Schrödinger, LLC, New York, NY, 2024.

47 K. Mansouri, C. M. Grulke, R. S. Judson and A. J. Williams, *Aust. J. Chem.*, 2018, **10**, 10.

48 K. Mansouri, J. T. Moreira-Filho and C. N. Lowe, *et al.*, *Aust. J. Chem.*, 2024, **16**, 19.

49 A. Gontier, P. F. Varela, C. Nemoz, V. Ropars, M. Aumont-Nicaise, M. Desmadril and J.-B. Charbonnier, *Methods Mol. Biol.*, 2021, **2247**, 125–143.

50 K. S. Pawelczak, B. J. Andrews and J. J. Turchi, *Nucleic Acids Res.*, 2005, **33**, 152–161.

51 J. Ji, S. Dragojevic, C. M. Callaghan, E. J. Smith, S. Talele, W. Zhang and M. A. Connors, *et al.*, *Mol. Cancer Ther.*, 2024, **23**, 662–671.

52 I. Berger, C. Tolzer and K. Gupta, *Emerging Top. Life Sci.*, 2019, **3**, 477–482.

53 K. S. Pawelczak and J. J. Turchi, *Nucleic Acids Res.*, 2008, **36**, 4022–4031.